Radio Resource Management for HSDPA and MC-DS-CDMA Systems

Radio Resource Management for HSDPA and MC-DS-CDMA Systems

A Dissertation

Presented to

The Academic Faculty

By

Chih-Wen Chang

In Partial Fulfillment

of the Requirements for the Degree of

Doctor of Philosophy in Communication Engineering

Department of Communication Engineering

National Chiao-Tung University

April, 2006

Abstract

Radio resource management (RRM) plays a key role in quality-of-service (QoS) control and capacity optimization for future wireless systems. In this dissertation, we investigate several critical RRM issues in the high speed downlink packet access (HSDPA) of wideband code division multiple access (WCDMA) system and the multi-carrier direct-sequence code division multiple access (MC-DS-CDMA) system.

In the first part of this dissertation, we focus on the stall issue of the parallel multi-channel stop-and-wait (SAW) hybrid auto-retransmission request (HARQ) mechanism for the HSDPA of WCDMA system. In the stall situation, the receiver may wait for a packet that will be no longer be sent by the transmitter and stops delivering the medium access control (MAC) layer packets to the upper layer. We present an analytical approach to evaluate three stall avoidance schemes — the timer-based, the window-based, and the indicator-based schemes based on a newly proposed performance metric — gap processing time. We demonstrate that the indicator-based stall avoidance scheme outperforms the timer-based and the window-based schemes. Finally, we further derive the closed-form expression for the gap-processing time of the indicator-based stall avoidance mechanism when applying the interleaving scheduling. The developed analytical approaches have several advantages including: (1) help determine a proper number of processes for the parallel SAW HARQ mechanisms and the number of acceptable fully loaded users for an admission control policy subject to the gap processing time constraint; (2) facilitate the MAC/radio link control (RLC) cross-layer design for the RLC timeout and RLC window size.

In the second part of this dissertation, we focus on the RRM issues in the MC-DS-CDMA systems, including power control, code admission, and subcarrier power allocation. We first analyze the joint effects of the power control errors (PCE) and the complete MAI in the multi-rate uplink MC-DS-CDMA system. We find that (1) the effect of PCE can exacerbate the impact of the complete MAI, or vice versa;

(2) increasing frequency or time domain spreading gain results in a higher sensitivity to the PCEs; (3) a larger PCE can possibly make the frequency domain diversity diminish faster than the gain obtained from the time-domain spreading.

For the downlink MC-DS-CDMA system, we develop an MAI-coefficient-based interference avoidance code assignment scheme. The *MAI coefficient* can be applied to quantitatively predict the MAI effect imposed on a particular code in a multi-rate MC-DS-CDMA system. We show that the proposed interference avoidance code assignment method can effectively reduce the MAI in a multi-rate MC-DS-CDMA system, while maintaining a very good call admission rate. Moreover, we further propose a joint subcarrier power allocation and code assignment scheme to optimize the received signal quality in the presence of MAI.

In summary, we investigate the performance tradeoffs between the gap processing time and throughput of the multi-process SAW HARQ mechanism in the HSDPA system. Moreover, we analyze the joint effects of PCEs and MAI in the uplink MC-DS-CDMA system. Finally, we investigate how to assign a code with less MAI and how to allocate the subcarrier power allocation for the downlink MC-DS-CDMA system.

Acknowledgments

First of all, I would like to express my deeply gratitude to my advisor Dr. Li-Chun Wang. Not only the important insights to research problems, encouragement, and support, he also taught me how to have a strong will power and how to be optimistic. Without his advice, guidance, comments, and all that, this work could not have been done. He indeed opened a door to the future for me.

Special thanks to my mates of Wireless Network Lab in NCTU. They gave me kindly help in many aspects. Anderson Chen, seated next to me, gave me many helpful suggestions. Yi-liang Lin and Tom Lee encouraged me every time when I felt frustrated. Wei-Cheng Liu helped me very much in the mathematic class. All in all, I was so lucky to have all the lab mates.

In the end, I have a lovely lady, I-Tin Lee, to thank. She gave me sincerely mental and emotional support and kept me company during this long journey. She indeed made every thing colorful. I would like to thank my dear sisters, too. They always warmly back me up. Most importantly, I am deeply indebted to my great parents whose love and understanding have been accompaning me through these years.

Contents

List of Tables

List of Figures

Glossary of Symbols

- 2D ≜ Two dimension

- 3G ≜ Third generation

- ACK ≜ Acknowledgement

- B3G ≜ Beyond the third generation

- BER ≜ Bit error rate

- CF ≜ Crowd-first-code

- CRC ≜ Cyclic redundancy check

- GHz ≜ Giga hertz

- GPT ≜ Gap processing time

- HARQ ≜ Hybrid auto-retransmission request

- HSDPA ≜ High speed downlink packet access

- IA ≜ Interference avoidance

- ISA ≜ Indicator-based stall avoidance

- MAC ≜ Media access control

- MAI ≜ Multiple access interference
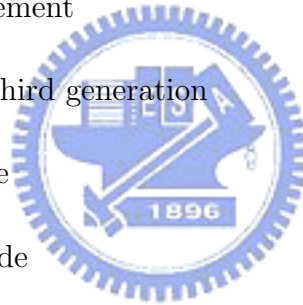
- MC-DS-CDMA $\triangleq$ Multi-carrier direct sequence code division multiple access

- MIMO $\triangleq$ Multiple input multiple output

- NACK $\triangleq$ Negative acknowledgement

- NDI $\triangleq$ New data indicator

- OFDM $\triangleq$ Orthogonal frequency division multiplexing

- OVSF $\triangleq$ Orthogonal variable spreading factor

- pmf $\triangleq$ Probability mass function

- pdf $\triangleq$ Probability density function

- PCE $\triangleq$ Power control error

- PKT $\triangleq$ Packet

- PR $\triangleq$ Process

- QoS $\triangleq$ Quality of service

- RM $\triangleq$ Random

- RLC $\triangleq$ Radio link control

- SAW $\triangleq$ Stop-and-wait

- SF $\triangleq$ Spreading factor

- SINR $\triangleq$ Signal to interference and noise ratio

- SPA $\triangleq$ Subcarrier power allocation

- STD $\triangleq$ Standard deviation

- TF $\triangleq$ Time and frequency

- TSN ≜ Transmission sequence number

- TTI ≜ Transmission time interval

- UMTS ≜ Universal mobile telecommunication services

- UTRA ≜ UMTS terrestrial radio access

- WCDMA ≜ Wide-band code division multiple access

- $\mathbf{A_u}$ ≜ User group, of which a user uses a time-domain spreading code the same as the reference user and a frequency-domain spreading code different from the reference user

- $\mathbf{B_u}$ ≜ User group, of which a user uses a time-domain spreading code different from the reference user and a frequency-domain spreading code different the same the reference user

- $\mathbf{C_u}$ ≜ User group, of which a user uses a time-domain spreading code and a frequency-domain spreading code both different from the reference user

- $\mathbf{A_o}$ ≜ User group, of which a user uses a time-domain spreading code not orthogonal to the reference user and a frequency-domain spreading code orthogonal to the reference user

- $\mathbf{B_o}$ ≜ User group, of which a user uses a time-domain spreading code orthogonal to the reference user and a frequency-domain spreading code not orthogonal to the reference user

- $\mathbf{C_o}$ ≜ User group, of which a user uses a time-domain spreading code and a frequency-domain spreading code both orthogonal to the reference user

- BW_c ≜ Coherent bandwidth of fading channel

- $C_{S,n}$ ≜ The n-th code in a code group with spreading gain S

- $C_{2^{l-1},n}^{(i)} \triangleq$ The n-th code of the code group in the l-th layer associated with the i-th code tree

- $C_n \triangleq$ The n-th code of a particular code set

- $C_V \triangleq$ The number of cycles involving all the processes in the multi-process SAW HARQ mechanism required to remove a Type-II gap

- $b \triangleq \ln 10/10$

- $b_{k,i}^{(\mathbf{X})}(t) \triangleq$ Waveform of user k of group $\mathbf{X}$ at the i-th substream

- $b_{k,i}^{(\mathbf{X})}[h] \triangleq$ The h-th bit of user k of group $\mathbf{X}$ at the i-th substream

- $b_{o,i}(t) \triangleq$ Waveform of the reference user at the i-th substream

- $c_k^{(\mathbf{X})}[j] \triangleq$ The j-th chip of the frequency-domain spreading code for the k-th user of group $\mathbf{X}$

- $c_o[j] \triangleq$ The j-th chip of the frequency-domain spreading code for the reference user

- $D \triangleq$ Expiry time of the timer

- $D_p \triangleq$ Order of Hermite or Laguerre polynomials

- $E_\alpha \triangleq$ Event of PR_m being ruled out in the k-th cycle

- $E_\beta \triangleq$ Event of $PR_2 \sim PR_{m-1}$ being ruled out within the k-th cycle

- $E_\gamma \triangleq$ Event of $PR_{m+1} \sim PR_M$ being ruled out within the $(k-1)$-th cycle

- $E_1 \triangleq$ The event that process 1 enters the STOP state within the k-th cycle

- $E_2 \triangleq$ The event that the first $m-2$ processes enter the STOP state within the k-th cycle

- $E_3 \triangleq$ The event that process m enters the STOP state at the k-th cycle

- $E_4 \triangleq$ The event that the last $M - m$ processes enter the STOP state before the k-th cycle

- $E_A \triangleq$ The event that process 1 is scheduling for transmission at the k-th cycle

- $E_B \triangleq$ The event that all the other $(M - 1)$ processes enter STOP state before the k-th cycle

- $E_b \triangleq$ Bit energy

- $E_o \triangleq$ Bit energy of the reference user

- $f_o \triangleq$ Main carrier frequency

- $f_{i,j} \triangleq$ Carrier frequency of the j-th carrier of the i-th substream

- $f_{z_v}(\cdot) \triangleq$ Probability density function of random variable z_v

- $f_{z_{kv}}(\cdot) \triangleq$ Probability density function of random variable z_{kv}

- $h_r \triangleq$ Number of allowable retransmissions

- $\mathbf{I}_A \triangleq \{NDI_{(rec)} = NEW\}$

- $\mathbf{I}_B \triangleq \{\{TSN_{(rec)} \neq TSN^*\} \cap \{NDI_{(rec)} = OLD\}\}$

- $g_o(t) \triangleq$ Time-domain spreading code of the reference user

- $g_k^{(\mathbf{X})}(t) \triangleq$ Time-domain spreading code of the k-th user of group $\mathbf{X}$

- $g_k^{(\mathbf{X})}[\ell] \triangleq$ The ℓ-th chip of the time-domain spreading code of user k of group $\mathbf{X}$

- $G_o \triangleq$ Time-domain spreading gain of the reference user

- $G_k^{(\mathbf{X})} \triangleq$ Time-domain spreading gain of user k of group $\mathbf{X}$

- $\overline{GPT} \triangleq$ Average gap processing time

- $\overline{GPT}_0 \triangleq$ Average gap processing time for case (I) of the indicator-based stall avoidance scheme

- $\overline{GPT}_1 \triangleq$ Average gap processing time for case (II) of the indicator-based stall avoidance scheme

- $\overline{GPT}_I \triangleq$ Average gap processing time for case (I) of the indicator-based stall avoidance scheme with interleaving scheduling

- $\overline{GPT}_{II} \triangleq$ Average gap processing time for case (II) of the indicator-based stall avoidance scheme with interleaving scheduling

- $GPT_c \triangleq$ Constraint of the gap processing time

- $\overline{GPT}_{indicator} \triangleq$ Average gap processing time of the indicator-based stall avoidance mechanism

- $\overline{GPT}(\ell) \triangleq$ Average gap processing time with ℓ Type-II gaps

- $\overline{GPT}_{timer} \triangleq$ Average gap processing time of the timer-based stall avoidance mechanism

- $\overline{GPT}_{window} \triangleq$ Average gap processing time of the window-based stall avoidance mechanism

- $h_m \triangleq$ Number of the minimum allowable retransmissions

- $h_r \triangleq$ Number of the allowable retransmissions

- $H(t) \triangleq$ Unit step function

- $I_{k,s,v}^{(\mathbf{X})} \triangleq$ Multiple access interference from of v-th subcarrier in the s-th substream for user k of group $\mathbf{X}$ in downlink transmission

- $I_{\mathbf{X},k}^{(1)} \triangleq$ Main subcarrier's multiple access interference from user k of group $\mathbf{X}$ in uplink transmission

- $I_{\mathbf{X},k}^{(2)} \triangleq$ Other subcarriers' multiple access interference from user k of group $\mathbf{X}$ in uplink transmission

- $I_{\mathbf{X},k}^{(2)'} \triangleq$ Other subcarriers' multiple access interference from user k of group $\mathbf{X}$ for case (a) in uplink transmission

- $I_{\mathbf{X},k}^{(2)''} \triangleq$ Other subcarriers' multiple access interference from user k of group $\mathbf{X}$ for case (b) in uplink transmission

- $I_{oc} \triangleq$ One average term of the multiple access interference from other subcarriers

- $J(\cdot) \triangleq$ Lagrange function

- $K_{\mathbf{X}} \triangleq$ Number of users of group $\mathbf{X}$

- $L_k^{(\mathbf{X})} \triangleq$ Ratio of the bit duration of the reference user and the interfering user k of group $\mathbf{X}$

- $L_g \triangleq$ Required TTIs to detect a Type-II gap

- $M \triangleq$ Frequency-domain spreading gain

- $n(t) \triangleq$ While Gaussian noise in the receiving end

- $n_{s,v} \triangleq$ White Gaussian noise of the v-th subcarrier in the s-th substream

- $N_0 \triangleq$ Power spectrum density of the while Gaussian noise

- $N_d \triangleq$ Network delay

- $N_p \triangleq$ Number of required parallel processes in the multi-process SAW HARQ to fully utilize the channel capacity

- $N_u \triangleq$ Number of acceptable full loaded users

- N→A $\triangleq$ NACK-to-ACK

- $NDI_{(rec)} \triangleq$ NDI of the received packet

- $P(\cdot) \triangleq$ Probability measure

- $P_\alpha(m, k) \triangleq$ Joint probability of events E_1, E_2, E_3, and E_4

- $P_e \triangleq$ Packet error rate

- $P(e) \triangleq$ Bit error rate

- $P(e|x) \triangleq$ Conditional error probability with a given condition x

- $P_G \triangleq$ Probability of a Type-II gap

- $P_{k,i,j}^{(\mathbf{X})} \triangleq$ Transmission power of user k of group $\mathbf{X}$ at the j-th subcarrier in the i-th substream

- $P_k^{(\mathbf{X})} \triangleq$ Transmission power of user k of group $\mathbf{X}$

- $P_o \triangleq$ Transmission power of the reference user

- $P_{o,i,j} \triangleq$ Transmission power of the reference user at the j-th subcarrier in the i-th substream

- $P_{T_c} \triangleq$ Chip waveform of a time-domain spreading code

- $P_{T_k^{(\mathbf{X})}} \triangleq$ Bit waveform of user k of group $\mathbf{X}$

- $P_{sch} \triangleq$ Probability of a process being scheduled

- $P_k^{(m)} \triangleq$ Probability of process PR_m being ruled out within the k-th cycle

- $P_N \triangleq$ Noise power

- $P_{N \to A} \triangleq$ Probability of the NACK-to-ACK error

- $P_{new} \triangleq$ Probability of receiving a new packet

- $P_{old} \triangleq$ Probability of receiving an old packet

- $PR_m \triangleq$ The m-th process of the multi-process SAW HARQ

- $P_s \triangleq$ Probability of successfully receiving a packet

- $\mathbf{P}(\mathbf{x}_\ell) \triangleq$ State probability vector of the multi-process SAW HARQ

- $P_V(m) \triangleq$ Probability of a new packet and a Type-II gap being separated by m seats in the detection window

- $Q(\cdot) \triangleq$ Q-function, defined as $Q(x) = \frac{1}{\sqrt{2\pi}} \int_x^\infty e^{-t^2/2} dt$

- $Q_d \triangleq$ Packet queuing delay

- $r_o(t) \triangleq$ Received signal of the reference user

- $R(t, \theta) \triangleq$ Auto-correlation function of the time-domain spreading code between the reference and the interfering users during the time interval $[0, t]$ with phase difference θ and subcarrier frequency difference $f_{i,j} - f_{s,v}$

- $\widetilde{R}(t, \theta) \triangleq$ Auto-correlation function of the time-domain spreading code between the reference and the interfering users during the time interval $\{t, T_o\}$ with phase difference θ and subcarrier frequency difference $f_{i,j} - f_{s,v}$

- $R_\ell(t, \theta) \triangleq$ Auto-correlation function of the time-domain spreading code between the reference and the interfering users during the time interval $[\ell T_k^{(\mathbf{X})}, \ell T_k^{(\mathbf{X})} + t]$ with phase difference θ and subcarrier frequency difference $f_{i,j} - f_{s,v}$

- $\widetilde{R}_\ell(t, \theta) \triangleq$ Auto-correlation function of the time-domain spreading code between the reference and the interfering users during the time interval $[\ell T_k^{(\mathbf{X})} + t, (\ell + 1)T_k^{(\mathbf{X})}]$ with phase difference θ and subcarrier frequency difference $f_{i,j} - f_{s,v}$

- $\mathbf{R}_c(\cdot) \triangleq$ Code set related to a particular code

- $R_d \triangleq$ Packet reordering delay

- $R_L \triangleq$ The lowest transmission rate

- $s_k^{(\mathbf{X})}(t) \triangleq$ Transmitted signal of user k of group $\mathbf{X}$

- $S_R \triangleq$ Retransmission state of the multi-process SAW HARQ.

- $S_T \triangleq$ STOP state of the multi-process SAW HARQ

- $S_0 \triangleq$ REQUEST state of the multi-process SAW HARQ

- $S_1, S_2 \triangleq$ RESCHEDULE state of the multi-process SAW HARQ

- $S_c \triangleq$ State variable $\in \{ACK, NACK, N \to A\}$

- $SF_t \triangleq$ Time-domain spreading factor

- $SF_f \triangleq$ Frequency-domain spreading factor

- $t_j \triangleq$ Elapsed time of the previous timer until the end of gap j

- $TSN_{(rec)} \triangleq$ TSN of the received packet

- $T_c \triangleq$ Chip duration

- $T_d \triangleq$ Packet delivery delay

- $T_o \triangleq$ Bit duration of the reference user after the serial-to-parallel converter

- $T_k^{(\mathbf{X})} \triangleq$ Bit duration of user k of group $\mathbf{X}$ after the serial-to-parallel converter

- $T_{b,k}^{(\mathbf{X})} \triangleq$ Bit duration of the source bit stream of user k of group $\mathbf{X}$

- $U \triangleq$ Number of substreams in the serial-to-parallel converter

- $V \triangleq$ Number of parallel processes in the multi-process SAW HARQ

- $W \triangleq$ Size of the detection window

- $x_\ell \triangleq$ State variable of the ℓ-th transmission cycle.

- $\mathbf{X} \triangleq$ Variable of user group

- $y_i \triangleq$ The i-th abscissa of the Hermite or Laguerre Polynomials

- $Y_{o,s} \triangleq$ Decision variable of the s-th substream for the reference user

- $Y_{o,s,v} \triangleq$ Output variable in the v-th subcarrier of the s-th substream for the reference user

- $z \triangleq$ Subcarrier distance between the j-th subcarrier of the i-th substream and the v-th subcarrier of s-th substream the, defined as $z = (i - s) + (j - v)U$, where U is the number of the substreams in the serial-to-parallel converter

- $z_v \triangleq$ Random variable representing the channel gain of the v-th subcarrier of the reference user, defined as $z_v = |\alpha_{o,s,v}|^2$

- $z_{kv} \triangleq$ Random variable representing the channel gain of the i-th subcarrier of user k of group $\mathbf{A_o}$, defined as $z_{kv} = |\alpha_{k,s,i}^{(\mathbf{A_o})}|^2$

- $z_{v,s} \triangleq$ The s-th abscissa of Laguerre polynomial for the v-th random variable for the reference user

- $z_{kv,s} \triangleq$ The s-th abscissa of Laguerre polynomial for the v-th random variable for the interfering user k

- $\alpha_{o,i,j} \triangleq$ Channel's amplitude of the reference user of the j-th subcarrier in the i-th substream

- $\alpha_{k,i,j}^{(\mathbf{X})} \triangleq$ Channel's amplitude of user k of group $\mathbf{X}$ of the j-th subcarrier in the i-th substream

- $\beta_{o,s,v} \triangleq$ Weights for a certain combining scheme of the reference user for the v-th subcarrier of the s-th substream

- $\gamma \triangleq$ Received signal to noise ratio

- $\gamma_c \triangleq$ The received signal to noise ratio of one particular subcarrier

- $\gamma_M \triangleq$ Combination of the channel gain from M subcarriers

- $\overline{\lambda} \triangleq$ Average power control error

- $\lambda_c \triangleq$ Call arrival rate

- $\lambda_L \triangleq$ Lagrange multiplier

- $\lambda_o \triangleq$ Power control error of the reference user

- $\lambda_k^{(\mathbf{X})} \triangleq$ Power control error of user k of group $\mathbf{X}$

- $\sigma_e \triangleq$ Standard deviation of power control error

- $\sigma_k^{\mathbf{A}} \triangleq$ Area of the grid for user k of group $\mathbf{A}$

- $\sigma_o \triangleq$ Area of the grid for the reference user

- $\omega_i \triangleq$ The i-th weight factor of Hermite or Laguerre polynomails

- $\omega_i, j \triangleq$ The j-th weight factor of Laguerre polynomails for the i-th random variable

- $\psi_{o,i,j} \triangleq$ Channel's phase of the reference

- $\psi_{k,i,j}^{(\mathbf{X})} \triangleq$ Channel's phase of user k of group $\mathbf{X}$

- $\varphi_{o,i,j} \triangleq$ Initial phase of the reference user

- $\varphi_{k,i,j}^{(\mathbf{X})} \triangleq$ Initial phase of user k of group $\mathbf{X}$ at the j-th carrier of the i-th substream

- $\phi_{i,j} \triangleq$ Initial phase of the j-th subcarrier in the i-th substream

- $\phi_{o,i,j} \triangleq$ Phase of the reference user in the receiving end

- $\phi_{k,i,j}^{(\mathbf{X})} \triangleq$ Phase of user k of group $\mathbf{X}$ of the j-th subcarrier at the i-th substream in the receiving end

- $\theta_{k,i,j}^{(\mathbf{X})} \triangleq$ Phase difference between the reference user and the interfering user, defined as $\theta_{k,i,j}^{(\mathbf{X})} = \phi_{k,i,j}^{(\mathbf{X})} - \phi_{o,s,v}$

- $\rho \triangleq$ Effective traffic load

- $\tau \triangleq$ Misalignment of transmission time between the reference user and the interfering user

- $\tau_o \triangleq$ Propagation delay of the reference user

- $\tau_k^{(\mathbf{X})} \triangleq$ Propagation delay of user k of group $\mathbf{X}$

- $\delta \triangleq$ Power control error in the real domain, defined as $10\log_{10}\lambda_o$

- $\Delta[\ell] \triangleq$ Random variable, defined as $\Delta[\ell] = \pm 1$ with equal probability for arbitrary positive integer ℓ

- $\Delta_f \triangleq$ Minimal frequency spacing between any two adjacent substreams with the same subcarrier index

- $\mu(\delta) \triangleq$ A function of the power control error, defined as $\mu(\delta) = \sqrt{\frac{10^{\delta/10}\gamma_c}{1+10^{\delta/10}\gamma_c}}$

- $\mu_c \triangleq$ Call departure rate

- $\zeta \triangleq$ Product of reference user's time-domain spreading gain and the combination of channel gain from M subcarriers, defined as $\zeta = G_o \sum_{v=1}^{M} |\alpha_{o,s,v}|^2$

- $\Phi_{j,\tau}^{(1)} \triangleq$ Phase difference between the main subcarrier of the reference user and the other subcarrier of the interfering user during the j-th chip of the reference user's time-domain spreading factor, defined as $\Phi_{j,\tau}^{(1)} = \frac{\pi z}{T_c}(2jT_c + \tau - hT_c) + \theta$, where h and θ are given positive integer and phase

- $\Phi_{j,\tau}^{(2)} \triangleq$ Phase difference between the main subcarrier of the reference user and the other subcarrier of the interfering user during the j-th chip of the reference user's time-domain spreading factor, defined as $\Phi_{j,\tau}^{(2)} = \frac{\pi z}{T_c}((2j+1)T_c+\tau-hT_c)+\theta$, where h and θ are given positive integer and phase

- $\kappa \triangleq$ MAI coefficient

- $E[\cdot] \triangleq$ Operator to take the average value

- $E_\tau[\cdot] \triangleq$ Operator to take the average over τ

- $E_\theta[\cdot] \triangleq$ Operator to take the average over θ

- $Var[\cdot] \triangleq$ Operator to take the variance value

- $\mathbf{max}(\cdot) \triangleq$ Operator to take the maximal value

- $\mathbf{min}(\cdot) \triangleq$ Operator to take the minimal value

- $\Delta_\kappa(\cdot) \triangleq$ Operator to calculate the incremental MAI coefficient of a code or code set

- $\kappa(\cdot) \triangleq$ Operator to calculate the MAI coefficient of a code or code set

Chapter 1

Introduction

As people are no longer satisfied with the conventional conversation service, the demand for versatile wireless multimedia services becomes a strong driving force for the birth of a new generation wireless communication systems. In recent years, the next generation wireless communication systems beyond the third generation (3G) will be developed to satisfy this increasing capacity demand. However, maintaining good quality-of-service (QoS), including the performance requirements of the end-to-end delay, error probability, call admission rate, and signal-to-interference-and-noise ratio (SINR) are essential for the B3G wireless systems. Thus, because radio resource management (RRM) techniques can improve the required QoS and the utilization of system capacity, the RRM techniques become the key to the success of the B3G wireless system. [1–5].

Specifically, power control and call admission control (CAC) are two important RRM techniques to decide the transmission power of a mobile terminal [6–9] and to determine whether a new session should be accepted [10–12], respectively. In the packet retransmission mechanism, the fast retransmission technique is an important technique to decide when and how to retransmit the erroneous packets [13–15]. Last, code assignment aims to select a good code for the new request [16–18]. In this dissertation, we study the aforementioned RRM techniques in two future systems, the high speed downlink packet accesss (HSDPA) in WCDMA and the multi-carrier direct-sequence code division multiple access (MC-DS-CDMA).

HSDPA, the alleged 3.5G system, is becoming an important feature for the wideband code division multiple access (WCDMA) system [19]. The objective of HSDPA in the WCDMA system is to provide a packet data service at rates up to 10 Mbits/sec [20, 21]. HSDPA integrates many techniques in both the physical and

MAC layers, including adaptive modulation and coding [22–24], fast packet scheduling [25–29], fast cell selection [30], multiple-input multiple-output (MIMO) antenna processing [31, 32], buffer overflow control [33], and fast HARQ mechanism [34].

MC-DS-CDMA, possessing both the advantages of the orthogonal frequency division multiplexing (OFDM) and spreading spectrum systems, has shown great potential for the next generation wireless communication systems [35–38]. The advantages of the MC-DS-CDMA system includes the robustness against the frequency-selective fading channel, the flexibility in system design, and the low detection complexity [39–42]. In general, MC-DS-CDMA can be divided into three categories: multi-carrier CDMA with pure frequency spreading and MC-DS-CDMA with pure time spreading as well as joint time and frequency spreading (TF-domain spreading). By adjusting spreading gains in both time and frequency domains, MC-DS-CDMA with TF-domain spreading can outperform other two MC-DS-CDMA schemes in supporting versatile multi-rate services in diverse environments [43–46].

In the first part of this dissertation, we investigate the stall avoidance techniques to enhance the media access control (MAC) layer performance of a parallel multi-process stop-and-wait (SAW) hybrid automatic repeat request (HARQ) mechanism in HSDPA. In the second part of this dissertation, we analyze the error rate performance of uplink MC-DS-CDMA. Last, we propose a novel code assignment strategy and a joint subcarrier power allocation and code assignment scheme for the downlink case. In the following, we discuss the problems and the solutions regarding the RRM issues of HSDPA and MC-DS-CDMA, respectively.

1.1 Problem and Solution

In this section, we will first briefly discuss how to resolve the stall issue in HSDPA. Then, we expound several important issues in MC-DS-CDMA, including the influ-

ence of power control errors (PCEs) on top of MAI, code assignment strategy, and subcarrier power allocation.

1.1.1 Analysis of Stall Avoidance Mechanisms for HSDPA in the WCDMA Systems

The HSDPA for the WCDMA system adopts the mutli-process SAW HARQ mechanism to enhance channel utilization [47–52]. Nevertheless, the so-called stall problem of the multi-process SAW HARQ mechanism can be a bottleneck when delivering the MAC layer data to the upper layer, and can seriously degrade the quality of service (QoS) from the higher-layer user's perspective. Specifically, the stall issue is defined as the situation when the transmitter mistakenly believes that a particular packet has already successfully reached the destination, while the receiver is still waiting for that lost or damaged packet in the retransmission process. The stall issue usually occurs when the negative acknowledgement (NACK) control signal is changed to an acknowledgement (ACK) control packet due to transmission errors in the wireless link. In this case, the transmitter will never send this packet and will make the receiver wait for that lost packet forever. It has been reported that the probability of the NACK signal becoming the ACK signal can be as high as 10^{-2} for a high speed mobile during handoff [53,54]. Thus, resolving the stall problem is the key to reducing the transmission delay in wireless data networks [55].

The objective of our work in this part is to develop analytical methods to evaluate the performances of these three stall avoidance methods: the timer-based, the window-based, and the indicator-based schemes. To characterize the performances of the stall avoidance schemes, a new performance metric, called the gap processing time, is introduced. The gap processing time is defined as the duration starting when the sequence of MAC layer data have a gap due to a NACK-to-ACK error until the

receiver recognizes that this gap cannot be recovered by the MAC layer retransmission scheme. We derive the probability mass functions and the closed-form expressions for the average value of gap processing time of the three considered stall avoidance techniques. By simulations and analyses, we find that the indicator-based stall avoidance scheme significantly reduces the gap processing time compared to the timer-based and the window-based schemes. When applying these three stall avoidance schemes, the presented analytical approach can provide important information for determining a proper number of processes in the parallel SAW HARQ mechanism. It can also be used to design the allowable retransmissions for the timer-based and the window-based schemes. Furthermore, the number of acceptable fully loaded users can also be designed by the proposed analytical approach when the admission control and the gap processing time are jointly considered.

1.1.2 Analysis of a Stall Avoidance Mechanism with Scheduling for HSDPA in the WCDMA System

This part presents the closed-form expression for the gap processing time of the indicator-based stall avoidance mechanism in the multi-process SAW HARQ mechanism for multi-user case. The gap processing time is related to the MAC-layer scheduling policy. Currently, two scheduling policies are considered for the HSDPA system to allocate radio resource to multiple users: scheduling-by-bundle policy and interleaving scheduling policy [56, 57]. The former policy schedules each user by a series of time slots, while the later policy schedules time slots for multiple users one at a time. Therefore, with the scheduling-by-bundle policy, the gap in the reordering buffer can be detected earlier by consecutively receiving a series of packets. However, the scheduling-by-bundle policy does not exploit multiuser diversity gain. Thus, the interleaving scheduling policy is adopted more commonly in current systems since it

can exploit the multiuser diversity gain [27, 28]. We will focus on the interleaving scheduling policy to derive the analytical model for the gap processing time of the indicator-based stall avoidance mechanism. The relations between the gap processing time and some system parameters in the physical layer and the MAC layer, such as as packet error rates, the number of users and the number of parallel processes in the HARQ mechanism, can be investigated by the developed analytical model. Since the gap processing time affects the delay performance and quality of service significantly, the developed analytical approach can help evaluate the overall performance of the HSDPA system from the higher layer user's perspective, while considering the lower physical layer impact.

1.1.3 Effects of Power Control Errors and Complete Multiple Access Interference on Uplink MC-DS-CDMA

Although MC-DS-CDMA has been extensively studied recently [39, 58–61], to our knowledge, the effects of power control errors (PCE) on MC-DS-CDMA seem to be neglected. Improper power control may significantly degrade the performance of the MC-DS-CDMA system. The key question is how to quantitatively analyze the impact of power control errors on the MC-DS-CDMA system. Unlike most current papers in the subject of MC-DS-CDMA assuming perfect power control, the first goal of this work is to investigate the impact of open-loop power control errors on the MC-DS-CDMA systems. In general, power control schemes can be divided into two categories: the closed-loop power control and the open-loop power control. The former technique is to combat the small scale fading such as the Rayleigh fading caused by multipath propagation, while the latter one aims to resolve the near-far effect, owing to the large-scale fading caused by path loss and shadowing, in a multi-user CDMA system. Note

that with open-loop power control to overcome the near-far effect, each subcarrier may still experience severe multi-path fast fading.

The second objective of this work is to analyze the effect of the *complete* multiple access interference (MAI) on top of power control errors for the *multi-rate* MC-DS-CDMA system. To support various types of services in the 4G system, MC-DS-CDMA becomes an attractive technique because it can adapt transmission rates by dynamically changing time and frequency spreading factors. However, most analytical models for the MC-DS-CDMA system are mainly focused on the single rate case. In a multi-rate MC-DS-CDMA system, the MAI issue becomes more involved because the users with different transmission rates may cause different levels of the MAI. In addition, asynchronous transmissions among users is another critical performance issue. Asynchronous users may destroy the orthogonality between subcarriers in the MC-DS-CDMA system. To our knowledge, the effect of the complete MAI (i.e. the interference from the main subcarrier and all the adjacent subcarriers of other users) has not yet been fully investigated in the context of the multi-rate MC-DS-CDMA system. Hence, we are motivated to develop an analytical model to evaluate the effects of the complete MAI of asynchronous multi-rate users for the MC-DS-CDMA system.

In summary, we develop an analytical model to characterize the joint effects of both the PCE and the complete MAI for the multi-rate MC-DS-CDMA system. Applying the developed analytical model, we obtain some important insights into the performance issues of the MC-DS-CDMA system. First, when both PCE and the complete MAI are jointly considered, the effect of PCE can exacerbate the impact of complete MAI on MC-DS-CDMA, or vice versa. That is, the joint impact of complete MAI and PCE is actually severer than the summation of the performance degradation from the complete MAI and PCE individually. Second, increasing the maximum total spreading gain by either increasing frequency or time domain spreading gain

can enhance the error rate performance for the multi-rate MC-DS-CDMA system, but it is necessary to pay attention to the side effect of higher sensitivity to power control errors. Third, for the same total time and frequency spreading gain, an MC-DS-CDMA system with a larger frequency domain spreading factor outperforms the system with a larger time domain spreading factor. However, the performance differences between the two are shrunk as power control errors increase.

1.1.4 Interference Avoidance Code Assignment for Downlink MC-DS-CDMA

To enhance the capacity of the MC-DS-CDMA system, the spectrum is shared by users with distinct codes in either time domain or frequency domain. Figure 1.1 shows an example of an MC-DS-CDMA system with two-dimensional orthogonal variable spreading factor (OVSF) codes, where time- and frequency-domain spread gains are 8 and 4, respectively. In principle, the total spreading gain is equal to the product of the time domain spreading gain and the frequency domain spreading gain, and a combination of a time-domain code and a frequency-domain code is allocated to each user. Ideally, any two time-domain spreading codes without the ancestor and child relation in the OVSF code tree are orthogonal even with the same frequency-domain spreading code. Similarly, any two (even the same) time-domain spreading codes in two distinct frequency-domain code trees of Fig. 1.1 are orthogonal in regardless of the ancestor and child relation.

However, in a high-speed wireless system, the frequency selective fading impairs the orthogonality of spreading codes. Thus, to reduce the impact of frequency-selective fading on the orthogonality of time-domain spreading codes, the MC-DS-CDMA system adopts a serial-to-parallel process to convert a high speed data stream into multiple slower data streams. Thus, instead of frequency selective fading, it

is the flat Rayleigh fading that influences the data in each subchannel after time-domain spreading. Hence, in the downlink case, the orthogonality between time-domain spreading codes can be maintained and the multiple MAI of using the same frequency-domain spreading codes is eliminated. Nevertheless, frequency-selective fading can still affect the orthogonality of frequency-domain spreading codes. In a multi-rate MC-DS-CDMA system, the imperfect orthogonality of frequency-domain spread codes even cause different amplitudes of MAI due to various transmit power levels for supporting multi-rate services.

Accordingly, a challenging issue arises: how can an MC-DS-CDMA system effectively assign a combination of frequency- and time-domain spreading codes for multi-rate users to avoid different amplitudes of MAI in a frequency selective fading channel. Another important concern for code assignment is to sustain the compactness of the tree structure of the OVSF codes for improving the call blocking performance. In this work, we propose an interference avoidance code assignment strategy to consider both the MAI and call blocking performance simultaneously. The proposed interference avoidance code assignment strategy can reuse spreading codes in both the time and frequency domains to enhance capacity, while controlling the incurred MAI due to reusing the time-domain spreading codes. The key to the proposed interference avoidance code assignment scheme is the newly defined performance metric — the *MAI coefficient*, which can quantitatively predict the incurred MAI before assigning a particular code. By choosing a code with the minimum incurred MAI in the multi-rate multiuser MC-DS-CDMA system, the signal quality can be improved significantly. Furthermore, the proposed code assignment strategy sustains the compactness of the code tree structure, thereby achieving very good call blocking rate performance.

code tree for frequency-domain
spreading code [1, -1, -1, 1]

code tree for frequency-domain
spreading code [1, -1, 1, -1]

code tree for frequency-domain
spreading code [1, 1, -1, -1]

code tree for frequency-domain
spreading code [1, 1, 1, 1]

4th tree

3rd tree

2nd tree

1st tree

code domain with frequency-
domain spreading

code domain with time-
domain spreading
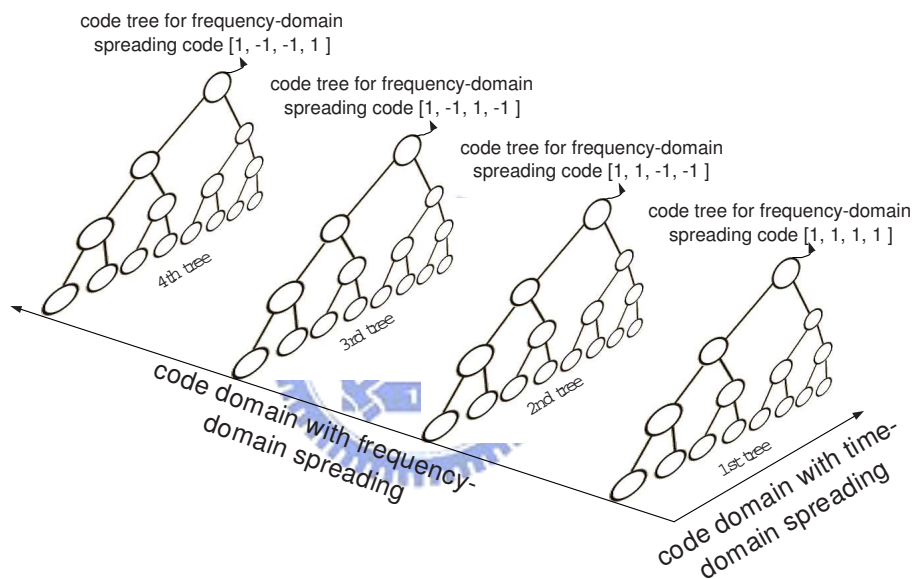
Fig. 1.1: A two dimensional OVSF code tree when the frequency-domain spreading factor is four.

1.1.5 Joint Interference Avoidance Code Assignment and Subcarrier Power Allocation for Downlink MC-DS-CDMA

In the multi-rate MC-DS-CDMA system with TF-domain spreading, subcarrier power is another degree of freedom. However, it is challenging to allocate subcarrier power in a multi-user environment. An optimal power allocation scheme with the maximized received signal power may also produce excessive interference to other users, which may also lower the call admission rate. Thus, we are motivated to propose a joint subcarrier power allocation and code assignment aiming to maximize the signal power through subcarrier power allocation while eliminating the MAI by a novel code assignment scheme. To achieve this goal, we first maximize the signal quality by allocating subcarrier power. On top of these allocated subcarrier power, we develop a code assignment strategy to maintain high call admission rates with less MAI. We define a new performance metric named as *MAI coefficient*. Through the bit error rate analysis associated with the subcarrier power allocation, we show that the MAI coefficient can quantitatively predict the incurred MAI before assigning a spreading code. Thus, with the help of MAI coefficient, an interference avoidance code assignment can be designed to choose a code with the minimum incurred MAI. The simulation results show that the proposed joint subcarrier power allocation and interference avoidance code assignment strategy can significantly improve the received signal quality. Furthermore, the code assignment considers the 2-dimension code tree structure in assigning a code to a user. Thus, the code assignment can also maintain good call admission rates.

1.2   Dissertation Outline

This dissertation consists of two themes. The first part is to investigate the performance issues of the fast HARQ mechanism in the MAC layer of HSDPA. The second part aims to investigate several RRM issues in MC-DS-CDMA. We analyze the joint effects of both the PCE and the complete MAI for the multi-rate MC-DS-CDMA system with TF-domain spreading for uplink transmission. For the downlink MC-DS-CDMA, we propose an interference code assignment strategy to eliminate the MAI, while maintaining a high call admission rate. Furthermore, a joint subcarrier power allocation and code assignment strategy is proposed to further enhance the performance of the MC-DS-CDMA system.

The remaining chapters of this dissertation are organized as follows. Chapter 2 reviews the some pivotal subjects for both HSDPA and MC-DS-CDMA, e.g., the multi-process SAW HARQ, stall issue and gap processing time for HSDPA and two-dimensional orthogonal variable spreading factor (OVSF) code tree structure for MC-DS-CDMA. Literature surveys of some related works are also provided. In Chapter 3, we develop an analytical model to evaluate the performances of three stall avoidance methods: the timer-based, the window-based, and the indicator-based schemes. Chapter 4 derives the closed-form expression for the gap processing time of the indicator-based stall avoidance mechanism for multi-user case. Chapter 5 analyzes the impact of PCEs and the complete MAI on the multi-rate MC-DS-CDMA system. In Chapter 6, we propose an interference avoidance code assignment strategy for the multi-rate MC-DS-CDMA system by reusing spreading codes in both the time and frequency domains. To further improve the received signal quality, a joint subcarrier power allocation and code assignment schemes is proposed in Chapter 7. At last, Chapter 8 provides the concluding remarks and some suggestions for future works.

Chapter 2

Background and Literature Survey

In this chapter, we survey related works to the stall issue of HSDPA and the performance analysis, the code assignment strategy, and the power allocation of MC-DS-CDMA. We also introduce the background for the multi-process SAW HARQ mechanism, the stall issue, and the gap processing time for HSDPA. Then, we review the power control mechanisms, the two-dimensional (2D) OVSF code tree structure, and the associated grip representation of the 2D-OVSF code tree.

2.1 HSDPA

2.1.1 Literature Survey

To resolve the stall issue for the multi-process SAW HARQ, there are two main research directions in the literature. The first direction is to improve the reliability of control packets by increasing the power of ACK or NACK signals [53]. The second direction is to design stall avoidance schemes to inform the receiver to stop waiting for the missing and nonrecoverable layer packets [55–57,63,64]. With a notice issued by a stall avoidance mechanism, the receiver starts forwarding all the received in-sequence packets to the upper layers even with a gap in a series of packets. As a result, the higher layer protocol stack can earlier request the transmitter to retransmit the missing packet. In [63], a timer-based stall avoidance mechanism was proposed to trigger a counter as soon as a gap appears in the HARQ reordering buffer. When the counter expires, the receiver starts forwarding received packets to the upper layer. In addition

to using a timer, a window-based stall avoidance mechanism in [64] utilized a sliding window to detect the stall situation earlier than the expiration of the timer. Recently in [55–57], the indicator-based stall avoidance mechanism applied the new data indicator (NDI) to monitor the activity of each HARQ process, thereby enhancing the capability to recognize the stall situation in sending the MAC layer data to the higher protocol layer. The basic principles of the indicator-based stall avoidance mechanism can be briefly introduced as follows. As long as all the HARQ processes are transmitting some other packets, instead of the expected missing packet, it is implied that the missing packet will not be retransmitted by the sender. Thus the receiver activates the process of forwarding data to the upper layer even before the timer expires or the window-based mechanism takes any actions. The performances of the above stall avoidance mechanisms were evaluated by extensive simulations in [34, 65, 66]. It was shown that a good cooperation between the radio link control (RLC) and MAC layers can reduce the peer-to-peer service data unit delay.

2.1.2 Multi-Process SAW HARQ Mechanism

The multi-process SAW HARQ mechanism is one of key techniques to provide the HSDPA service in the WCDMA system [19]. The basic idea of the multi-process SAW HARQ mechanism is to implement multiple parallel processes to fully utilize channel capacity, i.e. realize the so-called "keeping the pipe full" concept. Fig. 2.1(a) illustrates a dual-process SAW HARQ device consisting of an even process and an odd process to service one user [67]. As shown in Fig. 2.1(b), while the even process is waiting for the acknowledgement of packet 0 from the receiver, the odd process starts sending packet 1. With two processes sending data alternatively, the dual-process SAW HARQ mechanism can utilize the channel capacity more effectively and achieve higher throughput. In general, the required number of parallel processesc (N_p) to

fully utilize the channel capacity can be approximated by $N_p = RTT/TTI$, where RTT is the round trip time and the time transmission interval (TTI) indicates how often data arrives from higher layer to the physical layer.

Fig. 2.2 shows a scenario where a dual-process SAW HARQ device is serving multiple users. All the pairs of the source and destination devices share one downlink data channel. Thus, in the multi-user case, a system scheduler is responsible for selecting a particular customer to possess the right of using the shared channel.

2.1.3   The Stall Issue in Parallel SAW HARQ

The stall of delivering the MAC layer data to the upper layer is an important issue when providing real-time services (such as the streaming video or music) in the wireless channel. The stall issue is the dilemma for the receiver waiting for a missing packet that will no longer be sent by the transmitter. Fig. 2.3 shows an example of the stall issue in a dual-process SAW HARQ mechanism. In the figure, a NACK-to-ACK error occurs when the first receive process sends a NACK signal for the lost packet 0 in the feedback channel. In this situation, the first transmit process starts sending packet 4 because it mistakenly believes that packet 0 has already successfully reached the destination. Clearly packet 0 will never be sent again, but the first receive process will continue waiting for packet 0. As a result, delivering MAC layer data to the upper layer is stalled, thereby degrading higher layer QoS performance for the delay-sensitive services.

2.1.4   Gap Processing Time

In this dissertation, the gap processing time is used as a performance measure to quantify the impact of the stall issue on the multi-process SAW HARQ mechanism. Here a *gap* means an idle space reserved for a lost packet in the reordering buffer of

(a) Structure
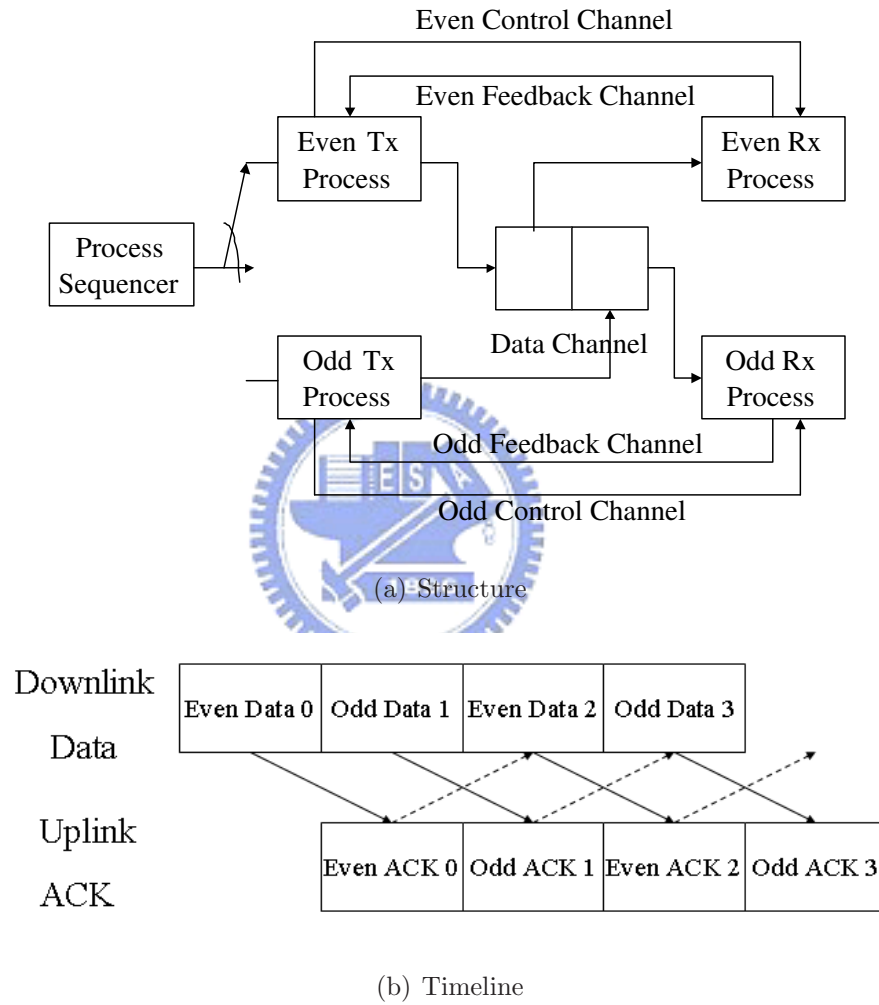
(b) Timeline

Fig. 2.1: The structure and timeline of the dual-process SAW H-ARQ mechanism.
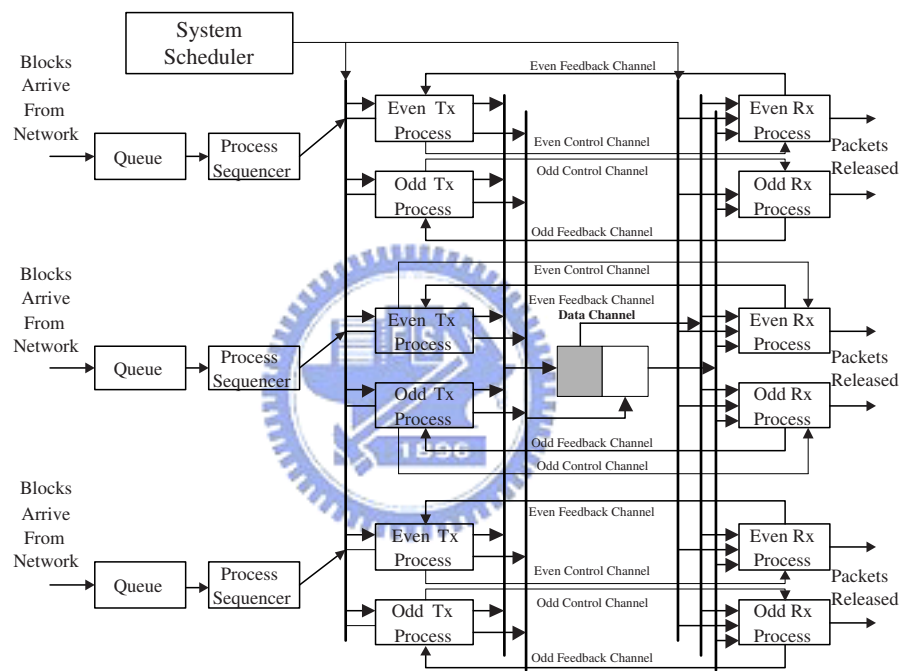
Fig. 2.2: The dual-process SAW HARQ mechanism with multiple users.
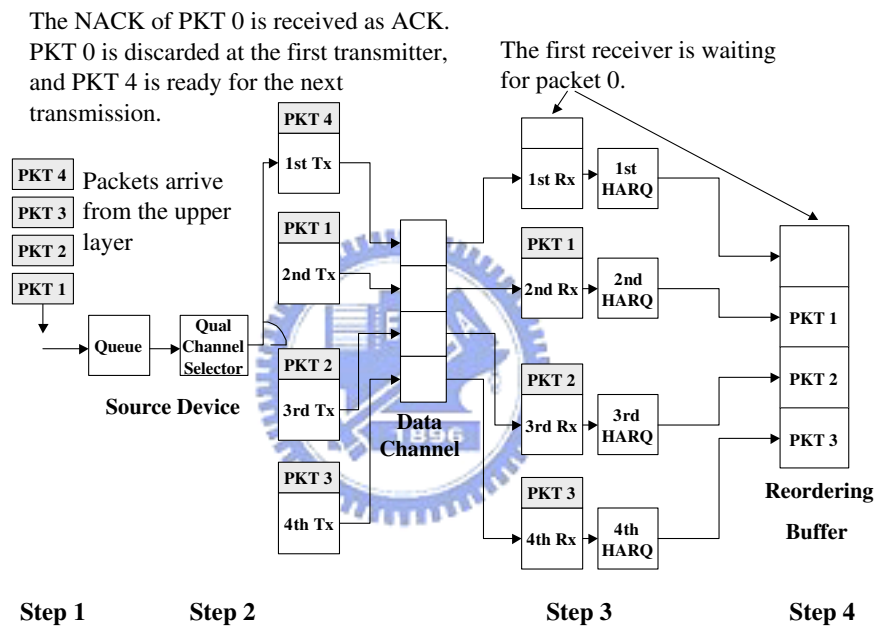
Fig. 2.3: A example of the stall issue in a qual-process SAW H-ARQ, where packet 0 is lost and packets 1, 2, and 3 are successfully received in the reordering buffer.

the receiver. Two types of gaps can be categorized in HSDPA: *Type-I gap* and *Type-II gap*. If it is still possibly recovered in future retransmissions, we call this type of gap the *Type-I gap*. In contrast, *Type-II gap* is the one that will never be sent again by the transmitter due to a NACK-to-ACK error. Whenever a Type-II gap appears in the reordering buffer, the process of sending packets to the upper layer is stalled.

The *gap processing time* is defined as the duration when a gap appears in the reordering buffer until the receiver confirms that it belongs to a Type-II gap. An HARQ process usually cannot easily distinguish a Type-II gap from a Type-I gap. Thus, a stall avoidance mechanism is required to detect the occurrence of the Type-II gap for the HSDPA system, and then to trigger the receiver to flush out the available packets in the reordering buffer to the upper RLC layer as well as this Type-II gap must be flushed out to the RLC layer. Next an RLC retransmission request is initiated for the missing Type-II gap [56, 57, 65].

2.2 MC-DS-CDMA

2.2.1 Literature Survey

Performance Analysis: In the literature, the studies on the performance of the MC-DS-CDMA system subject to power control errors and MAI can be summarized in two folds. On the one hand, from the standpoint of MAI, the authors in [68] analyzed the MAI's effect from the main subcarrier for a single-rate MC-DS-CDMA system. In [69], the authors analyzed the effect of the other inter-subcarriers' MAI in the MC-DS-CDMA system, but only for the single-rate case. The authors in [70] only analyzed the performance of the multi-rate multi-carrier DS-CDMA systems, but considered the effect of the MAI from the main subcarrier. On the other hand, from the view point of power control errors, most studies for the MC-DS-CDMA systems

were performed with the assumption of perfect power control [68–70]. Although power control has been extensively studied for the single-carrier DS-CDMA system in the literature [9, 71–74], extending these results from the single-carrier case to the multi-carrier case is a non-trivial task because the effect of power control errors in an MC-DS-CDMA system has to be jointly evaluated with the complete MAI from all inter-subcarriers.

Code Assignment and Power Allocation: In the literature, most code assignment techniques in the single carrier CDMA system were proposed without considering the impact of MAI. In [16, 75, 76], code assignment techniques were investigated with an aim to keep the code tree compact for the purpose of reducing the call blocking rate and the code reassignments in the single carrier CDMA system with OVSF codes. To eliminate asynchronous MAI in asynchronous MC-DS-CDMA, the interference-rejection and interference-free spreading codes were proposed in [77] and [78], respectively. In [79, 80], the authors proposed a code assignment strategy based on the dual quasi-orthogonal and Walsh codes to reduce the MAI in the MC-DS-CDMA systems. In [81], an MAI-minimized signature waveforms was proposed to minimize the MAI for the MC-DS-CDMA systems. To improve the signal quality, some subcarrier power allocation schemes aiming at improving the bit error rate performance have been proposed. In [82], the subcarrier power allocation was considered in a non-spread spectrum multi-carrier system. In [83], the authors proposed an adaptive subcarrier allocation policy for the frequency-hopping MC-DS-CDMA systems to avoid collision between users when loading bit to subcarriers. In the above MC-DS-CDMA systems, [77–81] all belong to MC-DS-CDMA with one-dimensional time-domain spreading.

For the MC-DS-CDMA system with time- and frequency-domain spreading, the authors in [45] proposed a novel two-dimension OVSF codes but ignore the impact

of frequency selective diversity. Furthermore, the MAI rejection property in [45] may not be applicable when the subcarriers carrying the same data bit experience independent fading channels because the zero autocorrelation sidelobes and the zero cross-correlation functions are no longer true as .

In this part of dissertation, we consider a downlink MC-DS-CDMA system with a constant frequency diversity gain. Furthermore, we investigate the MAI impact caused by reusing time-domain spreading codes in the MC-DS-CDMA, which is not considered in [45, 77–81].

2.2.2 Power Control Mechanism

In general, we can categorize power control schemes into two kinds. The first one is the open-loop power control (OLPC) and the other one is the closed-loop power control (CLPC). With open-loop power control, a mobile terminal decides its own transmission power by calculating the difference between the desired SIR and the target SIR. The goal of the open-loop power control is usually to compensate path loss and shadowing.

On the other hand, the CLPC scheme makes the base station determine the transmission power of the mobile terminal in the uplink case. After comparing the received SIR with the target SIR, the CLPC scheme issues either a "power up" or a "power down" command to the transmitter. After receiving this up/down power control command, the corresponding transmitter adjusts its transmission power accordingly. The block diagram of the CLPC scheme is shown in Fig. 2.4. In the figure, the CLPC has two feedback loops. The inner loop is to remove Rayleigh fading through fast power adjustment, while the outer loop is to set the target E_b/N_o for the inner loop power control.
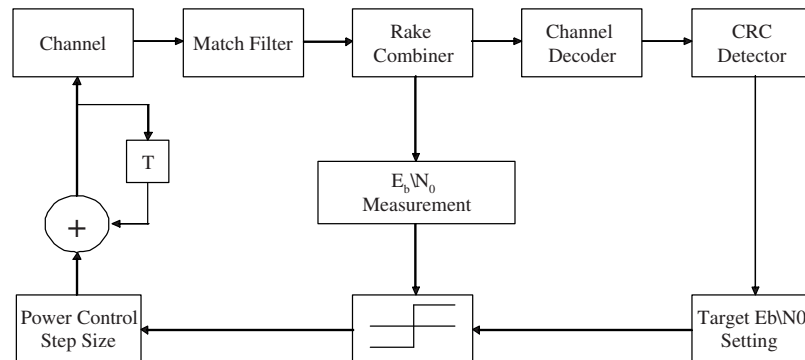
Fig. 2.4: The block diagram of the closed-loop power control scheme.

2.2.3 Two-Dimensional OVSF Code Tree

In the multi-rate MC-DS-CDMA system with TF-domain spreading, the orthogonal variable spreading factor (OVSF) code tree has a two-dimensional structure, as shown in Fig. 1.1. The OVSF codes have been used as the channelization codes in the universal mobile telecommunication services (UMTS) terrestrial radio access (UTRA) wide-band CDMA system [84]. The advantages of the OVSF codes include good cross-correlation and the flexibility of changing code length. In Fig. 1.1, the frequency-domain spreading factor is four and the time-domain spreading factor ranged 1 to 8 depending on the requested data rates by users. The OVSF spreading code in either time domain or frequency domain can be constructed according to the rules shown in Fig. 2.5, where $C_{S,n}$ denotes the n-th code in a code group with spreading gain S. On a layer of the OVSF code tree with spreading factor S, there are S mutually orthogonal codes. Any two codes on the different layers of the code tree are orthogonal if they do not have the ancestor-descendant relationship. In principle, different spreading factors, S correspond to different transmission rates. For example, the lowest data rate in Fig. 2.5 is associated with codes $C_{8,m}$ ($m = 1 \sim 8$). Then, a

code $C_{4,m}$ ($m = 1 \sim 4$) has two times higher data rates than $C_{8,m}$.

Now we discuss the orthogonality of the codes in the two dimension OVSF code tree. To easy the illustration, we spread the 2D code tree in Fig. 1.1 onto a plane as in Fig. 2.6. In the two-dimension OVSF code tree shown in Fig. 1.1, the total spreading factor is equal to $SF_f \times SF_t$, where $SF_f = 4$ is the frequency domain spreading factor and $SF_t = 1 \sim 8$ is the time-domain spreading code, respectively. Thus, an OVSF code tree with the maximum spreading factor of 8 is copied four times for each associated frequency-domain spreading code. Denote $C_{2^{l-1},n}^{(i)}$ ($n = 1, \ldots, 2^{(l-1)}$) the n-th code of the code group in the l-th layer associated with the i-th code tree, where the time-domain spreading factor $SF_t = 1 \sim 2^{(l-1)}$ from the top layer ($l = 1$) to the bottom layer ($l = 4$) of the OVSF code tree. Ideally, any two codes in two frequency-domain code trees are orthogonal thanks to the orthogonal frequency domain spreading codes. However, due to the frequency selective fading, this condition may no longer be true. We call two codes in the two dimensional OVSF code tree are *related codes* if they have ancestor-descendant relationship in the time domain. For example, $C_{4,1}^{(1)}=$[1 1 1 1] and $C_{8,1}^{(2)}=$[1 1 1 1 1 1 1 1]) are related codes, where $C_{4,1}^{(1)}$ and $C_{8,1}^{(2)}$ are associated with the frequency-domain spreading codes [1 1 1 1] and [1 1 -1 -1], respectively. Note that $C_{4,1}^{(1)}$ will interfere $C_{8,1}^{(2)}$ and vice versa.

2.2.4 Grid Representation of a 2-D Code Tree

For the sake of clearly illustrating and easily managing the code resources, we introduce a simple graphical *grid representation* of a 2D code tree in the MC-DS-CDMA with TF-domain spreading. In this grid representation, the codes with variant transmission rates are represented by a set of rectangles with different areas. The area of each rectangle is proportional to the transmission rate of the corresponding code channel (or inversely proportional to SF_t). A set of equal-sized rectangles construct
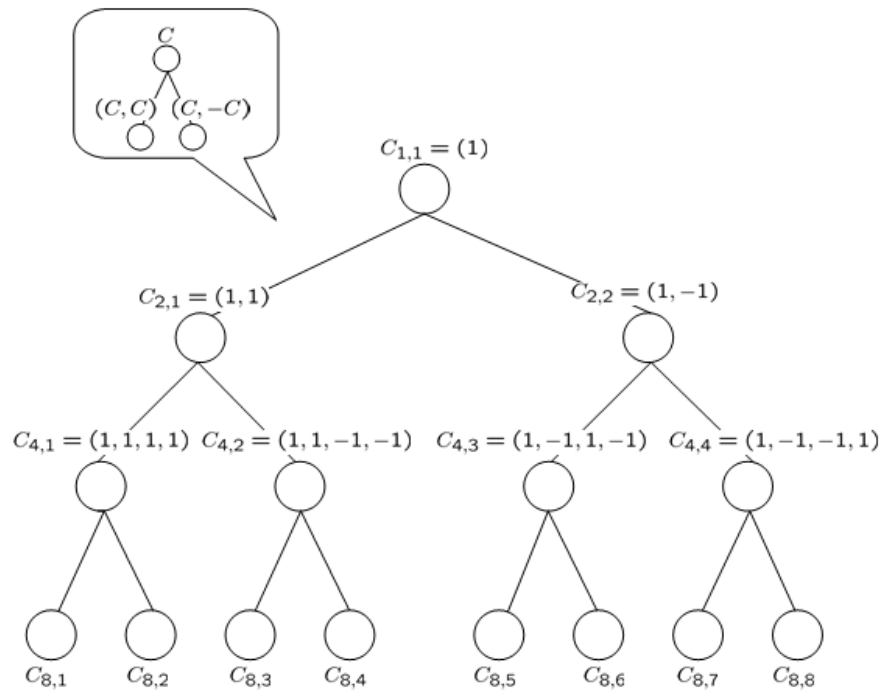
Fig. 2.5: An one dimensional OVSF code tree.

a block to present the code resources at each layer of the 2D code tree shown in Fig. 2.6. For the 2D code tree of Fig 2.6 with some allocated codes, the corresponding grid representation of available codes is shown in Fig. 2.7. In Figs. 2.6 and 2.7, "● (■)" and "● (■)" stand for the "used code" and "candidate code" for a requested code of $SF_t = 8$, respectively. As shown in Fig. 2.7, the code channels with $SF_t = 2$ at layer two are represented by a set of the largest equal-sized rectangles while code channels with $SF_t = 8$ at layer four are represented by the smallest equal-sized rectangles, each of which is sized up to one quarter of the size of a rectangle with $SF_t = 2$. At the bottom of Fig. 2.7, an aggregate of the blocks of layer 2∼4 summarizes the total used and free code resources. Now, with the aid of the grip representation, we can clearly define the related codes as:

$$Related\ Codes \equiv The\ used\ codes\ positioned\ in\ the\ same\ column\ of\ the\ grip\ representation\ .$$

$$(2.1)$$

For example, $\{C_{8,8}^{(1)}, C_{2,2}^{(2)}, C_{2,2}^{(3)}, C_{8,8}^{(4)}\}$ seated in the most right column is a set of related codes. Note that codes belong to the same set of related codes can interfere with each other.
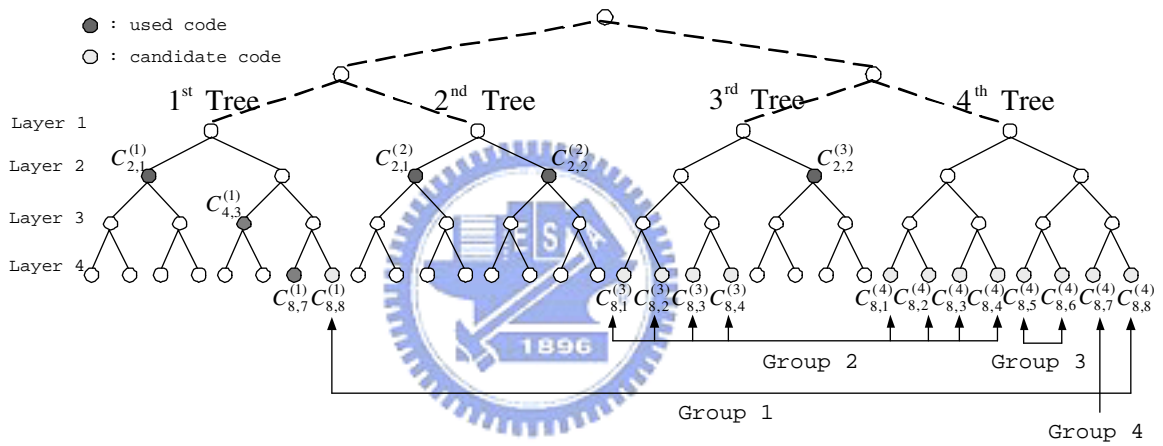
Fig. 2.6: An illustrating example of allocating a code with frequency-domain spreading factor $M = 4$ and time-domain spreading factor $SF = 8$ in the 2D code tree.
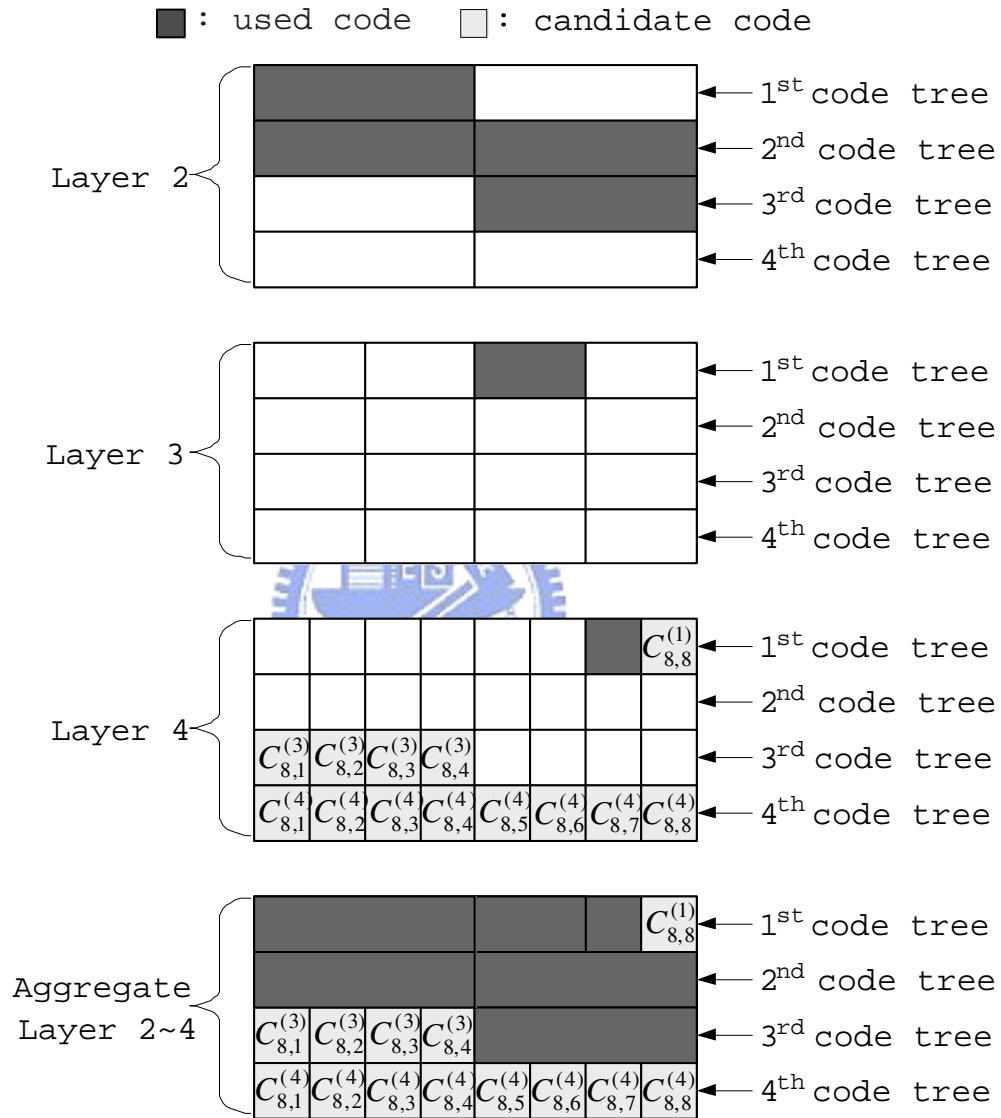
Fig. 2.7: The grid representation of Fig. 2.6 for the code resources in the MC-DS-CDMA system with time and frequency domain spreading.

Chapter 3

Analysis of Stall Avoidance Mechanisms for HSDPA in the WCDMA System

In this chapter, we study the stall issue in the parallel multi-channel stop-and-wait (SAW) hybrid automatic repeat request (HARQ) mechanism adopted in the high speed down-link packet access (HSDPA) of the wideband code division multiple access (WCDMA) system. The stall issue, resulted from the error of the negative acknowledgement (NACK) changing to the acknowledgement (ACK) in the control channel, is defined as the dilemma for the receiver waiting for a missing packet that will no longer be sent by the transmitter. In the stall situation, the receiver stops delivering the medium access control (MAC) layer packets to the upper layer. The stall issue seriously degrades the quality of service for the high speed mobile terminal owing to the high probability of NACK-to-ACK errors. The goal of this chapter is to develop an analytical model to evaluate the three stall avoidance mechanisms: the timer-based, the window-based, and the indicator-based stall avoidance schemes. To this end, we first propose a new performance metric — gap processing time, which is defined as the duration for a nonrecoverable gap appearing in the MAC layer reordering buffer until it is recognized. Second, we derive the probability mass functions and the closed-form expressions for the average gap processing time of these three stall avoidance schemes.

3.1 The Stall Avoidance Schemes

Because a NACK control signal may be corrupted during transmissions in a wireless channel, many stall avoidance schemes are proposed to prevent a receiver from waiting for a missing packet due to a NACK-to-ACK error. Not only can the stall avoidance schemes detect the Type-II gap, but also forward the already received packets at the MAC layer to the upper layer before triggering the RLC retransmission. Thus, compared to the purely RLC retransmission, the RLC transmission with the stall avoidance mechanism can expedite the delivery of the data by avoiding retransmitting the already received packets. In this section, we discuss three current stall avoidance schemes, the timer-based [63], the window-based [64], and the indicator-based schemes [55–57].

3.1.1 Timer-Based Scheme

The basic principles of the timer-based method in [63] are described as follows:

1. A timer is triggered when either a Type-I gap or a Type-II gap appears in the reordering buffer of the receiver.

2. As the timer expires, the receiver stops waiting for the lost packet and judge that the lost packet belongs to a Type-II gap.

3. The timer is reset if the missing packet is successfully retransmitted before the timer expires.

   Figure 3.1 illustrates the operation principles of the timer-based stall avoidance scheme. When packet 2 successfully arrives at the receiver, it is aware that packets 0 and 1 are missing and thus a timer is triggered. Note that only one timer is triggered

A timer is started for the first two continuous gaps

gap	gap	2

Because of receiving packet 2, the receiver becomes aware that packets 0 and 1 are lost. Only one timer is started.

gap	gap	2	3	4	gap	6	gap	8

When the first timer expires, the reordering buffer will discard the first two gaps and deliver packets 2, 3, and 4 to the upper layer.

gap	6	gap	8

After delivering packets 2, 3, and 4, a new timer is started for the gaps of packets 5 and 7.

Fig. 3.1: An example of the timer-based stall avoidance scheme.

for the consecutive gaps. Assume that packets 3, 4, 6 and 8 reach the receiver, but packets 5 and 7 are damaged. Based on the timer-bases stall avoidance scheme, a new timer will not be initiated for additional gaps until the previous timer expires. Thus, in this example, only after the timer set for packets 0 and 1 expires, a new timer will be set for the missing packets 5 and 7. After that, the receiver sends packets $2 \sim 4$ to the upper layer and requests for retransmitting packets 0 and 1 in the RLC layer.

3.1.2 Window-Based Scheme

In [64], the window-based method was suggested to detect Type-II gaps in the reordering queue on top of the timer-based scheme. To explain the operation of the window-based stall avoidance scheme, we define the *detection window*. The detection window means a set of packets that are expected to arrive at the receiver. The de-

tection window functions as a sliding window protocol. If a gap occurs, the detection window is initiated and two possible scenarios follow. For a Type-I gap, the detection window will shrink from the trailing edge after the gap is filled. For a Type-II gap, however, the trailing edge of the detection window is halted. Thus, the detection window expands from the leading edge when other subsequent packets arrive. In the long run, a pre-determined maximum threshold of the detection window size will be reached.

A fully-booked detection window means that all available slots/seats in the reordering buffer have been taken. The detection window size is usually designed large enough to guarantee a successful retransmission. Thus, the gaps halting the trailing edge of a fully booked detection window usually belong to Type-II gaps. As a consequence, when a new packet arrives and the detection window is fully booked, the window-based stall avoidance scheme forwards Type-II gaps and subsequent received in-sequence packets in the reorder buffer to the upper layer in regardless of timer expiration.

Figure 3.2 shows an example to illustrate the operation principles of the window-based stall avoidance scheme. Consider a detection window with a size of seven, which currently contains packets 2, 3, 4, and 6 and the gaps for missing packets 0, 1, and 5. Suppose that packets 0, 1, and 5 are Type-II gaps and new packets 7 and 8 arrive at this moment. Since the detection window is already *fully-booked* and its trailing edge is halted by packets 0 and 1, the window-based stall avoidance scheme can recognize that packets 0 and 1 are Type-II gaps. Accordingly, the receiver forwards packets 2, 3, 4 together with gaps of packets 0 and 1 to the upper layer. Now the detection window size becomes two and its trailing edge slides until the gap for packet 5. With more space available in the reordering buffer, packets 7 and 8 are accommodated and the detection window is reserved for packets 5 to 8.
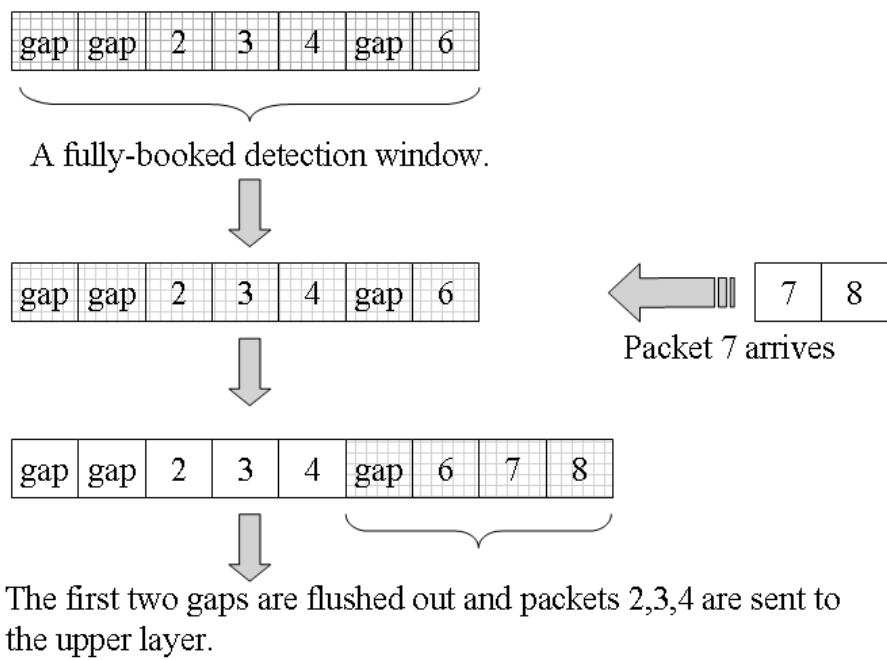
Fig. 3.2: An example of the window-based stall avoidance scheme with the detection window size equal to seven.

3.1.3   Indicator-Based Scheme

In [55–57], a new stall avoidance scheme is proposed by taking advantage of the new data indicator (NDI). The NDI (just a one-bit tag) is associated with every packet and is transmitted in the high speed downlink control channel [85]. The NDI is toggled for a new transmitted packet, but is not changed for a retransmitted old packet. By checking the NDI in the control channel and the transmission sequence number (TSN) in the traffic channel for each packet, the indicator-based stall avoidance scheme can determine whether the missing packet will be transmitted or not. If all HARQ processes are transmitting new packets or other old packets except for the expected missing packet, then this gap in the reordering buffer can be judged to be a Type-II gap.

Table 3.1 illustrates the status of a 4-process SAW HARQ mechanism for a particular user in two cycles. The cycle duration is defined as the sum of the transmission time interval (TTIs) with all different parallel processes transmitting one packet, e.g. the cycle duration is 4 TTIs in this case. The field in the table is filled with a triplet variable (TSN, S_c, NDI). Here $S_c \in \{ACK, NACK, \text{and } N{\rightarrow}A\}$ denotes one of the three events: "receiving an ACK", "receiving a $NACK$", and having a NACK-to-ACK error, respectively. The status NEW or OLD in the field NDI is equivalent to that the NDI is *changed* for a *new* packet or is *unchanged* for a retransmitted *old* packet, respectively. An empty field implies that this time slot is idle or assigned to other users. Assume that the target user requests to transmit five packets with TSN $= 0 \sim 4$ from the RLC layer. The functions of the indicator-based stall avoidance scheme associated with Table 3.1 are explained as follows:

1. In cycle 1, the four parallel processes transmit packets 0 to 3, respectively. Assume that packet 3 passes the cyclic redundancy check (CRC), but packets $0 \sim 2$ fail. In the feedback channel, suppose that a NACK-to-ACK error occurs

Tab. 3.1: An example of the statuses in a 4-process SAW HARQ mechanism for a Type-II gap being detected by receiving new packets in three processes and old packet in one process.

| Cycle | Process ID in 4-process SAW HARQ | | | |
| | Process 1 | Process 2 | Process 3 | Process 4 |
	(TSN,S_c,NDI)	(TSN,S_c,NDI)	(TSN,S_c,NDI)	(TSN,S_c,NDI)
1	(0,N→A,NEW)	(1,NACK,NEW)	(2,NACK,NEW)	(3,ACK,NEW)
2	(4,ACK,NEW)	(1,ACK,OLD)	(2,ACK,OLD)	

in process 1, and processes 2 and 3 successfully receive NACK for packets 1 and 2. The reordering buffer currently contains packet 3 together with the three gaps of packets $0 \sim 2$. At this moment, processes 1, 2, and 3 assume that the missing packets $0 \sim 2$ will be retransmitted, but are unsure which packet will be received. The stall avoidance scheme starts monitoring the statuses of processes 1, 2, and 3 to check whether these gaps belong to Type-II gaps.

2. In cycle 2, processes 1, 2, and 3 receive a new packet 4, and old packets 1 and 2, respectively. Now the holes of packets 1 and 2 in the reordering buffer are filled. Since the NDI statuses of processes 1 and 4 are NEW and the TSNs of processes 2 and 3 indicate that packets 1 and 2 are received, the subsequent packets arriving at the receiver will have TSNs higher than 4. Thus, no process is responsible for sending the missing packet 0. Consequently, it can be confirmed that the gap of packet 0 is a Type-II gap. Hence, the available in-sequence packets $1 \sim 4$ are forwarded to the upper layer together with packet 0.

3.2 Performance Measure and System Assumptions

3.2.1 Gap Processing Time

To measure the performance of the stall avoidance schemes, we define a new performance measure – *gap processing time (GPT)*. It is the duration from the occurrence of a Type II gap until a stall avoidance scheme recognizes the existence of nonrecoverable gaps. The gap processing time is an important performance metric to evaluate the quality of service (QoS) for HSDPA. On the one hand, when the gap processing time is shorter than the RLC timeout, with the help of the stall avoidance scheme an

RLC retransmission can be initiated sooner when the Type-II gap is detected. This is especially important for the delay sensitive services. On the other hand, without the help of the stall avoidance scheme, the excessive gap processing time may be longer than the RLC timeout. When a packet is sent out, an RLC timer is started at the transmitter. If the acknowledgement is not received correctly before the RLC timer is expired, the transmitter sends the packet again. When a Type-II gap halts the received packets at the MAC layer to be delivered to the RLC layer and the excessive gap processing time is longer than the RLC timeout, the so called "spurious" RLC retransmission occurs. In this situation, the RLC timeout triggers the retransmission of some already received packets, which are halted at the MAC layer due to an unrecoverable Type-II gap. Therefore, the analysis of gap processing time offered in the paper can be helpful in setting an appropriate value of the RLC timeout from a viewpoint of the receiver's MAC layer performance.

Although the probability of the NACK-to-ACK error is 0.01 [53, 54], the high allowable packet error rate in the MAC layer of HSDPA can still lead to serious stall problems. To boost the transmission rate, the packet error rate of the first transmission can be higher than 40% because a high level modulation and coding scheme is adopted [65]. For example, when the probability of a NACK-to-ACK error is equal to 0.01, average packet error rate is equal to 0.3, and the transmission time interval of 2 milli-seconds, the stall problem occurs 7.5 ($5/0.002 \times 0.3 \times 0.01$) times within five seconds. Thus, the impact of the NACK-to-ACK error cannot be ignored, especially for supporting delay sensitive services.

The stall problem affects the performance of the parallel HARQ mechanism in two folds. From the goodput aspect, the end-to-end goodput from the receiver's upper-layer viewpoint can be seriously degraded due to the long gap processing time. From the delay aspect, the end-to-end data delivery delay can also become longer due to the gap processing time. Referring to the analytical model in [86], the packet

delivery delay (denoted by T_d) in the third-generation (3G) WCDMA with transport control protocol (TCP) can be decomposed as

$$T_d = Q_d + R_d + N_d \ , \tag{3.1}$$

where Q_d, R_d, and N_d are the queuing delay, reordering delay, and the wireline network delay, respectively. However, the packet delivery delay of (3.1) does not consider the effect of NACK-to-ACK errors. To incorporate the effect of NACK-to-ACK errors into packet delivery delay, T_d can be modified as

$$T_d = Q_d + R_d + N_d + GPT \ . \tag{3.2}$$

Note that the reordering delay R_d is caused by Type-I gaps while the GPT is caused by Type-II gaps. Clearly, a longer period of gap processing time causes longer packet delay because Type-II gaps halt the procedure of forwarding the received packets to the upper layer.

A longer period of gap processing time also results in more accumulated packets in the MAC layer. As a result, the overflow probability of the reordering buffer is increased. Moreover, as more received packets are forwarded to the RLC layer due to longer gap processing time, a larger buffer in the RLC layer is required to accommodate these packets. With large enough buffers of both MAC and RLC layers, the received packets can be accommodated in the receiver. In this chapter, we focus on the analysis of the gap processing time for the three stall avoidance schemes. Gap processing time is influenced by the physical layer parameters, such as packet error rate (P_e) and the probability of a NACK becoming an ACK ($P_{N \rightarrow A}$), and the MAC layer parameters, e.g. the size of the reordering buffer and the number of processes in the parallel SAW HARQ mechanisms.

3.2.2 Assumptions

Being a function of both physical layer and MAC layer parameters, gap processing time is difficult to be computed analytically. To make the analysis tractable, we make the following assumptions:

1. Because a NACK-to-ACK error usually occurs when a mobile terminal moves at high speeds, it is assumed that the fast changing channel is modelled by an independent Rayleigh fading channel from one packet to another packet.

2. All packets are assumed to have the same priority.

3. All transmit processes in the HARQ mechanism always have packets ready for transmission.

4. Effects of incremental redundancy and Chase combining are not considered. The provided analysis in this chapter can be viewed as the worst-case analysis.

5. Assume the modulation and coding scheme and the packet length are not changed during the period of the gap processing time.

6. The feedback delay is not taken into account of the gap processing time.

3.3 Analysis of Timer-Based Stall Avoidance Scheme

In Proposition 1, we derive the average gap processing time for the timer-based stall avoidance scheme.

Proposition 1: *Denote P_s and $P_{N \to A}$ the probability of a packet being successfully received and that of having a NACK-to-ACK error, respectively. Then the*

probability with a Type-II gap (denoted by P_G) is equal to

$$P_G = (1 - P_s)P_{N \to A} \; . \tag{3.3}$$

Let D be the expiry time of the timer normalized to the transmission time interval (TTI). In terms of P_G and P_s and D, the average gap processing time for the timer-based stall avoidance scheme normalized to TTIs (denoted by $\overline{GPT}_{timer}$) in the single user case can be expressed as

$$\overline{GPT}_{timer} = \sum_{\ell=0}^{D} \overline{GPT}(\ell) \; , \tag{3.4}$$

where the average gap processing time with ℓ Type-II gaps (denoted by $\overline{GPT}(\ell)$) is

$$\overline{GPT}(\ell) = \begin{cases} (1 - P_G)^D [D + \sum\limits_{i=1}^{\infty} i(1 - P_s)^{i-1} P_s] & , \quad \ell = 0 \;\; ; \\ P_G^\ell (1 - P_G)^{D-\ell} \sum\limits_{t_1=1}^{D-\ell+1} \sum\limits_{t_2=t_1+1}^{D-\ell+2} \cdots \sum\limits_{t_\ell=t_{\ell-1}+1}^{D} \sum\limits_{j=1}^{\ell} \dfrac{2D - t_j}{\ell} & , \quad \ell = 1, \cdots, D \; , \end{cases} \tag{3.5}$$

and t_j is defined as the elapsed time of the previous timer until the end of gap j ($j = 1, \cdots, \ell$).

    Proof: Assume that a timer is already initiated for a certain gap. We consider the following two scenarios:

(I) <u>No new Type-II gap occurs in a period of D, $\ell = 0$:</u>

    Referring to Figure 3.3(a), let gap 0 occur after the previous timer expires. Suppose that i TTIs later a packet PKT^* with a higher TSN than gap 0's is successfully received. Then, a new timer is then initiated for gap 0. In this case, the gap processing time of gap 0 is i plus the expiration time of the timer D. Now, we approximate the probability of receiving PKT^* after i TTIs by $(1 - P_s)^{i-1} P_s$. Note that the successful received PKT^* may not always have a TSN higher than that of gap 0. Because the probability of not having new Type-II gap within D TTIs is
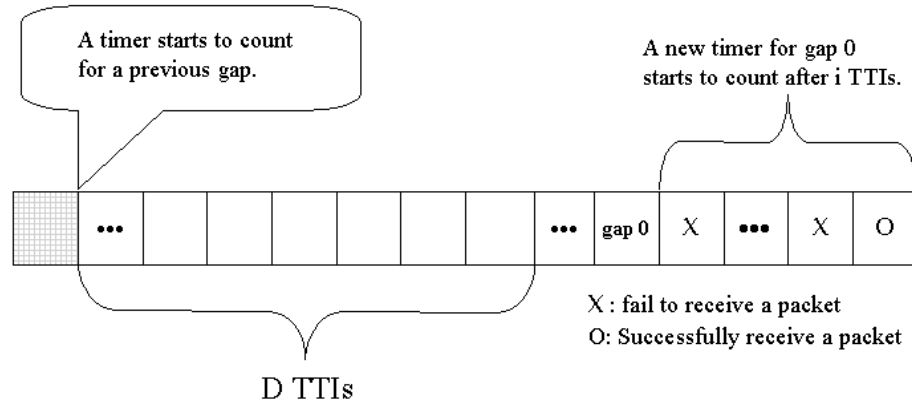
(a) No new Type-II gap occurs before the timer expires for a previous gap.
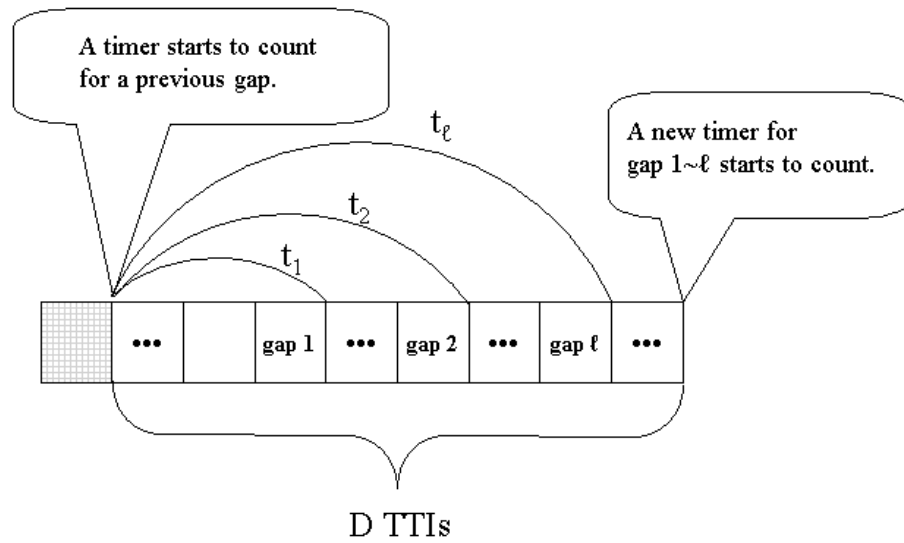
(b) Some new Type-II gaps occur before the timer expires for a previous gap.

Fig. 3.3: Two scenarios for the timer-based stall avoidance scheme to remove a Type-II gap.

$(1 - P_G)^D$, the probability mass function (pmf) for the gap processing time (GPT) equal to $D + i$ TTIs can be expressed as

$$P(GPT = i + D) = (1 - P_G)^D (1 - P_s)^{i-1} P_s \ . \tag{3.6}$$

The average gap processing time in the case of $l = 0$ can be computed as follows:

$$
\begin{aligned}
\overline{GPT}(0) &= \sum_{i=1}^{\infty} (i + D) P(GPT = i + D) \\
&= \left[D + \sum_{i=1}^{\infty} i (1 - P_s)^{i-1} P_s \right] (1 - P_G)^D \ .
\end{aligned}
\tag{3.7}
$$

Thus, the first part of Proposition 1 is proved.

(II) ℓ Type-II gaps occur before the timer expires, $\ell \neq 0$:

Assume that ℓ new Type-II gaps occur before the timer expires, as shown in Fig. 3.3(b). For gap j, $(j = 1, ..., \ell)$, a period of time $(D - t_j)$ is needed before its own timer starts. Recall that t_j is defined as the elapsed time of the previous timer until the end of gap j. In this case, the total gap processing time for gap j is equal to $(2D - t_j)$ and the probability of having ℓ Type-II gaps conditioned on known $t_1, \cdots, t_\ell$ is $P_G^\ell (1 - P_G)^{D-\ell}$. Note that the value of $P_G^\ell (1 - P_G)^{D-\ell}$ is small for $\ell \geq 2$ in real cases. Thus, we can approximate the exact gap processing time for the ℓ gaps by an average value over the ℓ gaps as

$$\overline{GPT}(\ell | t_1, \cdots, t_\ell) = \sum_{j=1}^{\ell} \frac{2D - t_j}{\ell} \ . \tag{3.8}$$

Then, the pmf of the gap processing time for having ℓ gaps conditioned on known $t_1, \cdots, t_\ell$ can be expressed as

$$P(GPT = \overline{GPT}(\ell | t_1, \cdots, t_\ell)) = P_G^\ell (1 - P_G)^{D-\ell} \ . \tag{3.9}$$

By considering all the possible occurrence time of ℓ Type-II gaps in D TTIs, we have

$$
\begin{aligned}
\overline{GPT}(\ell) &= \sum_{t_1=1}^{D-\ell+1} \sum_{t_2=t_1+1}^{D-\ell+2} \cdots \sum_{t_\ell=t_{\ell-1}+1}^{D} \sum_{j=1}^{\ell} \frac{2D-t_j}{\ell} \times P(GPT = \overline{GPT}(\ell|t_1,\cdots,t_\ell)) \\
&= P_G^\ell (1-P_G)^{D-\ell} \sum_{t_1=1}^{D-\ell+1} \sum_{t_2=t_1+1}^{D-\ell+2} \cdots \sum_{t_\ell=t_{\ell-1}+1}^{D} \sum_{j=1}^{\ell} \frac{2D-t_j}{\ell} \qquad (3.10)
\end{aligned}
$$

Hence, we prove the second part of Proposition 1.

∎

3.4   Analysis of Window-Based Stall Avoidance Scheme

Proposition 2, we derive the average gap processing time for the window-based stall avoidance scheme.
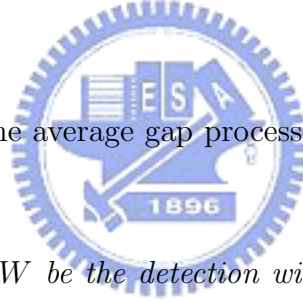
Proposition 2: *Let W be the detection window size of the window-based stall avoidance scheme for an V-process SAW HARQ mechanism. Denote P_{new} and P_{old} the probability of receiving a new packet and that of receiving a retransmitted old packet, respectively. From the definitions of P_s and $P_{N \to A}$ in Proposition 1, P_{new} and P_{old} can be expressed as*

$$
P_{new} = P_s + (1-P_s)P_{N \to A} \ , \qquad (3.11)
$$

and

$$
P_{old} = (1-P_s)(1-P_{N \to A}) \ . \qquad (3.12)
$$

Then the average gap processing time of the window-based stall avoidance scheme normalized to TTI in the single user case can be computed in terms of pa-

gap* and PKT* are separated by
m seats with probability $P_V(m)$.

Remaining (V-m) processes
retransmit old packets to
refill the holes in the
reordering buffer.

Other (m-1) processes
transmit new packets

gap*   •••   PKT*

A Type-II gap appears in PR*

Detection window   Remaining seats
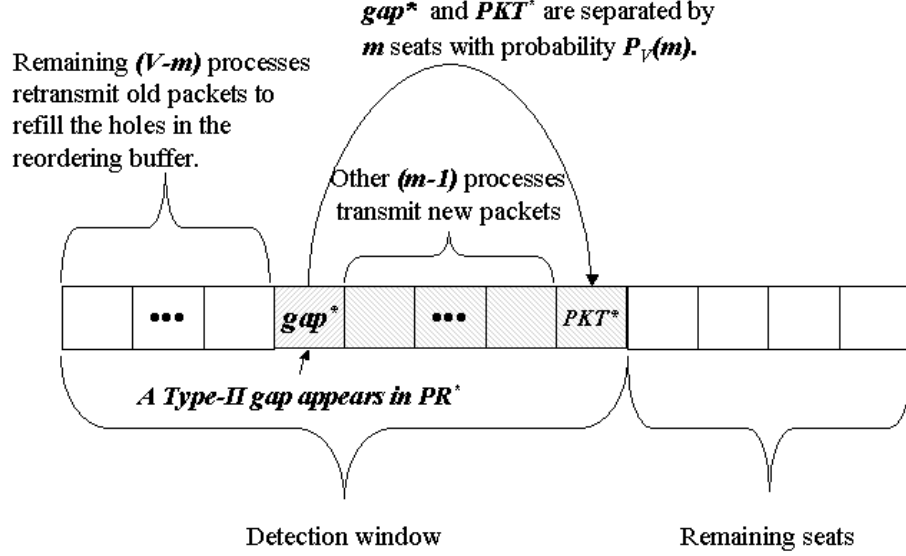
Fig. 3.4: An illustrative example of the seat allocation in a detection window for the window-based stall avoidance scheme.

rameters P_{new}, P_{old}, W, and V as follows:

$$\overline{GPT}_{window} = V + \sum_{m=1}^{V} \left[(W-m) \sum_{n=1}^{\infty} n P_{new} P_{old}^{n-1} \right] \binom{V-1}{m-1} P_{new}^{m-1} P_{old}^{V-m} .$$

(3.13)

Proof: The gap processing time for the window-based stall avoidance scheme is derived in two steps. In the following, we will prove that

$$\overline{GPT}_{window} = cycle\ duration + residual\ detection\ time ,$$
(3.14)

where the cycle duration is defined in Section 3.1.3 and the residual detection time is defined as the extra time to detect a Type II gap in addition to one cycle duration.

1. cycle duration: The minimum gap processing time for the window-based stall avoidance scheme is equal to one cycle duration (V TTIs). Consider the small-

est detection window $W = V$. The detection window size (or equivalently the reordering buffer size) is usually larger than the number of parallel HARQ processes, i.e. $W \geq V$. Suppose that a Type-II gap occurs in process PR^* in i-th cycle. If subsequent $V - 1$ processes transmit new packets successfully, process PR^* intends to send a new packet (PKT^*) in the $(i+1)$-th cycle due to a NACK-to-ACK error. However, because the detection window is fully-booked, the gap in the i-th cycle for process PR^* can be judged to be a Type-II gap according the rule of the window-based stall avoidance scheme. In this situation, the gap processing time is equal to one cycle duration (i.e. V TTIs).

2. residual detection time: The *residual detection time* is defined as the extra time after one cycle duration for the detection window becoming fully-booked. The residual detection time spans in the following two cases (a) $W > V$ and (b) $W = V$ with some of the $V - 1$ processes subsequent to process PR^* receiving old packets after the occurrence of the Type-II gaps in step 1.

   (a) $\underline{W > V}$: Now let's examine the seat allocation of a detection window, as shown in Fig. 3.4. Recall in step 1 that process PR^* produced a type-II gap (gap^*) in cycle i. Thus, process PR^* will transmit a new packet PKT^* in cycle $i + 1$. Without loss of generality, choose $(m - 1)$ processes out of the total other $(V - 1)$ processes to send new packets, and the remaining $(V - m)$ processes to send old packets. Clearly, the probability of $(m - 1)$ processes transmitting new packets is P_{new}^{m-1} and that of $(V - m)$ processes retransmitting old packets is P_{old}^{V-m}. Since there are $\binom{V-1}{m-1}$ choices, the probability of PKT^* and gap^* being separated by m seats is equal to

$$P_V(m) = \binom{V-1}{m-1} P_{new}^{m-1} P_{old}^{V-m} \ , \tag{3.15}$$

where $\sum_{m=1}^{V} P_V(m) = 1$. A Type-II gap will finally halt the trailing edge of

a detection window and is seated at the first place of the detection window. Hence, PKT^* will be positioned at the $(m+1)$-th seat. Accordingly, there will be another $(W - m - 1)$ available seats remained in the detection window. Note that the detection window extends its leading edge only when receiving a new packet and the old packets just fill in the empty holes in the reserved seats of the reordering buffer. Thus, the Type-II gap gap^* can be detected when the remaining $(W - m - 1)$ plus one seats in the ordering buffer are occupied.

The gap processing time for gap^* will be $cycle\ duration + (W - m)$ TTIs when $W - m$ consecutive new packets arrive the receiver successfully with conditional probability P_{new}^{W-m}. Note that $cycle\ duration = V$. In this case, the probability of gap processing time equal to $V + (W - m)$ TTIs is $P_{new}^{W-m}P_V(m)$. However, the gap processing time will be longer than $V + (W - m)$ TTIs if one or more of the $W - m$ new packets fail the CRC at their first trials to reach the receiver. Thus, the gap processing time will be $V + (W - m) + 1$ TTIs if one of the $W - m$ new packets takes two transmissions (one transmission with probability P_{new} and one retransmission with probability P_{old}) to reach the receiver. In this case, the probability is $(W - m)P_{new}^{W-m}P_{old}P_V(m)$.

Now we assume that there are $W - m$ transmissions and total $n - (W - m)$ retransmissions before these $W - m$ new packets successfully reach the receiver. The gap processing time is $n + V$ TTIs in this case. Because these total $n - (W - m)$ retransmissions may be responsible for some of the $W - m$ packets, there are $\frac{(n-1)!}{(W-m-1)!(n-(W-m))!} = \binom{n-1}{W-m-1}$ choices in this case, for each of which the probability is $P_{new}^{W-m}P_{old}^{n-(W-m)}$. Thus, the probability of the gap processing time equal to $n + V$ (denoted by $P(GPT = n + V)$)

can be expressed as

$$P(GPT = n + V) = P(GPT = n + V | PKT^* \text{ at } (m+1)\text{-th seat}) P_V(m)$$

$$= \binom{n-1}{W-m-1} P_{new}^{W-m} P_{old}^{n-(W-m)} \binom{V-1}{m-1} P_{new}^{m-1} P_{old}^{V-m}$$

$$= \binom{n-1}{W-m-1} \binom{V-1}{m-1} P_{new}^{W-1} P_{old}^{n+V-W} \quad . \tag{3.16}$$

Note that

$$\sum_{m=1}^{V} \sum_{n=W-m}^{L_g} P(GPT = n + V) = 1 \quad , \tag{3.17}$$

where L_g is the required TTIs to detect a Type-II gap. The average gap processing time for the case of $W > V$ can be calculated by

$$\overline{GPT}_{window} = \sum_{m=1}^{V} \sum_{n=W-m}^{L_g} (n + V) P(GPT = n + V)$$

$$= \sum_{m=1}^{V} \sum_{n=W-m}^{L_g} (n+V) \binom{n-1}{W-m-1} \binom{V-1}{m-1} P_{new}^{W-1} P_{old}^{n+V-W} \quad .$$

$$\tag{3.18}$$

(b) <u>W=V:</u> Recall that the residual time for $W = V$ lasts when some of the $V - 1$ processes subsequent to process PR^* receive old packets after the occurrence of the Type-II gaps in step 1. Following the same approach of obtaining (3.15) in the case of $W > V$, we assume that the $(m - 1)$ processes of the subsequent $(V - 1)$ processes send new packets and the remaining $(V - m)$ processes send old packets. In this situation, gap^* can be recognized as a Type-II gap when the remaining $(V - m - 1)$ plus one seats in the ordering buffer are occupied. Then, one can easily find that the residual time for $W = V$ is just a special case of that for $W > V$.

However, one should note that (3.16) is not valid for $W = V$ and $m = V$. For $W = V$ and $m = V$, $P(GPT = n + V | PKT^*$ at $(V + 1)$-th seat$) = P_{new} P_{old}^n$ because PKT^* may successfully reach the receiver and overbook the detection window after $n + 1$ transmissions, where $n \geq 0$.

In order to obtain a general closed-form expression of average gap processing time for the window-based stall avoidance scheme, an alternative derivation of Proposition II is provided in the following. Since the probability of a new packet arriving at the reordering buffer within n TTIs is equal to $P_{new} P_{old}^{n-1}$, the average time for the detection window extending its leading edge by one seat (denoted by T_0) can be computed by

$$T_s = \sum_{n=1}^{\infty} n P_{new} P_{old}^{n-1} \ . \tag{3.19}$$

As a result, it takes extra $(W - m - 1)T_s$ TTIs to have a fully-booked window in addition to one cycle duration. When another new packet arrives in the next T_s, the receiver can judge the gap at the first seat of the window is a Type-II gap and start the process of forwarding the received packets with the type II gap to the upper later. From (3.15) and (3.19) and the above discussion, the total residual detection time in addition to one cycle duration is calculated as

$$residual\ detection\ time = \sum_{m=1}^{V} \left[(W - m)T_s \right] P_V(m)$$

$$= \sum_{m=1}^{V} \left[(W - m) \sum_{n=1}^{\infty} n P_{new} P_{old}^{n-1} \right] \binom{V - 1}{m - 1} P_{new}^{m-1} P_{old}^{V-m} \ .$$

$$\tag{3.20}$$

Adding the residual detection time (3.20) to the cycle duration (V TTIs), we obtain the closed-form expression of the average gap processing time for the

window-based stall avoidance scheme as shown in (3.13). Note that the average gap processing time calculated by (3.20) plus the cycle duration V is equal to that obtained in (3.18).

∎

3.5 Analysis of Indicator-Based Stall Avoidance Scheme

In Proposition 3, we derive the average gap processing time for the indicator-based stall avoidance scheme.

Proposition 3: *Consider an V-process SAW HARQ mechanism. The gap processing time normalized to TTIs for the indicator-based scheme in the single user case can be calculated in terms of parameters V, P_s, P_{new}, and P_{old} as follows:*

$$\overline{GPT}_{indicator} = V(P_{new} + P_{old}P_s)^{V-1} + \sum_{k=1}^{C_V} \sum_{m=2}^{V} (m - 1 + kV)P(x_k = S_T) \times$$

$$\left[\sum_{i=0}^{k} P(x_i = S_T) \right]^{m-2} \left[\sum_{j=0}^{k-1} P(x_j = S_T) \right]^{V-m} ,$$

$$(3.21)$$

where

$$P(x_0 = S_T) = P_{new} + P_{old}P_s \qquad (3.22)$$

and

$$P(x_\ell = S_T) = P_{old}^\ell (1 - P_s)P_{new} \quad for \quad \ell \geq 1 . \qquad (3.23)$$

C_V is the number of cycles involving all the processes in the V-process SAW HARQ mechanism required to detect a Type-II gap.

Proof: Recall that the basic idea of the indicator-based stall avoidance scheme is to examine the status of each HARQ process by the use of the NDI in the control channel and the TSN in the traffic channel to confirm whether the missing packet will be transmitted or not. To ease our discussion, the status of an HARQ process are described by the following two events:

$$\mathbf{I}_A \triangleq \{NDI_{(rec)} = NEW\} \ ; \tag{3.24}$$

$$\mathbf{I}_B \triangleq \{\{TSN_{(rec)} \neq TSN^*\} \cap \{NDI_{(rec)} = OLD\}\} \ , \tag{3.25}$$

where $NDI_{(rec)}$ and $TSN_{(rec)}$ are the NDI and the TSN of the received packet; TSN^* is the TSN of the missing gap. If either event $\mathbf{I}_A$ or event $\mathbf{I}_B$ is sustained for a HARQ process, then this HARQ process is ruled out to be the candidate for sending the missing packet TSN^*. If all the HARQ processes are ruled out, it implies that the existing gap in the reordering buffer belongs to the nonrecoverable Type-II gap since no HARQ process will transmit the missing packet. However, if none of events $\mathbf{I}_A$ and $\mathbf{I}_B$ happens (denoted by $\overline{\{\mathbf{I}_A \cup \mathbf{I}_B\}}$), the receiver believes that the HARQ process still possibly transmits the packet TSN^* to fill the gap of the reordering buffer in the future. Note that when $TSN_{(rec)} = TSN^*$, this Type-I gap is filled in the reordering buffer, which will not cause the stall issue.

Assume that a Type-II gap appears in the first process (PR_1) of the V-processes SAW HARQ mechanism in the cycle 0 $(\ell = 0)$ as shown in Fig. 3.5. To begin the proof, we first define a semi-Markov chain to describe the status of each HARQ process. Fig. 3.6 shows this Markov chain with two states defined as follows:

1. Retransmission state (S_R): If event $\overline{\{\mathbf{I}_A \cup \mathbf{I}_B\}}$ happens, this HARQ process enters the retransmission state. Denote x_ℓ the state variable in the l-th cycle. If

a process in the retransmission state in the $(\ell - 1)$-th cycle, the receiving process will issue a NACK signal for requesting a retransmission in the ℓ-th cycle. However, if the NACK signal is changed to an ACK signal, a new packet will be transmitted in the ℓ-th cycle instead. Based on the definition of event $\mathbf{I}_A$ in (3.24), we have

$$P(\mathbf{I}_A | x_{\ell-1} = S_R) = P_{N \to A} \ , \tag{3.26}$$

where $P_{N \to A}$ is the probability of having a NACK-to-ACK error. On the contrary, if the NACK signal arrives the transmitter correctly, the missing packet will be retransmitted in the ℓ-th cycle. Note that probability of the NACK signal arriving the transmitter correctly is $(1 - P_{N \to A})$ and the probability of successfully retransmitting packet to the receiver is P_s. According to the definition of (3.25), the occurrence probability of event $\mathbf{I}_B$ is equal to

$$P(\mathbf{I}_B | x_{\ell-1} = S_R) = (1 - P_{N \to A}) P_s \ . \tag{3.27}$$

Because events $\mathbf{I}_A$ and $\mathbf{I}_B$ are mutually exclusive and from (3.26) and (3.27), we can obtain

$$
\begin{aligned}
P(x_\ell = S_R | x_{\ell-1} = S_R) &= P(\{\overline{\mathbf{I}_A \cup \mathbf{I}_B}\} | x_{\ell-1} = S_R) \\
&= 1 - [P(\mathbf{I}_A | x_{\ell-1} = S_R) + P(\mathbf{I}_B | x_{\ell-1} = S_R)] \\
&= 1 - [P_{N \to A} + (1 - P_{N \to A}) P_s] \\
&= (1 - P_{N \to A})(1 - P_s) \\
&= P_{old} \ . \tag{3.28}
\end{aligned}
$$

Recall that in (3.12), we define $P_{old} = (1 - P_{N \to A})(1 - P_s)$. According to the definition of S_R, when a process receives a retransmitted old packet which fails

the CRC, it enters state S_R. Thus, the initial probability of a process at S_R can be expressed as

$$P(x_0 = S_R) = P_{old}(1 - P_s) \ . \tag{3.29}$$

2. Stop state (S_T): If either event $\mathbf{I}_A$ or event $\mathbf{I}_B$ happens, the state of process will enter the stop state. From Fig. 3.6 and (3.26) and (3.27), the probability of a process in the stop state S_T in the ℓ-th cycle can be expressed as

$$
\begin{aligned}
P(x_\ell = S_T | x_{\ell-1} = S_R) &= P(\mathbf{I}_A \cup \mathbf{I}_B | x_{\ell-1} = S_R) \\
&= P(\mathbf{I}_A | x_{\ell-1} = S_R) + P(\mathbf{I}_B | x_{\ell-1} = S_R) \\
&= P_{N \to A} + (1 - P_{N \to A})P_s \\
&= P_s + (1 - P_s)P_{N \to A} \\
&= P_{new} \ .
\end{aligned}
\tag{3.30}
$$

Recall that in (3.11), we define $P_{new} = P_s + (1 - P_s)P_{N \to A}$. According to the definition of state S_T, when a process receives a new packet or successfully receives a retransmitted old packet, it will enter state S_T. Thus, the initial probability of a process at S_T can be expressed as

$$P(x_0 = S_T) = P_{new} + P_{old}P_s \ . \tag{3.31}$$

From (3.28) and (3.30), we obtain the state transition probability matrix $\mathbf{\Gamma}$ of

	$\ell = 0$	$\ell = 1$	$\ell = 2$	$\ell = 3$	$\ell = 4$	$\cdots$	$\ell = k$	$\cdots$
PR_1	**gap** TSN^*	V				$\cdots$		$\cdots$
PR_2		1+V	1+2V	1+3V	1+4V	$\cdots$	1+kV	$\cdots$
PR_3		2+V	2+2V	2+3V	2+4V	$\cdots$	2+kV	$\cdots$
$\vdots$	$\vdots$	$\vdots$	$\vdots$	$\vdots$	$\vdots$	$\vdots$	$\vdots$	$\vdots$
PR_m		(m-1)+V	(m-1)+2V	(m-1)+3V	(m-1)+4V	$\cdots$	(m-1)+kV	$\cdots$
$\vdots$	$\vdots$	$\vdots$	$\vdots$	$\vdots$	$\vdots$	$\vdots$	$\vdots$	$\vdots$
PR_V		(V-1)+V	(V-1)+2V	(V-1)+3V	(V-1)+4V	$\cdots$	(V-1)+kV	$\cdots$

Fig. 3.5: An illustration for the gap processing time of the indicator-based stall avoidance scheme.

the two-state Markov chain in Fig. 3.6 as follows:

$$
\mathbf{\Gamma} \triangleq \left[\begin{array}{cc} P(x_\ell = S_R | x_{\ell-1} = S_R) & P(x_\ell = S_T | x_{\ell-1} = S_R) \\ P(x_\ell = S_R | x_{\ell-1} = S_T) & P(x_\ell = S_T | x_{\ell-1} = S_T) \end{array} \right]
$$

$$
= \left[\begin{array}{cc} P_{old} & P_{new} \\ 0 & 0 \end{array} \right] . \tag{3.32}
$$

Then from (3.29) and (3.31), a state probability vector $\mathbf{P}(\mathbf{x}_\ell) \triangleq [P(x_\ell = S_R),\ P(x_\ell = S_T)]$ can be obtained by

$$
\mathbf{P}(\mathbf{x}_\ell) = \mathbf{P}(\mathbf{x}_{\ell-1})\mathbf{\Gamma} = \mathbf{P}(\mathbf{x}_0)\mathbf{\Gamma}^\ell
$$

$$
= [P_{old}^{\ell+1}(1 - P_s),\ P_{old}^\ell(1 - P_s)P_{new}] . \tag{3.33}
$$

Now referring to Fig. 3.5, we derive the average gap processing time for the following two possible scenarios.

(I) Detect Type-II gap right after cycle 0:

$$1 \;-\; P(\mathbf{I}_A|x_{\ell-1} = S_R)$$
$$-\; P(\mathbf{I}_B|x_{\ell-1} = S_R)$$

$$P(\mathbf{I}_A|x_{\ell-1} = S_R)$$

$$S_R$$

$$S_T$$

$$P(\mathbf{I}_B|x_{\ell-1} = S_R)$$

Retransmission state

Stop state

$$\mathbf{I}_A \quad \{NDI_{(rec)} = NEW\}$$
$$\mathbf{I}_B \quad \{\{TSN_{(rec)} \neq TSN^*\} \cap \{NDI_{(rec)} = OLD\}\}$$
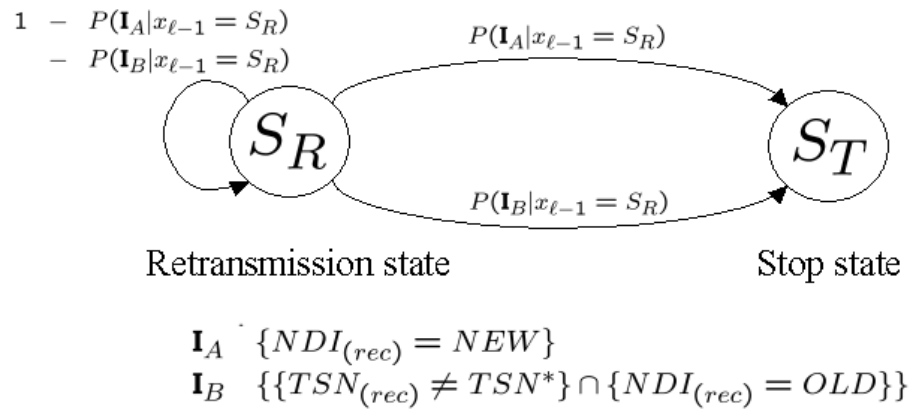
Fig. 3.6: The state transition diagram for the indicator-based stall avoidance scheme.

If in cycle 0 processes $PR_2 \sim PR_V$ are all in state S_T, the gap TSN^* can be detected as a Type-II gap right after the end of cycle 0. Due to a NACK-to-ACK error, PR_1 transmits a new packet in cycle 1. As long as process PR_1 receives the NDI and finds $NDI = NEW$, the receiver can confirm that the missing packet TSN^* is a Type-II gap since all processes are handling other packets except for TSN^*. In this case, the receiver spends V TTIs to detect this Type-II gap. Thus, from (3.31), the probability of gap processing time equal to V can be expressed as

$$
\begin{aligned}
P(GPT = V) &= [P(x_0 = S_T)]^{V-1} \\
&= (P_{new} + P_{old}P_s)^{V-1} .
\end{aligned}
\tag{3.34}
$$

Then, the average gap processing time for detecting a Type-II gap immediately after cycle 0 can be calculated as

$$
\begin{aligned}
\overline{GPT}_0 &= V \times P(GPT = V) \\
&= V(P_{new} + P_{old}P_s)^{V-1} .
\end{aligned}
\tag{3.35}
$$

(II) Detect the Type-II gap more than one cycle:

Recall that if a process is in state S_T, this process is ruled out to be the candidate for sending the missing packet TSN^*. When all the processes are all ruled out, the remaining gap in the reordering buffer is the Type-II gap. As shown in Fig. 3.5, $GPT = m - 1 + kV$ when the Type-II gap is detected in the k-th cycle by PR_m, where $m \geq 2$ and $k \geq 1$. To compute the probability of $GPT = m - 1 + kV$, three event E_α, E_β, and E_γ are defined as follows:

$$
E_\alpha = \{PR_m \text{ is ruled out in the } k\text{-th cycle.}\}
\tag{3.36}
$$

$$
E_\beta = \{PR_2 \sim PR_{m-1} \text{ are ruled out within } k\text{-th cycle.}\}
\tag{3.37}
$$

$$
E_\gamma = \{PR_{m+1} \sim PR_V \text{ are ruled out within } (k-1)\text{-th cycle.}\}
\tag{3.38}
$$

From the state probability of the Markov chain in (3.33), it is obvious that

$$P(E_\alpha) = P(x_k = S_T) .$$

$$(3.39)$$

Before calculating $P(E_\beta)$, we first denote $P_k^{(m)}$ the probability of process PR_m being ruled out within k-th cycle. Because all processes send data independently, the probability for processes $PR_2 \sim PR_{m-1}$ being ruled out within k-th cycle can be expressed as

$$P(E_\beta) = \overbrace{P_k^{(2)} \times P_k^{(3)} \times \cdots \times P_k^{(m-1)}}^{(m-2)}$$

$$= \left[\sum_{i=0}^{k} P(x_i = S_T) \right]^{m-2} .$$

$$(3.40)$$

Similarly, for event E_γ we can have

$$P(E_\gamma) = \left[\sum_{j=0}^{k-1} P(x_j = S_T) \right]^{V-m} .$$

$$(3.41)$$

Combining (3.39), (3.40), and (3.41), we can obtain the pmf of the GPT of the indicator-based stall avoidance scheme as

$$P(GPT = m - 1 + kV) = P(x_k = S_T) \left[\sum_{i=0}^{k} P(x_i = S_T) \right]^{m-2} \left[\sum_{j=0}^{k-1} P(x_j = S_T) \right]^{V-m} .$$

$$(3.42)$$

Then, we can express the average gap processing time for case (II) as follows:

$$\overline{GPT}_1 = \sum_{k=1}^{C_V} \sum_{m=2}^{V} (m - 1 + kV) P(GPT = m - 1 + kV)$$

$$= \sum_{k=1}^{C_V} \sum_{m=2}^{V} (m - 1 + kV) P(x_k = S_T) \left[\sum_{i=0}^{k} P(x_i = S_T) \right]^{m-2} \left[\sum_{j=0}^{k-1} P(x_j = S_T) \right]^{V-m} ,$$

$$(3.43)$$

where C_V is the number of cycles involving all the processes in the V-process SAW HARQ mechanism required to remove a Type-II gap. For given parameters P_{new}, P_{old}, P_s, and V, the value of C_V can be obtained from

$$(P_{new} + P_{old}P_s)^{V-1} + \sum_{k=1}^{C_V} \sum_{m=2}^{V} P(x_k = S_T) \times$$

$$\left[\sum_{i=0}^{k} P(x_i = S_T) \right]^{m-2} \left[\sum_{j=0}^{k-1} P(x_j = S_T) \right]^{V-m} = 1 . \tag{3.44}$$

Combining (3.35) and (3.43), the average gap processing time for the indicator-based stall avoidance scheme can be computed by

$$
\begin{aligned}
\overline{GPT}_{indicator} &= \overline{GPT}_0 + \overline{GPT}_1 \\
&= V(P_{new} + P_{old}P_s)^{V-1} + \sum_{k=1}^{C_V} \sum_{m=2}^{V} (m - 1 + kV)P(x_k = S_T) \times \\
&\qquad \left[\sum_{i=0}^{k} P(x_i = S_T) \right]^{m-2} \left[\sum_{j=0}^{k-1} P(x_j = S_T) \right]^{V-m} . \tag{3.45}
\end{aligned}
$$

∎

3.6   Numerical Results and Discussions

In this section, by analysis and simulations, we investigate the average gap process-ing time and the corresponding probability mass functions for the timer-based, the window-based, and the indicator-based stall avoidance schemes. We will discuss the relation between the gap processing time, the allowable retransmissions, and the num-ber of acceptable fully loaded users for different stall avoidance schemes. For these

---

[1] To boost the transmission rate, the packet error rate of the first transmission can be higher than 40% because a high level modulation and coding scheme is adopted [65].

Tab. 3.2: The Simulation Environment

Channel model	Rayleigh fading
Doppler frequency	100 Hz
Packet size	320 bits
CRC bits	16 bits
No. of parallel HARQ processes	4, 6, 8
TTI	2 msec
E_b/N_0 (dB)	$10 \sim 20$ dB
1st transmission P_e [1]	$0.09 \sim 0.42$

purposes, we conduct a simulation cross physical and MAC layers under the assumptions of Section 3.2.2. In the simulation, each packet is transmitted through the flat Rayleigh fading channel. The Doppler frequency of the Rayleigh fading channel is 100 Hz, which is equivalent to a vehicle speed of 54 km/hour with a carrier frequency of 2 GHz. The correctness of each received packet is checked by CRC. If the received packet passes CRC, an ACK signal will be sent through the feedback control channel otherwise a NACK signal is sent. If a NACK-to-ACK error occurs in the feedback control channel, a Type-II gap will appear in the reordering buffer. The gap processing time of the Type-II gap is calculated from its appearance until it is detected. To confirm the correctness of simulation results, we run 100000 packets for each simulation. The simulation parameters are shown in Table 3.2. In the discussion of the number of acceptable fully loaded users, we assume that all fully loaded users are selected from multiple users and under the same QoS requirements, i.e. the required gap processing time should be lower than 100 TTIs. A fair scheduling policy is implemented to allocate resource to fully loaded users.

3.6.1 Average Gap Processing Time of the Timer-Based Scheme

Figure 3.7 shows the average gap processing time of the timer-based stall avoidance scheme with various settings on the timer's expiration (D). It is shown that the analytical results are close to the simulation results. In the case of $D = 20$ TTIs and $E_b/N_0 = 14$ dB, the analytical average gap processing time (21.7 TTIs) is only 2.7% smaller than the simulation value (22.3 TTIs). Regarding the 2.7% discrepancy between the simulation and the analytical results, we summarized the reason as what follows.

To ease the derivation of the computational formula of the gap processing time
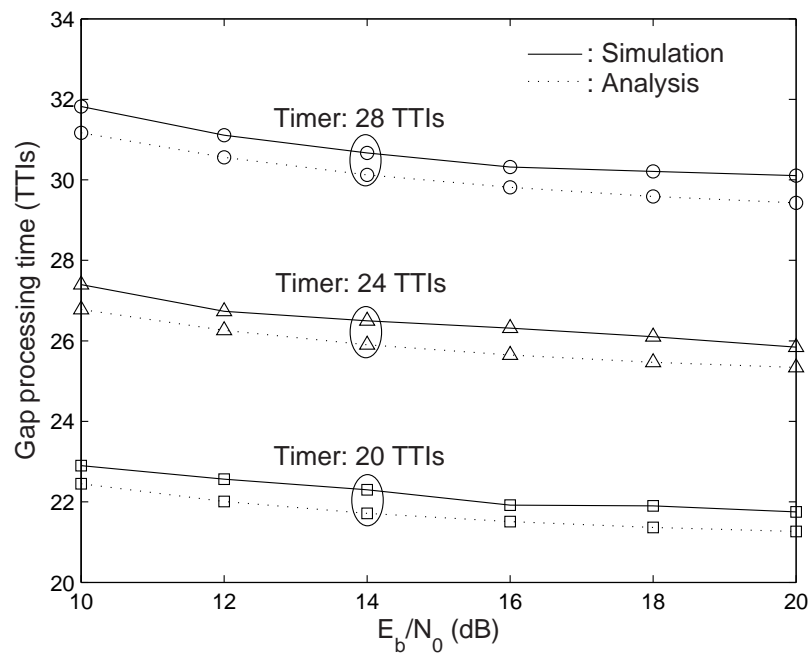
Fig. 3.7: The average gap processing time of the timer-based stall avoidance scheme with different timer expiration for the 4-process SAW HARQ mechanism in the Rayleigh fading channel with Doppler frequency of 100 Hz.

for the timer-based avoidance schemes, we assume that the transmission sequence number (TSN) of the missing packet is smaller than that of the first successfully received consequent packet. Having a packet with a larger TSN after the missing packet with a smaller TSN, the receiver can find a gap in a series of received packets, thereby initiating the timer counting for the timer-based scheme. In general, it is possible that the receiver may receive a packet with a smaller TSN than the previous missing packet. In this case, the receiver does not know to initiate the timer counting for the missing gap until the reception of another packet with a larger TSN than the previous missing packet's TSN. However, the analysis of gap processing time for the general case is quite involved, which is not discussed in this chapter. Hence, Propositions I shows the lower bound on the average gap processing time for the timer-based stall avoidance mechanisms.

The timer's expiration impacts the MAC layer performance of HSDPA in two folds. On the one hand, as shown in the figure, a longer timer results in longer gap processing time. For $D = 20$ TTIs at $E_b/N_0 = 14$ dB, the average gap processing time ($\overline{GPT}_{timer}$) is 21.7 TTIs , while for $D = 28$ TTIs $\overline{GPT}_{timer} = 30.1$ TTIs. On the other hand, a larger value of time expiration allows more retransmissions. Specifically, for an V-process SAW HARQ mechanism, the allowable number of retransmissions (h_r) is equal to D/V in the single user case. A properly designed timer expiration is to allow enough retransmissions to recover the lost packet, and in the meanwhile not to cause too long gap processing time. From Proposition 1, we can rapidly evaluate the impact of the allowable retransmissions ($h_r = D/V$) on the gap processing time ($\overline{GPT}_{timer}$) for different values of P_s and $P_{N \to A}$ without time consuming simulations.

Furthermore, the derived analytical method of computing the gap processing time can also be applied to design the proper number of acceptable fully loaded users from the admission control standpoint. Let GPT_c be the constraint on the maximum allowable gap processing time. Then the acceptable fully loaded users in the system

can be approximated by $\lfloor GPT_c/\overline{GPT}_{timer} \rfloor$, where $\lfloor x \rfloor$ is the largest integer less than or equal to x. According to the above guidelines, Figure 3.8 shows the number of acceptable fully loaded users of the timer-based stall avoidance scheme versus the number of allowable retransmissions (n) for different numbers of parallel processes (V) subject to the constraint of $GPT_c = 100$ TTIs. As shown in the figure, the more the allowable retransmissions (h_r), the fewer the users can be accepted. For $V = 4$, as the value of h_r increases from 2 to 6, the number of acceptable fully loaded users decreases from 10 to 3. This is because for a given V, a larger value of h_r leads to a longer timer expiration ($D = h_r \times V$ in the single user case), thereby resulting in a longer period of the gap processing time. That is, more retransmissions increases the gap processing time and thus decreases the number of acceptable fully loaded users. Similarly, as the number of parallel HARQ processes increases, the effect of increasing gap processing time will reduce the acceptable fully loaded users.

3.6.2 Average Gap Processing Time of the Window-Based Scheme

Figure 3.9 shows $\overline{GPT}_{window}$ against E_b/N_0 for various window sizes. The accuracy of the derived average gap processing time (i.e. (3.13)) of the window-based stall avoidance scheme is validated by simulations. As shown in the figure, the analytical results match the simulations well. Most importantly, Fig. 3.9 also provides important insights into designing an admission control policy subject to the gap processing time constraint GPT_c. Consider a fair scheduling policy. The number of acceptable fully loaded users (N_u) in the system can be approximated by

$$N_u = \lfloor GPT_c/\overline{GPT}_{window} \rfloor \ , \tag{3.46}$$

where $\lfloor x \rfloor$ is the largest integer less than or equal to x. For $E_b/N_0 = 14$ dB in Fig. 3.9, one can observe that $\overline{GPT}_{window} = 15.3, 19.2, 23.1$ TTIs for W $= 12, 15, 18$,
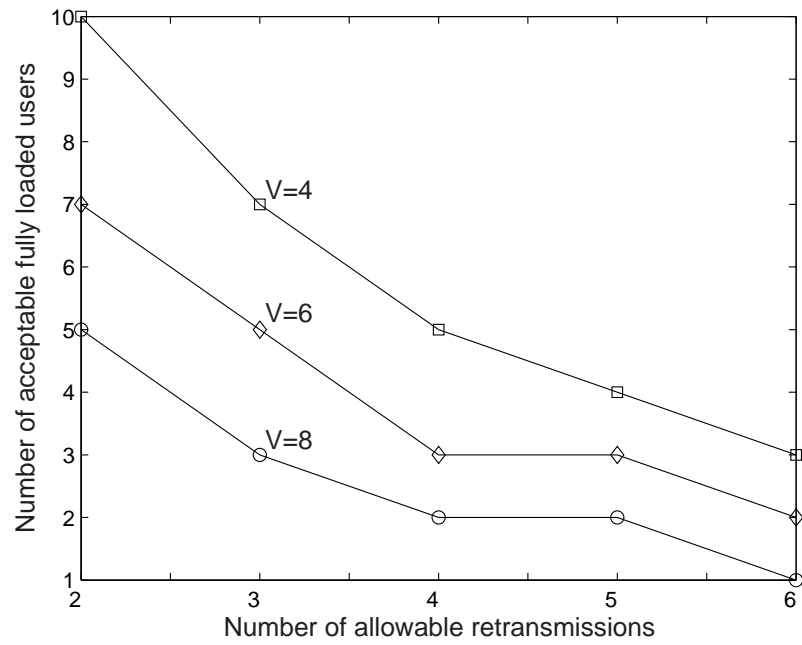
Fig. 3.8: The number of acceptable fully loaded users of the timer-based stall avoidance scheme versus the numbers of allowable retransmissions (h_r) for various number processes (V) in the parallel SAW HARQ mechanism subject to a constraint of gap processing time 100 TTIs.
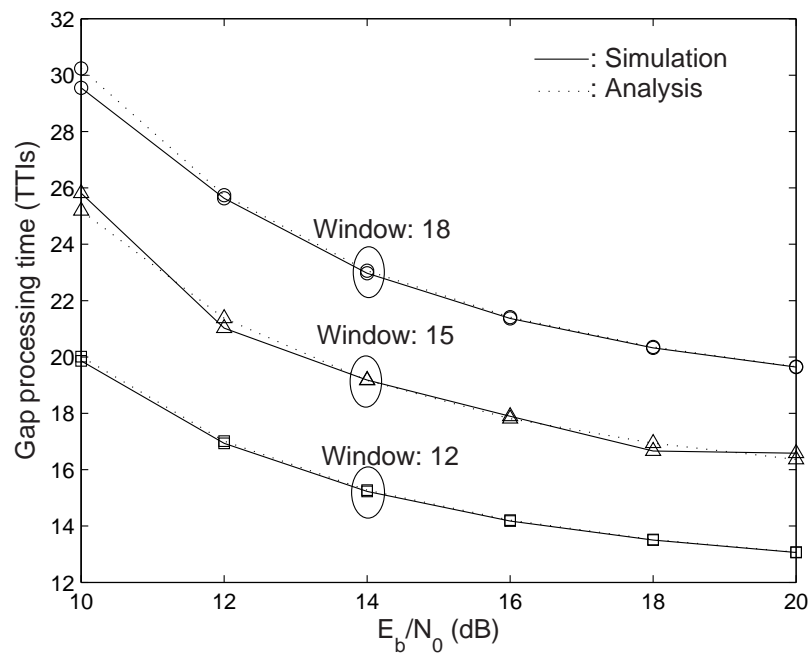
Fig. 3.9: The average gap processing time of the window-based stall avoidance scheme with different window sizes for the 4-process SAW HARQ mechanism in the Rayleigh fading channel with Doppler frequency of 100 Hz.

respectively. For the maximal gap processing time constraint $GPT_c = 100$ TTIs, the allowable users are therefore equal to 6, 5, and 4 for the window of size of 12, 15, and 18, respectively.

As a matter of fact, the window size is a function of the allowable minimum retransmissions (h_m) and the number of HARQ processes (V). In the single user case, for an V-process SAW HARQ mechanism with a window of size of W, the allowable retransmissions (h_m) of a missing packet is at least

$$h_m = \frac{W}{V - 1} - 1 \ . \tag{3.47}$$

For $V = 4$ and $W = 12$, the missing packet can be retransmitted by $\frac{W}{V-1} - 1 = 3$ times. Assume one process keeps transmitting a missing packet and the other 3 processes transmit new packets successfully. After 4 cycles, a window with a size of 12 is fully occupied. Because the window has no more space for the missing packet, this packet will not be transmitted.

Hence, the admission control policy subject to the gap processing time requirement can also be designed for different combinations of parameters h_m and V. Take $V = 4$ as an example. Figure 3.10 shows the number of acceptable fully loaded users versus E_b/N_0 with various minimum allowable retransmissions (h_m) subject to a gap processing time constraint of 100 TTIs. These curves are obtained by mapping Fig. 3.9 according to (3.46). From (3.47), $h_m = 3$, 4, and 5 correspond to $W = 12$, 15, and 18, respectively. As shown in the figure, the acceptable fully loaded users is reduced from 7 to 4 as h_m increases from 3 to 5 for 16 dB $\leq E_b/N_0 \leq 18$ dB.

Figure 3.11 shows the number of acceptable fully loaded users of the window-based stall avoidance scheme against packet error rate (P_e) with various numbers of parallel processes (V), where the maximal allowable gap processing time $GPT_c = 100$ TTIs and the minimum allowable retransmission $h_m = 3$. These curves are obtained by substituting the parameters V, W, P_s, and $P_{N \to A}$ into (3.13). Note that $P_e = 1 - P_s$

and the corresponding window size $W = 12$, 20, and 28 is obtained from $W = (n + 1)(V - 1)$ according to (3.47). This figure can be associated with an admission control policy subject to gap processing time by observing P_e. According to the CRC results and P_e, suitable number of allowable users to maintain the QoS can be determined from the standpoint of meeting the gap processing time requirement. In the figure, we find that more parallel SAW HARQ processes results in fewer allowable users in the system subject to the total gap processing time requirement. For $P_e = 0.15$, the number of acceptable fully loaded users decreases from 7 to 3 as V increases from 4 to 8. Recall $h_m = \frac{W}{V-1} - 1$ in (3.47). For a fixed h_m, a larger value of V also leads to a lager value of W and longer gap processing time. Hence, the number of acceptable fully loaded users is reduced for a larger value of V to satisfy the gap processing time requirement.

3.6.3 Average Gap Processing Time of the Indicator-Based Scheme

Figure 3.12 shows the analytical average gap processing time for the indicator-based stall avoidance scheme obtained from (3.21) and simulations. As shown in the figure, the differences between simulation and the analytical approximation are quite small. Similar to the reason for the timer-based scheme, the receiver may possibly receive a packet with a smaller TSN than the previous missing packet. In this situation, the procedure of monitoring the status of the HARQ process can start only after another packet with a larger TSN arrives. Hence, Proposition III shows a lower bound on the average gap processing time for the indicator-based stall avoidance mechanism.

Comparing to Figs. 3.7, 3.9, and 3.12, the indicator-based scheme outperforms the timer-based and the window-based schemes in terms of the gap processing time. For a 4-process SAW HARQ mechanism with $E_b/N_0 = 14$ dB, the gap processing
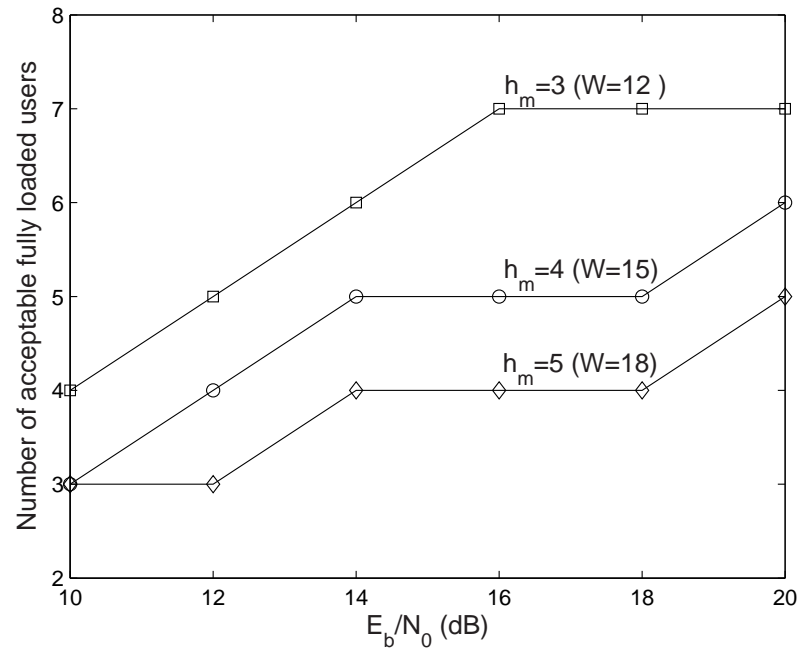
Fig. 3.10: The number of acceptable fully loaded users of the window-based stall avoidance scheme versus E_b/N_0 with various number minimum allowable retransmissions ($h_m = 3, 4, 5$) in the 4-process SAW HARQ mechanism subject to a gap processing time constraint of 100 TTIs.
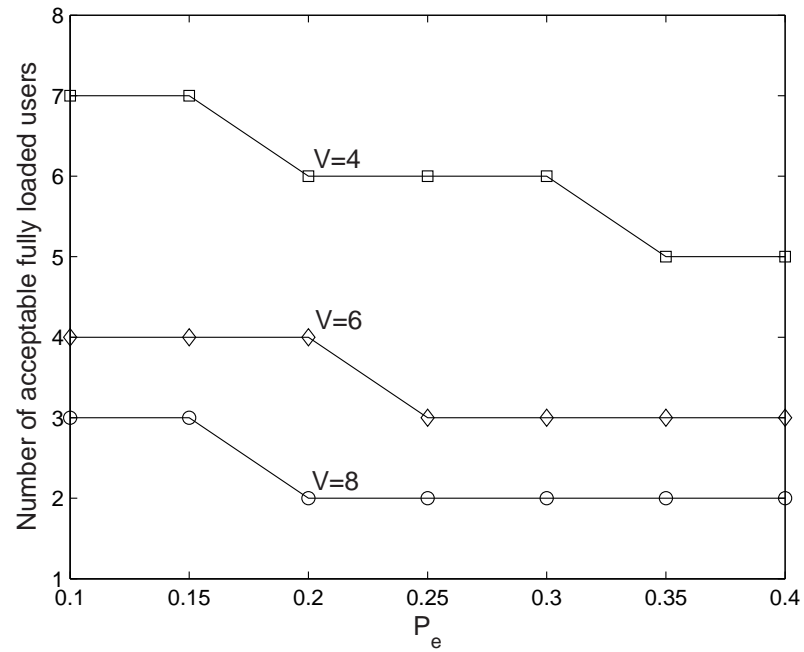
Fig. 3.11: The number of acceptable fully loaded users of the window-based stall avoidance scheme versus P_e with various number processes (V) in the parallel SAW HARQ mechanism subject to a gap processing time constraint of 100 TTIs. The minimum allowable retransmission (h_m) is three.
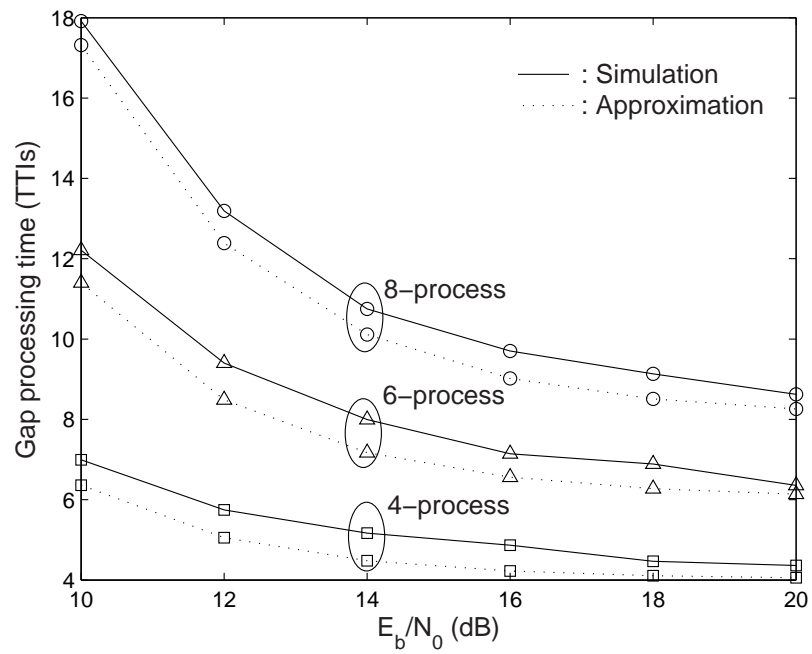
Fig. 3.12: Effect of the number of processes in the multi-process SAW HARQ mechanism on the gap processing time for the indicator-based avoidance scheme in the Rayleigh fading channel with Doppler frequency of 100 Hz .

time of the indicator-based scheme is 4.9 TTIs; the gap processing time is 21.7 TTIs for the timer-based scheme with a timer expiration of 20 TTIs; the gap processing time is 15.27 TTIs for the window-based scheme with a window of a size of 12. Also, it is found that the more the parallel HARQ processes, the longer the average gap processing time.

The developed gap processing time computation method for the indicator-based scheme can be applied to determine the acceptable fully loaded users through $\lfloor GPT_c / \overline{GPT}_{indicator} \rfloor$ as the timer-based and the window-based schemes, where GPT_c is a given constrain on the gap processing time. Figure 3.13 shows the number of acceptable fully loaded users of the indicator-based stall avoidance scheme against P_e with various numbers of parallel HARQ processes (V) under a constraint of the gap processing time 100 TTIs. One can find that with the aid of the indicator-based stall avoidance scheme, an HSDPA system can accommodate more users compared to the window-based scheme. For $V = 4$ at $P_e = 0.2$, the number of acceptable fully loaded users are 4, 6, and 24 for the timer-based, the window-based, and the indicator-based schemes, respectively. Furthermore, although more parallel HARQ processes can enhance throughput, the side effect of increasing gap processing time can not be ignored. As V increases from 4 to 12 at $P_e = 0.2$, it is necessary to reduce the acceptable fully loaded users from 24 to 6 if the gap processing time requirement is fulfilled.

3.6.4 Probability Mass Function of the Gap Processing Time

Figure 3.14 shows the probability mass functions of the gap processing time for the timer-based, the window-based, and the indicator-based stall avoidance schemes, where the timer's expiration $D = 24$ and the detection window size $W = 20$ with
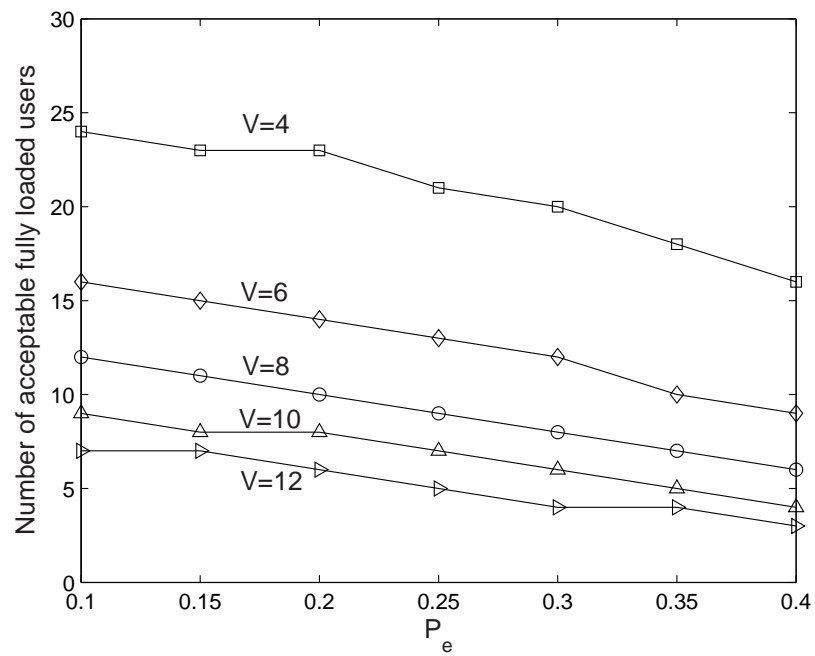
Fig. 3.13: The number of acceptable fully loaded users of the indicator-based stall avoidance scheme versus P_e with various number processes (V) in the parallel SAW HARQ mechanism subject to a gap processing time constraint of 100 TTIs.

$V = 6$ parallel HARQ processes at $E_b/N_0 = 14$ dB. The analytical pmf for the timer-based scheme can be obtained by evaluating (3.6) and (3.9). For the window-based scheme, we obtain the analytical pmf by evaluating (3.16), while the pmf for the indicator-based scheme can be obtained by calculating (3.35) and (3.43). From the figure, one can see that the analytical results can approximate the simulation results. Most importantly, the gap processing time for the timer-based and the indicator-based schemes are centralized while that of the window-based scheme is widely spread. For example, 78% and 71% of the gap processing time of the timer-based and the indicator-based schemes are lower than 26 and 8 TTIs, respectively, where the corresponding average gap processing times are 26.8 and 8.4 TTIs. However, for the window-based scheme, only 53% of the gap processing time are lower than the average value of 25.6 TTIs. Thus, we can conclude that indicator-based scheme is more capable of maintaining stable and better QoS for HSDPA.

3.7 Chapter Summary

In this chapter, we have defined a new performance metric – gap processing time – to evaluate the stall avoidance schemes for HSDPA. We derive the probability mass functions and the closed-form expressions for the average gap processing time of the timer-based, the window-based, and the indicator-based stall avoidance schemes. Through analyses or simulations, we find that the indicator-based stall avoidance scheme outperforms the other two schemes in terms of the gap processing time. The proposed analytic model can also be used to design the proper size in the reordering buffer in the MAC layer, the window size in the RLC layers, the RLC timeout period, and the number of acceptable fully loaded users in the radio resource management layer.
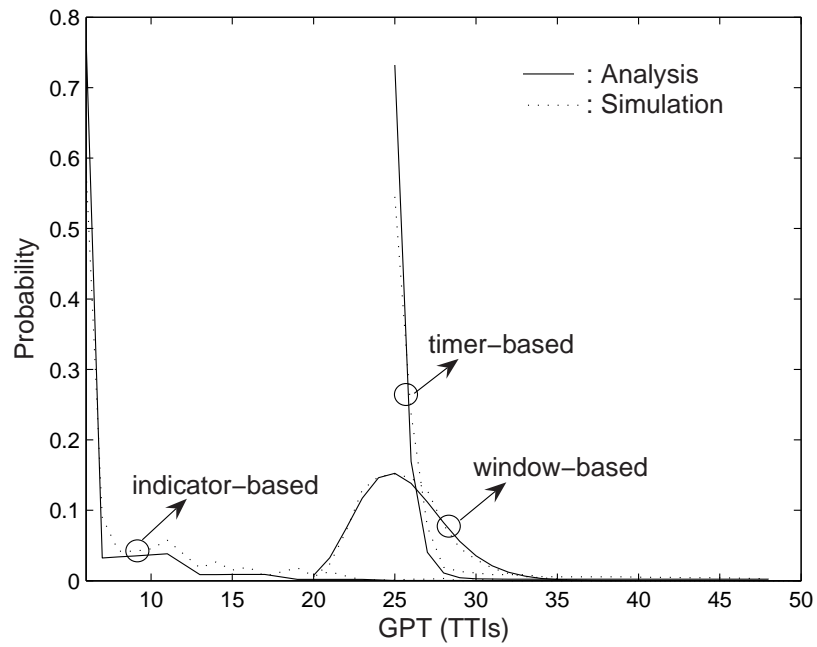
Fig. 3.14: The probability mass functions of the gap processing time for the timer-based, the window-based, and the indicator-based stall avoidance schemes, where the timer's expiration $D = 24$ and the detection window size $W = 20$ with $V = 6$ parallel HARQ processes at $E_b/N_0 = 14$ dB.

Chapter 4

Analysis of a Stall Avoidance Mechanism with Scheduling for HSDPA in the WCDMA Systems

The objective of this chapter is to derive a formula of gap processing time for the indicator-based stall avoidance mechanism (ISA) with interleaving scheduling. In general, the scheduling policies of the high speed down link packet access (HSDPA) can be divided into two categories: scheduling-by-bundle and interleaving scheduling policies. The former policy allocates a subsequent time slots to each user, while the later policy schedules time slots for multiple users one at a time. In the previous chapter, we have compared the three current stall avoidance mechanisms with the scheduling-by-bundle policy. Through the results of Chapter 3, we have concluded that the indicator-based scheme can outperform the timer-based and window-based schemes with scheduling-by-bundle. Thus, in this chapter, we extend the analysis of the average gap processing time for the indicator-based scheme from the case with scheduling-by-bundle to that with interleaving scheduling.

4.1 ISA Mechanism

4.1.1 Principles

The indicator-based stall avoidance (ISA) mechanism introduced the new data indicator (NDI) to monitor the activity of each process in the multi-process SAW HARQ mechanism [55–57]. The NDI is simply a one-bit tag transmitted in the control chan-

nel. The status of the NDI is toggled whenever a new data packet is sent, or remained to be the same for the retransmitted packets. The basic principles of the indicator-based stall avoidance mechanism is illustrated in Fig. 4.3. We assume that a gap for packet PKT^* appears in the reordering buffer and process i receives packet PKT^+ with a sequence number larger than PKT^*. If it is a Type-I gap, the missing packet PKT^* may be transmitted by other $V - \{i\}$ processes, where V is the set of all parallel processes in the SAW HARQ mechanism. In contrast, if it is a Type-II gap, it will not be recovered by the MAC layer retransmission scheme. Note that an HARQ process with current transmission sequence number (TSN) will have a higher TSN for the subsequent packets. Thus, process i will not be able to transmit PKT^*. Then the indicator-based stall avoidance (ISA) mechanism is initialized and starts monitoring the states of all the other processes $V - \{i\}$. If these processes transmit new packets or other missing packets except for the expected PKT^*, it is implied that the gap PKT^* observed by receiving PKT^+ in process i will not be transmitted again. In the case, these processes terminate the monitoring procedures (i.e. enter the STOP state). Now PKT^* can be confirmed to be a Type-II gap. Hence, the stall avoidance mechanism starts the process of forwarding the received packets to the upper layer.

Note that the performance of the indicator-based stall avoidance mechanism highly relies on the robustness of the NDI. On the one hand, from the receiver perspective, if the control signal is damaged due to transmission errors, the receiver can not attain NDI information. Without the aid of NDI, the monitoring procedure of the indicator-based stall avoidance mechanism for a Type-II gap will be terminated. In this situation, the receiver should wait for a new control signal and then resume the monitoring procedure of the indicator-based stall avoidance mechanism [55]. As a result, the gap processing time will be further delayed. Moreover, the receiving packet in the traffic channel corresponding to the missing control signal will be dropped because even this packet passes the CRC test, the receiver can not know to which

Tab. 4.1: Nomenclatures of symbols

V	No. of parallel processes in SAW H-ARQ mechanism
S_0	REQUEST state
S_1, S_2	RESCHEDULE states
S_T	STOP state
x_n	State variable at the n-th transmission
P_e	Packet error rate
P_{old}	Probability of generating a retransmitted packet
P_{new}	Probability of generating a new packet
P_{sch}	Probability of a precess being scheduled
$P_{N \to A}$	Probability of a NACK-to-ACK error

process this packet belongs without the information of process identification carried by the control signal. On the other hand, from the transmitter perspective, the transmitter will randomly receives an erroneous NACK or ACK signal. If an erroneous NACK is received, the dropped data packet due to an erroneous control packet with the NDI information will be retransmitted. On the contrary, if an erroneous ACK is received, the dropped packet will not be retransmitted and a new Type-II gap appears in the reordering buffer at the receiving side. The analysis to include effect of damaged NDI goes beyond the scope of this chapter. Here, we only focus on the performance analysis of the indicator-based stall avoidance mechanism with the correct NDI information.

4.1.2 Problem Formulation

Referring to Fig. 4.1, we explain the monitoring procedure of the indicator-based stall avoidance mechanism with respect to each HARQ process. Fig. 4.2 shows the state transition diagram of the monitoring procedure. Table 4.1 lists the nomenclatures of the symbols used in the following. The state of a SAW HARQ process can be categorized into three different states: the REQUEST state, the RESCHEDULE states, and the STOP state. These three states are explained as follows:

1. REQUEST state (S_0):

   The REQUEST state (S_0) of a particular process in the SAW HARQ mechanism is the situation when a retransmitted packet is in error. Since the transmitted packet fails the the cyclic redundancy check (CRC) test, the TSN of this packet can not be known. Denote x_n the state variable at the n-th transmission. Then we have

   $$P(x_0 = S_0) = P_{old}P_e \ , \tag{4.1}$$

   where P_{old} is the probability of generating a retransmitted packet and P_e is its associated packet error rate (i.e. the probability of failing the CRC test for a packet). While the receiver requests retransmissions, the missing PKT^* may be still possibly transmitted by this HARQ process. The stall avoidance mechanism continues monitoring the state of this process until the receiver obtains the TSN information (i.e. the retransmitted packet passes the CRC), or the NDI changes to the NEW state. During this period, the HARQ process moves to the RESCHEDULE state, which will be discussed next.

2. RESCHEDULE states (S_1 and S_2):

   After the REQUEST state S_0, the receive process sends a NACK control signal back to its transmit process through its feedback control channel and then

enter the RESCHEDULE state: S_1 or S_2. If a NACK-to-ACK error occurs, the process transits to state S_1; otherwise, it changes to state S_2.

(a) The case with a NACK-to-ACK error (S_1):

Denote $P_{N \to A}$ the probability of a NACK becoming an ACK. From Fig. 4.1, we have the initial condition for state S_1:

$$P(x_0 = S_1) \;\; = \;\; P_{old} P_e P_{N \to A} \;. \tag{4.2}$$

The process will be latched in the reschedule state until it is scheduled to transmit a certain packet. Let the probability of a process being scheduled be P_{sch}. Then as shown in the left part of Fig. 4.2, the state transition probability between the REQUEST state S_0 and the RESCHEDULE state S_1 can be expressed as

$$P(x_n = S_1) \;\; = \;\; P(x_n = S_0) P_{N \to A} + P(x_{n-1} = S_1)(1 - P_{sch}) \;. \tag{4.3}$$

In this case, the NDI in the control channel will be changed to the NEW state for the subsequent packet and move to the STOP state, which will be discussed later.

(b) The case without a NACK-to-ACK error (S_2):

Referring to Fig. 4.1, the initial condition of S_2 can be written as

$$P(x_0 = S_2) \;\; = \;\; P_{old} P_e (1 - P_{N \to A}) \;. \tag{4.4}$$

In this chapter, the retransmitted packet will be scheduled for transmission with probability P_{sch} for the sake of fairness concern [48, 52]. Similar to the explanation in S_1, the HARQ process will remain in state S_2 until it is scheduled for transmission. Thus, from the right branch of Fig. 4.2, we

have

$$P(x_n = S_2) = P(x_n = S_0)(1 - P_{N \to A}) + P(x_{n-1} = S_2)(1 - P_{sch}) \ .$$

$$(4.5)$$

If the retransmitted packet in state S_2 fails the CRC test, the HARQ process returns to the REQUEST state S_0 and the TSN information can not be obtained. From Fig. 4.1, the state transition probability from S_2 to S_0 can be expressed as

$$P(x_{n+1} = S_0) = P(x_n = S_2)P_{sch}P_e \ . \qquad (4.6)$$

On the other hand, if the retransmitted packet in state S_2 passes the CRC test, the TSN information can be known and the HARQ process moves to the STOP state (S_T), which will be discussed next.

3. STOP state (S_T):

When the receiver receives a new packet or a retransmitted packet successfully, the state of the HARQ process will change to the STOP state (S_T). If this new packet is received, the stall avoidance mechanism knows that the missing packet will not be transmitted by this HARQ process.

If the retransmitted old packet is received, the stall avoidance mechanism can check the TSN to judge whether the received packet is the missing packet (PKT^*) or not. If so, as shown in Fig. 4.1, the indicator-based stall avoidance mechanism will terminate the monitoring procedures of all the HARQ processes because the hole in the receiving buffer is already filled. If not, the stall avoidance mechanism confirm that the missing packet will never be retransmitted by this process, either. The reason for this argument can be explained as follows. Due to the requirement of chase combining, it is usually the same pair of
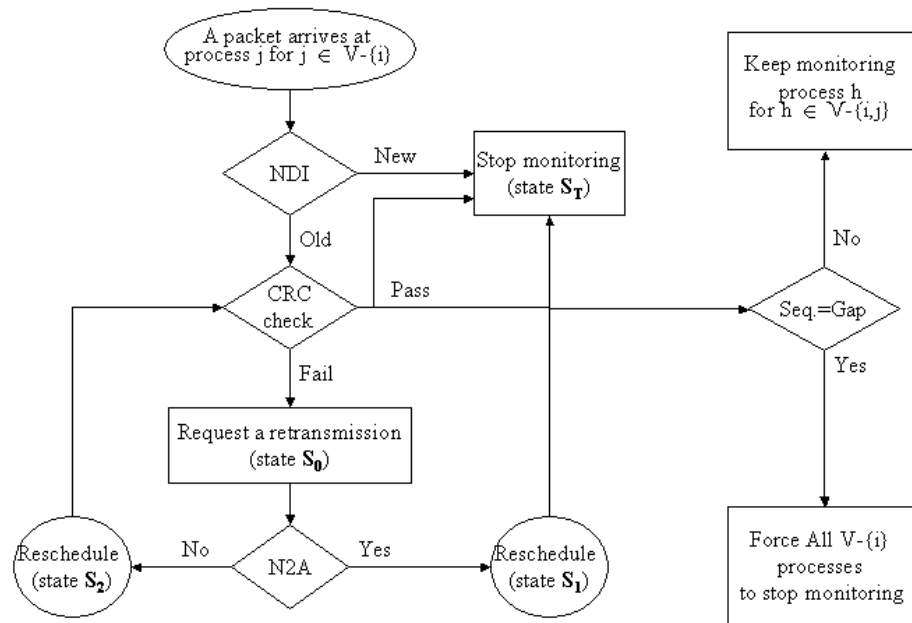
Fig. 4.1: The monitoring procedure of the indicator-based stall avoidance mechanism with respect to a particular process.

transmit and receive processes that is responsible for retransmitting the missing packet. That is, if a packet (PKT^*) is lost during the transmission in a certain HARQ process (PR^*), other parallel HARQ processes will not send the packet PKT^* for process PR^*. Consequently, process PR^* will be responsible for transmitting packet PKT^* before sending any other packets. As a result, when the TSN for the retransmitted packet is decoded successfully in a process and is not equal to that of the missing PKT^*, the stall avoidance mechanism stop monitoring this process.

According to the above discussions and Figs. 4.3 and 4.1, the state trans-
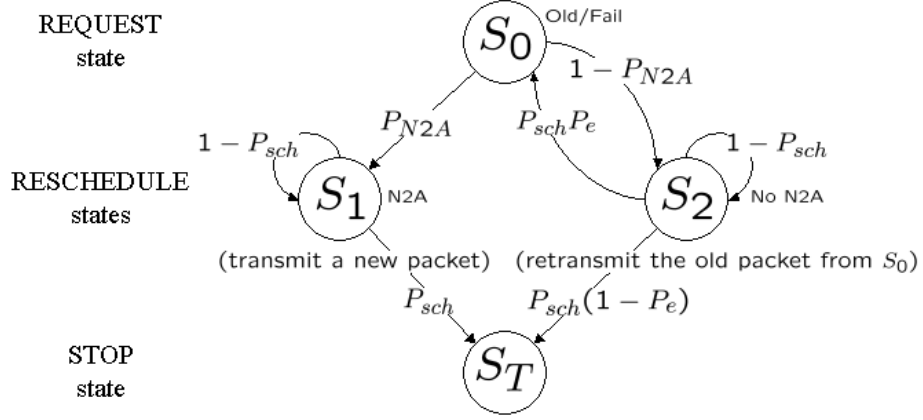
Fig. 4.2: The state transition diagram for the indicator-based stall avoidance mechanism.

mission between RESCHEDULE states and S_T can be expressed as

$$
\begin{aligned}
P(x_n = S_T) &= \text{Prob(receive a new packet due to a NACK-to-ACK error)} + \\
&\quad \text{Prob(receive an old packet and decode TSN successfully)} \\
&= P(x_{n-1} = S_1)P_{sch} + P(x_{n-1} = S_2)P_{sch}(1 - P_e) \ . \qquad (4.7)
\end{aligned}
$$

The initial condition of the STOP state S_T can be written as

$$
P(x_0 = S_T) = P_{new} + P_{old}(1 - P_e) \ , \qquad (4.8)
$$

where P_{new} is the probability of generating a new packet.

As shown in Fig. 4.3, when all the HARQ processes are in STOP state and the gap for the missing packet PKT^* still exists in the reordering buffer, then this gap can be identified as an unrecoverable Type-II gap. Now the stall avoidance mechanism can initiate the process of forwarding the received in-sequence packets
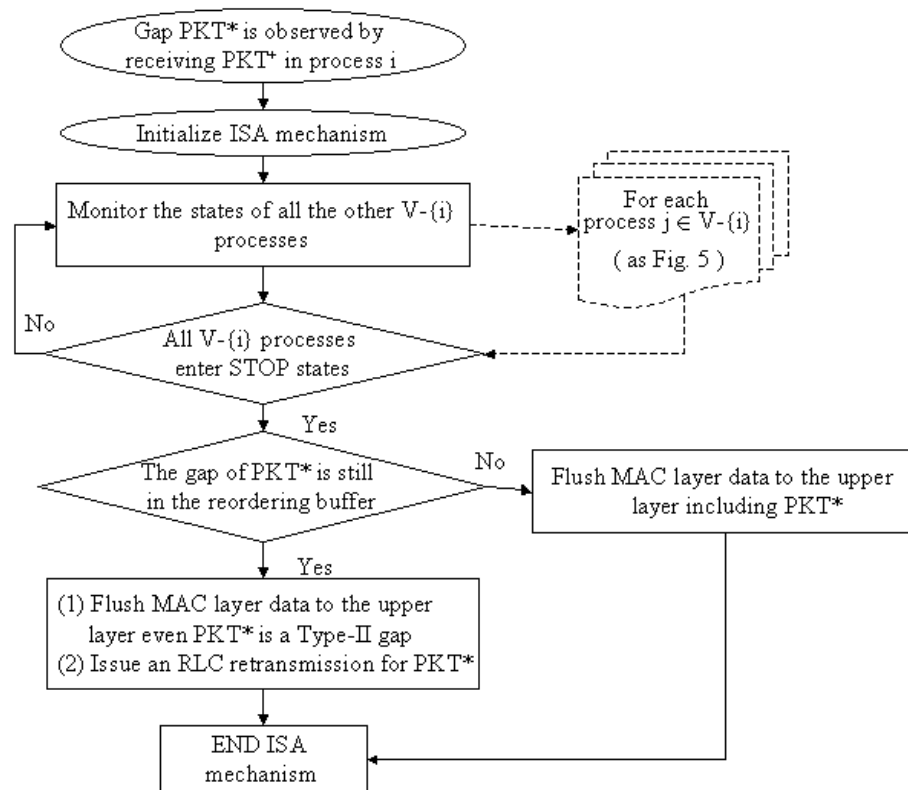
Fig. 4.3: The flowchart of the operations for the indicator-based stall avoidance mechanism.

with this Type-II gap from the MAC layer to the upper layer. In the meanwhile, a RLC layer retransmission request is issued for the missing packet PKT^*. Next we give an example to illustrate the function of the indicator-based stall avoidance mechanism.

4.1.3 Example

In this example, we consider a qual-process SAW HARQ mechanism. These four parallel HARQ processes are shared by multiple users. Thus, different HARQ processes may be assigned to transmit its data packets for a particular user depending on the

Tab. 4.2: An example of a Type-II gap being removed by the indication of receiving both new and old packets in a 4-process SAW HARQ mechanism.

Cycle	Process ID in 4-process SAW HARQ			
	Process 1 $(\text{TSN},S_c,\text{NDI})$	Process 2 $(\text{TSN},S_c,\text{NDI})$	Process 3 $(\text{TSN},S_c,\text{NDI})$	Process 4 $(\text{TSN},S_c,\text{NDI})$
i-1	...	...	...	...
i	(10,N→A,NEW)		(11,NACK,NEW)	
i+1				(12,NACK,NEW)
i+2		(13,ACK,NEW)	(11,ACK,OLD)	
i+3				(12,NACK,OLD)
i+4				(12,ACK,OLD)
i+5	(14,NACK,NEW)			

multiple users' requests in different cycles. Table 4.2 illustrates an example of the states of the qual-process SAW HARQ mechanism for a user from cycles i to $i + 5$. Here the period of one cycle is equal to four TTIs. Each field in the table is filled with a triplet variable, (TSN, S_c, NDI). TSN stands for the transmission sequence number. S_c is one of the three events in the feedback control channel: receive an ACK without errors (denoted by ACK), receive a $NACK$ without errors (denoted by $NACK$), and a NACK-to-ACK error occurs (denoted by $N{\rightarrow}A$). NDI is either NEW or OLD. Empty fields in the table mean the time slots that are assigned to other users or idle. In this example, we want to show that both the NDI in the control channel and the TSN in the data channel can be used to identify an unrecoverable Type-II gap. In this example, assume that packets with TSN $= 0 \sim 9$ of a particular user have been transmitted successfully by cycle $i - 1$. Now this target user has five packets with TSN $= 10 \sim 14$ requested for transmissions from the RLC layer. In the MAC layer, a scheduler will assign a number of HARQ processes to transmit these packets for this user in every 4-TTI cycle.

1. In cycle i, processes 1 and 3 send packets 10 and 11 for the target user, respectively, and both processes 2 and 4 are idle or used by other users. Assume that packet 10 is lost and its NACK signal is changed to an ACK signal, while the NACK signal of packet 11 is successfully sent to the corresponding process in the transmitter. The states of the four processes are $(-, -, -, -)$, where "$-$" stands for the NULL state. Note that the NACK signal for packet 10 is changed to ACK. The problem here is how the receiver knows the occurrence of the NACK-to-ACK error. This can be done by the help of the stall avoidance mechanism.

2. In cycle $i + 1$, packet 12 is scheduled for transmission in process 4. Assume this packet reaches the receiver successfully, but fails the CRC test. Hence, a NACK

signal is issued to request a retransmission. Up to now, packets 10, 11, and 12 are lost in process 1, 3, and 4, respectively. The HARQ mechanism still believes that these packets can be recovered by the normal retransmission procedures. Since the stall avoidance mechanism is not started yet, the states of the four parallel HARQ processes are still in $(-, -, -, -)$.

3. In the second TTI of cycle $i + 2$, processes 2 receives a new packet 13. When receiving packet 13, the receiver moves this packet to the reordering buffer of this user and makes this HARQ available for other new packets in the next cycle. However, packets 10, 11, 12 have not been received yet so that three holes for packets $10 \sim 12$ occur in the reordering buffer. To ensure these gaps can be filled in future transmissions, the stall avoidance mechanism is initiated to identify whether these missing packets are either recoverable Type-I gaps or unrecoverable Type-II gaps. Since packets 10, 11, and 12 will be transmitted by processes 1, 3, and 4 from a receiver viewpoint, the stall avoidance mechanism starts monitor the states of these processes. In the current situation with a new packet arriving at process 2, the states of the four parallel HARQ processes are $(-, S_T, -, -)$ according to Fig. 4.1.

In the the third TTI of cycle $i + 2$, process 3 receives a retransmitted old packet 11 and pass the CRC test. Note that due to the requirement of Chase combining, the retransmitted packet 11 is sent by the same HARQ process 3 in cycles i and $i + 2$. Since the hole of packet 11 is filled in the reordering buffer, the reordering buffer contains packets 11 and 13. In the meanwhile, process 3 enters the STOP state according to Fig. 4.3. Thus, the states of four HARQ processes change to $(-, S_T, S_T, -)$ and the stall avoidance mechanism keeps monitoring the states of processes 1 and 4.

4. In the forth TTI of cycle $i+3$, process 4 is scheduled to transmit an old packet 12

for the target user. Assume that packet 12 fails the CRC test again. According to the Fig. 4.1, process 4 enters the REQUEST state (S_0) and the states of the four parallel processes become ($-$, S_T, S_T, S_0). During the REQUEST state S_0, the receive process of the HARQ process 4 requests a retransmission for packet 12 by sending a NACK signal to the corresponding transmit process. Assume that this NACK signal successfully reaches the the transmit process, the state of process 4 changes to the RESCHEDULE state (S_2). Thus the states of the four parallel HARQ processes are now ($-$, S_T, S_T, S_2).

5. In the forth TTI of cycle $i+4$, process 4 is scheduled to retransmit packet 12 for the target user. This time packet 12 passes the CRC test and the TSN of packet 12 is obtained. Based on the information of TSN, packet 12 is moved to the reordering buffer and fills its gap. From Fig. 4.1, the state of process 4 enters the STOP state and the states of the four processes become ($-$, S_T, S_T, S_T). At this stage, packets 11, 12, and 13 are in the reordering buffer and an empty space is reserved for the missing packet 10. The stall avoidance mechanism continues monitoring process 1, which is the only left process possibly transmitting packet 10.

6. In cycle $i+5$, process 1 transmits a new packet 14 because the NACK signal of packet 10 is reverted to an ACK signal due to transmission errors in cycle i in the feedback control channel. Here, we assume that the new packet 14 is lost and a NACK signal is sent backed to the corresponding process in the transmitter. Since packet 14 is a new packet, the NDI in the control channel becomes the *NEW* state. Without the information of TSN of this packet in the traffic channel, the process 4 enters the STOP state (S_T). This shows the advantage of using NDI to shorten the gap processing time in the HARQ mechanism. According to Fig. 4.1 the status of the four parallel HARQ processes are now

$(S_T, \ S_T, \ S_T, \ S_T)$. Because the four processes are all in the STOP state and the gap for packet 10 is still in the reordering buffer, it is implied that the missing packet 10 is a nonrecoverable Type-II gap. Hence, the HARQ process should no longer wait for packet 10. As a consequence, the available in-sequence packets $11 \sim 13$ should be forwarded to the upper layer and an RLC layer retransmission request is issued for packet 10.

In the above example, we have shown how the indicator-based stall avoidance mechanism can recognize Type-II gap with the aids of NDIs in the control channel and TSNs in the data channel. In the considered example, the NDIs of processes 1 and 2 are used to confirm that these two processes do not possibly retransmit the missing packet 10. In addition, the information of TSN of processes 3 and 4 in the user data channel is used to judge that these two processes will not transmit the missing packet 10, either. With the cooperation of the NDI in the control channel and the TSN in the data traffic channel, the indicator-based stall avoidance can realize the fast physical/MAC layer retransmission for the HARQ mechanism. In the following section, we will present the analysis of the gap processing time of the indicator-based stall avoidance mechanism according to state transition diagram shown in Fig. 4.2.

4.2   Analysis

In this section, we present an analytical formula to calculate the average gap processing time of the indicator-based stall avoidance mechanism. The average gap processing time is an important performance metric for the high speed retransmission mechanism in both the MAC and RLC layers. For example, if a Type-II gap occurs, the received packets are queued in the reordering buffer of the MAC layer. Thus, a longer gap processing time causes a higher overflow probability in the MAC layer

reordering buffer. Furthermore, a Type-II gap will trigger an RLC retransmission. Thus, if the gap processing time is too long, a large-sized buffer in the RLC layer is required to accommodate the packets forwarded from the MAC layer. However, it is difficult to evaluate the gap processing time of the indicator-based stall avoidance mechanism in an analytic way. The gap processing time is a function with parameters from both the physical and the MAC layers. For example, in the physical layer, the packet error rate and the probability of a NACK becoming an ACK should be incorporated in this function, while in the MAC layer, the impact of the scheduling policy on the gap processing time should also be considered. Hence, to make the analysis tractable, we has made the following assumptions:

1. A fair scheduler independently assigns each process to each user with a probability of $P_{sch} = 1/K$, where K is the number of users in the system.

2. Because a NACK-to-ACK error usually occurs when a mobile terminal moves at high speeds, it is assumed that the fast changing channel is modelled by an independent Rayleigh fading channel from one packet to another packet.

3. In the receiving end, a reordering buffer is assigned to a user to handle the received packets from multiple parallel HARQ processes.

4. Effects of incremental redundancy and Chase combining have not been considered in the analytical model yet. Thus the provided analysis can be viewed as a worst-case analysis compared to the cases applying incremental redundancy and Chase combining.

5. The feedback delay of sending an ACK or a NACK in an individual HARQ process is not taken into account of the gap processing time. In HSDPA, multiple parallel HARQ processes transmit data packets alternately to fully utilize the channel capacity. Thus the feedback delay of sending control signals does

not affect the gap processing time. In the feedback channel, only the impact of NACK-to-ACK errors is considered.

Now we prove that the average gap processing time of the indicator-based stall avoidance mechanism for the multiple parallel HARQ processes can be calculated by the following proposition.

Proposition 1: *Consider an V-process SAW HARQ process. For a given packet error rate (P_e) and the probability of an NACK-to-ACK error ($P_{N \to A}$), define the probability of generating new packets and old packets as*

$$P_{new} = (1 - P_e) + P_e P_{N \to A} \tag{4.9}$$

and

$$P_{old} = P_e(1 - P_{N \to A}) \ , \tag{4.10}$$

respectively. Then, the gap processing time for the indicator-based stall avoidance method can be calculated as follows:

$$\overline{GPT} = \sum_{k=1}^{C_V} \left\{ kV P_{sch}(1 - P_{sch})^{k-1} \left[\sum_{i=0}^{k-1} P(x_i = S_T) \right]^{V-1} + \sum_{m=2}^{V} (m - 1 + kV) \times \right.$$

$$\left. \sum_{\ell=1}^{k} P_{sch}(1 - P_{sch})^{\ell-1} \left[\sum_{i=0}^{k} P(x_i = S_T) \right]^{m-2} P(x_k = S_T) \left[\sum_{j=0}^{k-1} P(x_j = S_T) \right]^{V-m} \right\}.$$

$$\tag{4.11}$$

where

$$P(x_0 = S_T) = P_{new} + P_{old}(1 - P_e) \ ,$$

and

$$P(x_n = S_T) = P_{old}P_{sch} \left[P_e P_{N \to A} + P_{old}(1 - P_e) \right] \left[P_{sch}P_{old} + (1 - P_{sch}) \right]^{n-1} n \geq 1 \ .$$

$$\tag{4.12}$$

The parameter C_V in (4.11) is the required cycles to involve all processes in the V-process SAW HARQ to remove a Type-II gap, and the other parameters V, P_{sch}, and $P(x_n = S_T)$ are already defined in Section 4.1.

Proof: Assume that a Type-II gap appears in cycle 0 of process PR_1 as shown in Fig. 4.4. We now consider the following two possible scenarios to calculate the average gap processing time.

(I) Type-II gap can be removed at process 1:

When all the SAW HARQ processes except PR_1 enter the STOP state (S_T), the gap will be removed at process 1 when process 1 enters the STOP state in the future. Process 1 will transmit a new packet whenever it is scheduled to transmit a packet in the k-th cycle because the NACK signal for the missing packet is contaminated to be an ACK signal. Hence, this new packet sent by process 1 is associated with a NEW NDI state. Consequently, the state of process 1 enters the STOP state at k-th cycle. Since all (V) processes enter the STOP state and the gap of the missing packet is still in the reordering buffer, the receiver can judge that the missing packet is a Type-II gap and will never be retransmitted. In this case, the receiver takes a period of kV TTIs to remove this Type-II gap from the reordering buffer, where other ($V-1$) processes turn to the STOP state before k-th cycle. Denote E_A and E_B the event that process 1 being scheduled for transmission at the k-th cycle and that all other ($V-1$) processes enter the STOP state before the k-th cycle, respectively. Then, it is followed that

$$P(E_A) = P_{sch}(1 - P_{sch})^{k-1} \tag{4.13}$$

and

$$P(E_B) = \left[\sum_{i=0}^{k-1} P(x_i = S_T)\right]^{V-1}. \tag{4.14}$$

Recall that

$$P(x_n = S_T) = P(x_{n-1} = S_1)P_{sch} + P(x_{n-1} = S_2)P_{sch}(1 - P_e) \ , \ \ n \geq 1 \ .$$

By iteratively substituting (4.2)-(4.6) into (4.7), we obtain

$$P(x_n = S_T) = P_{old}P_{sch}\left[P_e P_{N \to A} + P_{old}(1 - P_e)\right]\left[P_{sch}P_{old} + (1 - P_{sch})\right]^{n-1}, n \geq 1 \ .$$

$$(4.15)$$

Because events E_A and E_B are mutually independent, the probability of the Type-II gap being removed in the k-th cycle of process 1 can be expressed as

$$P(E_A \cap E_B) = P(E_A)P(E_B) \ . \tag{4.16}$$

Combining (4.13), (4.14), and (4.15), the average gap processing time to remove a Type-II gap at process 1 is

$$\overline{GPT}_I = \sum_{k=1}^{C_V} kV \times P(E_A)P(E_B)$$

$$= \sum_{k=1}^{C_V} kV \times P_{sch}(1 - P_{sch})^{k-1}\left[\sum_{i=0}^{k-1} P(x_i = S_T)\right]^{V-1}, \tag{4.17}$$

where C_V is the required cycles of involving all processes in the V-process SAW HARQ to remove a Type-II gap.

(II) Type-II gap can be removed at process m, for $m \geq 2$:

Assume that the Type-II gap is removed in the k-th cycle of process m, where $m \geq 2$ and $k \geq 1$. In this case, the gap processing time is $(m-1+kV)$ TTIs, as shown in Fig. 4.4. Denote $P_\alpha(m, k)$ as the probability of process m removing the Type-II gap in the k-th cycle for different combinations of k and m. Then, the average gap processing time for the Type-II gap being removed at process m, where $m \geq 2$, can

be expressed as

$$\overline{GPT}_{II} = \sum_{k=1}^{C_V} \sum_{m=2}^{V} (m - 1 + kV) P_\alpha(m, k) \ , \tag{4.18}$$

where C_V is defined in (4.17). The probability $P_\alpha(m, k)$ is the joint probability of following four independent events:

$$\begin{cases} P(E_1) & = & P(\text{Process 1 enters the STOP state within the } k\text{-th cycle}) \\ P(E_2) & = & P(\text{The first } m - 2 \text{ processes enter the STOP state within the } k\text{-th cycle}) \\ P(E_3) & = & P(\text{The Process } m \text{ enters the STOP state at the } k\text{-th cycle}) \\ P(E_4) & = & P(\text{The last } V - m \text{ processes enter the STOP state before the } k\text{-th cycle}) \ . \end{cases} \tag{4.19}$$

Note that

$$P_\alpha(m, k) = P(E_1)P(E_2)P(E_3)P(E_4) \ . \tag{4.20}$$

Similar to the procedures of deriving (4.13) and (4.14), we can rewrite (4.19) as

$$\begin{cases} P(E_1) = \sum_{\ell=1}^{k} P_{sch}(1 - P_{sch})^{\ell-1} \\ P(E_2) = [\sum_{i=0}^{k} P(x_i = S_T)]^{m-2} \\ P(E_3) = P(x_k = S_T) \\ P(E_4) = [\sum_{j=0}^{k-1} P(x_j = S_T)]^{V-m} \ . \end{cases} \tag{4.21}$$

Substituting (4.20) and (4.21) into (4.18), we can have the probability of removing the Type-II gap at process m, where $m \geq 2$, as

$$\overline{GPT}_{II} = \sum_{k=1}^{C_V} \sum_{m=2}^{V} (m - 1 + kV) P_\alpha(m, k)$$

$$= \sum_{k=1}^{C_V} \sum_{m=2}^{V} (m - 1 + kV) \overbrace{\sum_{\ell=1}^{k} P_{sch}(1 - P_{sch})^{\ell-1}}^{Process\ 1} \overbrace{\left[\sum_{i=0}^{k} P(x_i = S_T)\right]^{m-2}}^{The\ first\ m-2\ processes} \overbrace{P(x_k = S_T)}^{Process\ m} \times$$

$$\overbrace{\left[\sum_{j=0}^{k-1} P(x_j = S_T)\right]^{V-m}}^{The\ last\ V-m\ processes} . \tag{4.22}$$

Note that the value of C_V can be obtained by satisfying the following equation:

$$\sum_{k=1}^{C_V} \left\{ P_{sch}(1 - P_{sch})^{k-1} \left[\sum_{i=0}^{k-1} P(x_i = S_T)\right]^{V-1} + \sum_{m=2}^{V} \sum_{\ell=1}^{k} P_{sch}(1 - P_{sch})^{\ell-1} \times \right.$$

$$\left. \left[\sum_{i=0}^{k} P(x_i = S_T)\right]^{m-2} P(x_k = S_T) \left[\sum_{j=0}^{k-1} P(x_j = S_T)\right]^{V-m} \right\} = 1 . \tag{4.23}$$

With (4.17) and (4.22), the average gap processing time for the indicator-based stall avoidance mechanism with multiuser communications is equal to

$$\overline{GPT} = \overline{GPT}_I + \overline{GPT}_{II}$$

$$= \sum_{k=1}^{C_V} \left\{ kV P_{sch}(1 - P_{sch})^{k-1} \left[\sum_{i=0}^{k-1} P(x_i = S_T)\right]^{V-1} + \sum_{m=2}^{V} (m - 1 + kV) \times \right.$$

$$\left. \sum_{\ell=1}^{k} P_{sch}(1 - P_{sch})^{\ell-1} \left[\sum_{i=0}^{k} P(x_i = S_T)\right]^{m-2} P(x_k = S_T) \left[\sum_{j=0}^{k-1} P(x_j = S_T)\right]^{V-m} \right\} . \tag{4.24}$$

	Cycle 0	Cycle 1	Cycle 2	Cycle 3	Cycle 4	···	Cycle k	···
PR_1	G	V	2V	3V	4V	···	kV	···
PR_2		1+V	1+2V	1+3V	1+4V	···	1+kV	···
PR_3		2+V	2+2V	2+3V	2+4V	···	2+kV	$\}$ m-2 ···
	⋮	⋮	⋮	⋮	⋮	⋮	⋮	⋮
PR_m		(m-1)+V	(m-1)+2V	(V-1)+3V	(m-1)+4V	···	(m-1)+kV	···
	⋮	⋮	⋮	⋮	⋮	⋮	⋮	$\}$ V-m ⋮
PR_M		(V-1)+V	(V-1)+2V	(V-1)+3V	(V-1)+4V	···	(V-1)+kV	···

Fig. 4.4: An illustration for the gap processing time of the indicator-based stall avoidance mechanism.

■
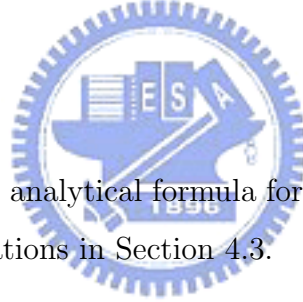
The accuracy of the analytical formula for estimating the gap processing time will be validated by simulations in Section 4.3.

4.3   Numerical Results

In this section, through simulations and analysis, we investigate the performance of the indicator-based stall avoidance mechanism in the Rayleigh fading channel. In the considered case, each process in the multi-process SAW HARQ mechanism is shared by multiple users based on the Round-Robin scheduling policy.

Fig. 4.5 compares the average gap processing time of the multi-process SAW HARQ mechanism for various numbers of processes. We consider a time varying Rayleigh fading channel with the Doppler frequency equal to 100 Hz, which is the case when a mobile moves at the speeds of 54 km/hour with a carrier frequency of

2 GHz. Let the packet error rate (P_e) be 0.12. As shown in the figure, the more the parallel processes in the SAW HARQ mechanism, the longer the average gap processing time. The analytical results are validated by the simulation results. In the case with 9 users, the average gap processing times for the V-process SAQ HARQ mechanism are 38.84, 57.86 and 79.23 TTIs for $V = 4$, 6, and 8, respectively. Each TTI is equal to 2 msec. One can observe that the average gap processing time of the 8-process SAW HARQ mechanism is about two times higher than that of the 4-process SAW HARQ mechanism. From [66], delay is suggested to be less than 50 TTIs (i.e., 0.1 sec) in order to provide acceptable QoS. The developed analytical formula of average gap processing time can be used to compute the appropriate number of allowable users in the system. For instance, based on the results shown in the figure, 5 users can be allowed to stay in a 8-process SAW HARQ system, whereas 11 users can be supported in a system with 4 parallel SAW HARQ processes. This example shows that the gap processing time significantly affects the RLC retransmission delay, thereby becoming an important issue in QoS provisioning when the number of users is large.

One of advantages in the proposed analytical models is to abstract physical layer impacts into some key parameters, such as packet error rates (P_e). Since users may have various traffic types and accordingly different requirements on P_e, the developed analytical model can quickly estimate the gap processing time for various values of P_e and various numbers of parallel HARQ processes, as shown in Fig. 4.6. In the case with five users, we see that when $P_e < 0.2$, the gap processing time is linearly proportional to the number of processes in the multi-process SAW HARQ mechanism. However, if $P_e > 0.25$, the gap processing time exponentially increases as the number of the parallel processes of the SAW HARQ mechanism increases. This observation indicates that the sharply increasing gap processing time can not be ignored when P_e requirement is stringent. For example, as the delay constraint is
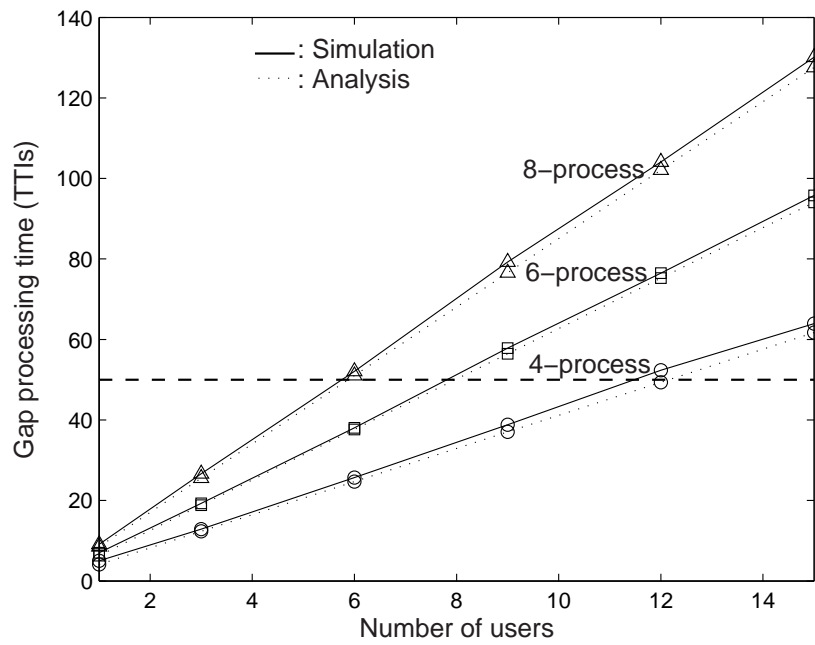
Fig. 4.5: The impact of number of users on the average gap processing time for 4, 6, 8-process SAW HARQ mechanisms in a Rayleigh channel with Doppler frequency of 100 Hz and $P_e = 0.12$.
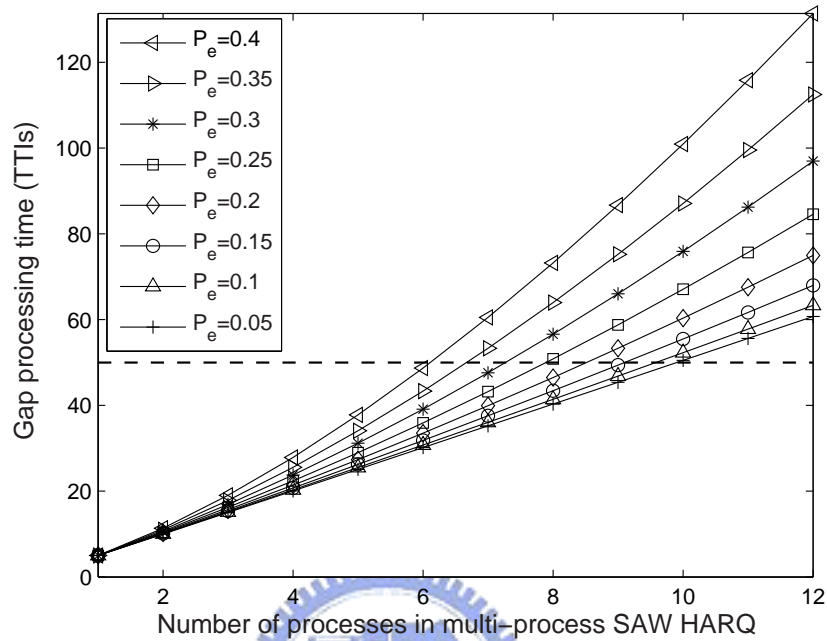
Fig. 4.6: The impact of number of processes in the multi-process SAW HARQ mechanism on the performance of average gap processing time for different P_es with 5 users in the system.

set to be less than 50 TTIs, the allowable numbers of parallel SAW HARQ processes are 5 and 10 for $P_e = 0.4$ and 0.05, respectively. An interesting research topic is to determine the optimal number of parallel SAW HARQ processes to improve the overall system performance by taking both throughput and gap processing time into account.

Another interesting application of the developed analytical model is to evaluate the number of allowable users in the system from the QoS provision perspective. Fig. 4.7 illustrates the average gap processing time against the number of users for various P_e requirement in a 6-process SAW HARQ mechanism. As shown in the figure, as the number of users increases, the gap processing time increases linearly. The slope of the

performance curve between the gap processing time against the number of users with high P_e region is steeper than that with low P_e region. Furthermore, for a required RLC delay constraint, the higher the value of P_e, less the number of user can be supported by the system. For example, for a RLC delay constraint of 50 TTIs, the allowable numbers of users in the system with a 50 TTIs delay limit are 4 and 8 when $P_e = 0.4$ and 0.05, respectively. The reason for this phenomenon is that the TSN information in the data traffic channel can be obtained earlier when the P_e is lower. With the aid of the TSN information, the indicator-based stall mechanism can enter the STOP state earlier. Thus, in a channel with high P_e, it is implied that a suitable call admission control scheme is necessary for the SAW HARQ system to guarantees the QoS provisioning.

4.4   Chapter Summary

In this chapter, we have presented a closed-form expression for the average gap processing time of the indicator-based stall avoidance mechanism for the HSDPA system with interleaving scheduling. If a NACK-to-ACK error occurs in the MAC layer HARQ mechanism, a non-recoverable gap also appears in the reordering buffer of the received packets for a specific user. Longer gap processing time will delay the necessary higher layer RLC retransmissions, thereby degrading the system performance seriously from a higher layer user perspective. Thus, it is of importance to develop an analytical method to calculate the gap processing time from both physical layer and MAC perspectives without time-consuming simulations.

The developed analytical model can facilitate the evaluation of the gap processing time of the multi-process SAW HARQ mechanism in the HSDPA system for different packet error rates, the numbers of allowable users, and the numbers of parallel processes in the SAW HARQ mechanism. From our analytical and simulation
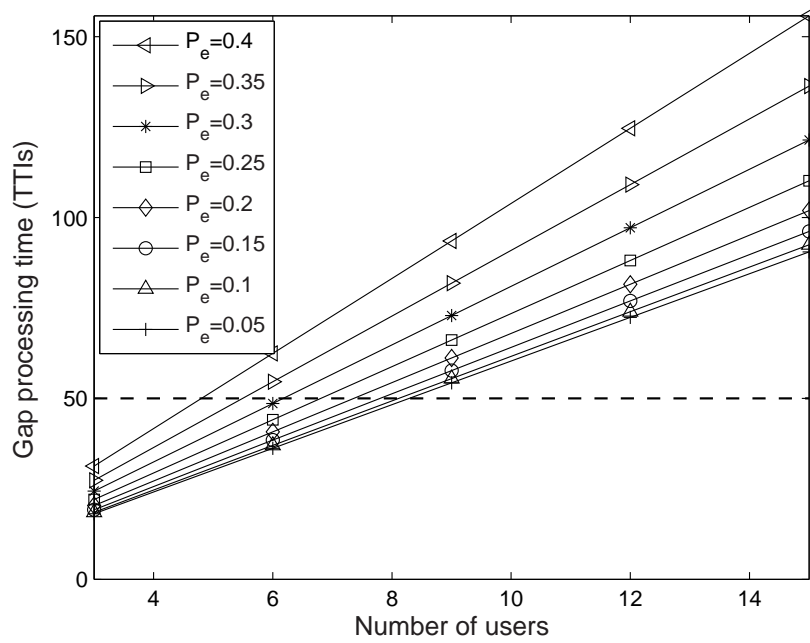
Fig. 4.7: The impact of the number of users on the average gap processing time with various packet error rates in a 6-process SAW HARQ mechanism.

results in a Rayleigh fading channel, we find that throughput enhancement by adding the parallel processes in the SAW HARQ mechanism comes at the cost of longer average gap processing time. For moderate packet error rates, the gap processing time is linearly proportional to the number of users and the number of the parallel HARQ processes. However, in the situation of high packet error rates, the average gap processing time almost exponentially increases when the number of parallel SAW HARQ processes increases.

Chapter 5

Effects of Power Control Errors and Complete Multiple Access Interference on Uplink MC-DS-CDMA

In this chapter, we will develop an analytical method to evaluate the joint effects of the power control errors (PCEs) and the complete multiple access interference (MAI) on the multi-rate multi-carrier direct-sequence code division multiple access (MC-DS-CDMA) system. MC-DS-CDMA becomes an attractive technique for the future fourth generation (4G) wireless system because it can flexibly adapt transmission rates by changing both time and frequency spreading factors and possesses many physical layer advantages in dispersive fading channels. However, the PCE and complete MAI from all the inter-subcarriers may significantly degrade the performance of the MC-DS-CDMA system. Conventionally, the influence of the PCE for the single-carrier DS-CDMA was analyzed by the first order Taylor expansion method. However, the analysis is only valid for a small PCE and small diversity order. Thus, in this chapter, we apply the Hermite summation method to evaluate the effect of a larger PCE and a higher diversity order for the multi-carrier DS-CDMA system.

5.1 System Model

5.1.1 Transmitted Signal

The transmitter structure in the MC-DS-CDMA system using both time and frequency domain spreading codes is shown in Fig. 5.1. First, the serial-to-parallel pro-
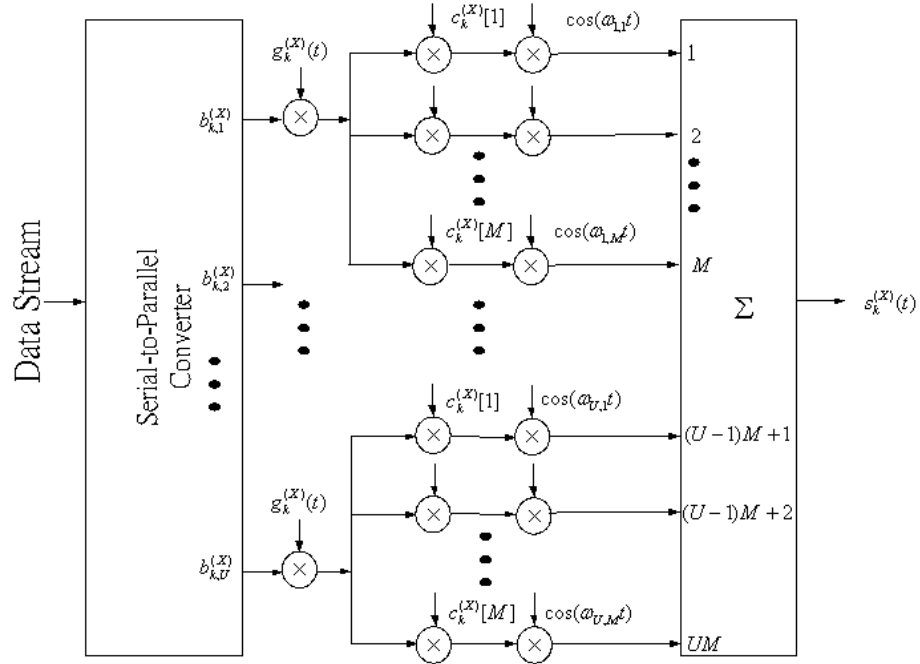
Fig. 5.1: The transmitter structure of the MC-DS-CDMA system using time and frequency domain spreading codes.

cess converts a data streams with the duration of $T_{b,k}^{(\mathbf{X})}$ to U slower parallel with bit duration $T_k^{(\mathbf{X})} = UT_{b,k}^{(\mathbf{X})}$, where k is the user index and the user group $\mathbf{X} \in \mathbf{A_u}, \mathbf{B_u}, \mathbf{C_u}$ will be defined later. After the serial-to-parrel processing, unlike that the original data stream is transmitted in a frequency selective fading channel, each substream is now transmitted in a frequency flat (or non-dispersive) fading channel. In the next step, the data in each substream are spread by a time domain spreading code $g_k^{(\mathbf{X})}(t)$. Being copied to M subcarriers, each substream is multiplied by a frequency domain spreading code $\{c_k^{(\mathbf{X})}[j]\}$.

The transmitted signal of user k in group $\mathbf{X}$ can be expressed as

$$s_k^{(\mathbf{X})}(t) = \sum_{i=1}^{U} \sum_{j=1}^{M} \sqrt{\frac{2\lambda_k^{(\mathbf{X})} P_k^{(\mathbf{X})}}{M}} b_{k,i}^{(\mathbf{X})}(t) g_k^{(\mathbf{X})}(t) c_k^{(\mathbf{X})}[j] \cos(2\pi f_{i,j} t + \varphi_{k,i,j}^{(\mathbf{X})}) \ , \quad (5.1)$$

where $P_k^{(\mathbf{X})}$ and $\lambda_k^{(\mathbf{X})}$ respectively represent the transmitted power and the power control errors (PCE), while $\{f_{i,j}\}$ and $\{\varphi_{k,i,j}^{(\mathbf{X})}\}$ represent the subcarrier frequency and the initial phase for the j-th carrier of the i-th substream, respectively. The waveform in the i-th substream $b_{k,i}^{(\mathbf{X})}(t) = \sum_{h=-\infty}^{\infty} b_{k,i}^{(\mathbf{X})}[h] P_{T_k^{(\mathbf{X})}}(t - hT_k^{(\mathbf{X})})$ consists of a sequence of independent rectangular pulses with duration $T_k^{(\mathbf{X})}$, where $b_{k,i}^{(\mathbf{X})}[h] = \pm 1$ with equal probability. The time domain spreading code $g_k^{(\mathbf{X})}(t) = \sum_{\ell=-\infty}^{\infty} g_k^{(\mathbf{X})}[\ell] P_{T_c}(t - \ell T_c)$ represents the chip sequence of the rectangular pulses of duration T_c, where $g_k^{(\mathbf{X})}[\ell] = \pm 1$ with equal probability. Note that the time domain spreading factor of user k in the group $\mathbf{X}$ is $G_k^{(\mathbf{X})} = T_k^{(\mathbf{X})}/T_c$.

The user group $\mathbf{X}$ is defined as follows. Let $g_o(t)$ and $c_o[j]$ be the time domain spreading code and frequency domain spreading code of the reference user, respectively. As in [68], we categorize the interfering users into three groups:

1. group $\mathbf{A_u}$: the user utilizing a time domain spreading code $g_k^{(\mathbf{A_u})}(t) = g_o(t)$ and a frequency domain spreading code $c_k^{(\mathbf{A_u})}[j] \neq c_o[j]$.

2. group $\mathbf{B_u}$: the user utilizing a time domain spreading code $g_k^{(\mathbf{B_u})}(t) \neq g_o(t)$ and a frequency domain spreading code $c_k^{(\mathbf{B_u})}[j] = c_o[j]$.

3. group $\mathbf{C_u}$: the user utilizing a time domain spreading code $g_k^{(\mathbf{C_u})}(t) \neq g_o(t)$ and a frequency domain spreading code $c_k^{(\mathbf{C_u})}[j] \neq c_o[j]$.

Noteworthily, $g_k^{(\mathbf{X})}(t) \neq g_o(t)$ (or $c_k^{(\mathbf{X})}[j] \neq c_o[j]$) can also be the case with the same particular pseudo-noise sequence offset by two different values.

5.1.2 Received Signal

Since each substream is sent in the flat Rayleigh fading channel, the received signal
of the reference user (denoted by r_o), can be expressed as:

$$
\begin{aligned}
r_o(t) &= \sum_{i=1}^{U}\sum_{j=1}^{M}\sqrt{\frac{2\lambda_o P_o}{M}}\alpha_{o,i,j}b_{o,i}(t-\tau_o)g_o(t-\tau_o)c_o[j]\cos(2\pi f_{i,j}t+\phi_{o,i,j}) + \\
&\quad \sum_{\mathbf{X}\in\{\mathbf{A_u},\mathbf{B_u},\mathbf{C_u}\}}\sum_{k=1}^{K_{\mathbf{X}}}\sum_{i=1}^{U}\sum_{j=1}^{M}\sqrt{\frac{2\lambda_k^{(\mathbf{X})}P_k^{(\mathbf{X})}}{M}}\alpha_{k,i,j}^{(\mathbf{X})}b_{k,i}^{(\mathbf{X})}(t-\tau_k^{(\mathbf{X})}) \times \\
&\quad g_k^{(\mathbf{X})}(t-\tau_k^{(\mathbf{X})})c_k^{(\mathbf{X})}[j]\cos(2\pi f_{i,j}t+\phi_{k,i,j}^{(\mathbf{X})}) + n(t)\ ,
\end{aligned}
\tag{5.2}
$$

where P_o and λ_o respectively represent the transmitted power and the power control
errors (PCE) of the reference user; $\alpha_{o,i,j}$ and $\alpha_{k,i,j}^{(\mathbf{X})}$ are the channel's amplitude of the
reference user and that of the k-th user in group $\mathbf{X}$, respectively; τ_o is the propagation
delay for the reference user which is assumed to be $\tau_o = 0$ without loss of general-
ity; $\tau_k^{(\mathbf{X})}$ is the misalignment with respect to the reference user, which is uniformly
distributed in the time interval $[0, T_k^{(\mathbf{X})})$; $K_{\mathbf{X}}$ is the number of users in the group $\mathbf{X}$;
and $n(t)$ is the white Gaussian noise with double-sided power spectrum density of
$N_0/2$. In (7.2), $\phi_{o,i,j} = \varphi_{o,i,j} + \psi_{o,i,j} - 2\pi f_{i,j}\tau_o$ and $\phi_{k,i,j}^{(\mathbf{X})} = \varphi_{k,i,j}^{(\mathbf{X})} + \psi_{k,i,j}^{(\mathbf{X})} - 2\pi f_{i,j}\tau_k^{(\mathbf{X})}$
are uniformly distributed in $[0, 2\pi)$, where $\varphi_{o,i,j}$ and $\psi_{o,i,j}$ are the initial phase and
the channel's phase of the reference user, and $\varphi_{k,i,j}^{(\mathbf{X})}$ and $\psi_{k,i,j}^{(\mathbf{X})}$ are those for the k-th
user in group $\mathbf{X}$, respectively.

The receiver structure of the MC-DS-CDMA system using time-domain and
frequency-domain spreading codes is shown in Fig. 5.2. Without loss of generality, let
the bit of interest be the first bit in the s-th substream of the reference user (denoted
by $b_{o,s}[0]$). After time domain despreading, the output variable in the v-th subcarrier

of the s-th substream for the reference user can be expressed as:

$$Y_{o,s,v} = \int_0^{T_o} r_o(t)\beta_{o,s,v}g_o(t)c_o[v]\cos(2\pi f_{s,v}t + \phi_{o,s,v})dt$$

$$= \sqrt{\frac{\lambda_o P_o}{2M}}T_o\left\{b_{o,s}[0]\alpha_{o,s,v}\beta_{o,s,v} + \sum_{\mathbf{X}\in\{\mathbf{A_u},\mathbf{B_u},\mathbf{C_u}\}}\left[\sum_{k=1}^{K_{\mathbf{X}}}I_{\mathbf{X},k}^{(1)} + \sum_{k=1}^{K_{\mathbf{X}}}\underbrace{\sum_{i=1}^{U}\sum_{j=1}^{M}}_{j\neq v \text{ for } i=s}I_{\mathbf{X},k}^{(2)}\right] + n_{s,v}\right\},$$

$$(5.3)$$

where P_o and T_o are the transmit power and the bit duration of the reference user; $\beta_{o,s,v}$ is the weights for a certain combining scheme; $I_{\mathbf{X},k}^{(1)}$ and $I_{\mathbf{X},k}^{(2)}$ denote the MAI from the main subcarrier and that from other inter-subcarriers, respectively; and $n_{s,v}$ is the white Gaussian noise with zero mean and variance of $\frac{|\beta_{o,s,v}|^2}{2\lambda_o}(\frac{E_o}{MN_0})^{-1}$, where $E_o = P_oT_o$ is the bit energy of the reference user. Combining M subcarriers, the decision variable of $b_{o,s}[0]$ for the reference user becomes

$$Y_{o,s} = \sum_{v=1}^{M}Y_{o,s,v} \;, \qquad (5.4)$$

where $Y_{o,s,v}$ is given in (5.3).

5.1.3 Assumption

To make $Y_{o,s}$ have the maximal diversity combining gain, we assume that the associated M subcarriers in (5.4) experience independent fading. For this purpose, any two neighboring subcarriers in the same substream are at least separated by the maximal coherent bandwidth, denoted by $\mathbf{max}(BW_c)$. Denote Δ_f the minimal frequency spacing between any two adjacent substreams with the same subcarrier index. Then $f_{i,j}$ (the frequency of the j-th subcarrier of the i-th substream) can be determined by
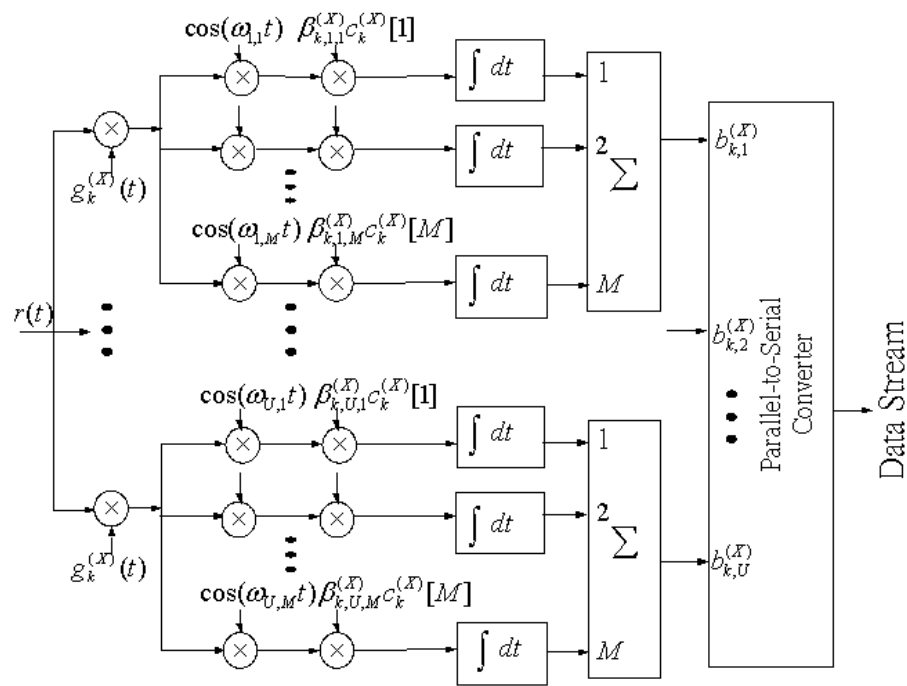
Fig. 5.2: The receiver structure of the MC-DS-CDMA system using time and frequency domain spreading codes.

the following rule:

$$f_{i,j} = f_o + [(i-1) + (j-1)U]\Delta_f, \text{ for } \begin{cases} 1 \le i \le U \\ 1 \le j \le M \end{cases}, \tag{5.5}$$

where f_o is the main carrier frequency. In order to achieve the maximum diversity combining gain in (5.4), the following condition

$$U\Delta_f \ge \mathbf{max}(BW_c) , \tag{5.6}$$

should be satisfied, where U is the size of the serial-to-parallel process. Note that the system bandwidth is proportional to UMG_o/T_o. For a fixed total number of subcarriers (UM), U should be large enough to satisfy the condition of (5.6). Otherwise, the assumption of independent subcarriers may become less realistic.

5.2   Effect of Complete MAI on BER Performance

5.2.1   Motivation

The complete MAI in a multi-rate MC-DS-CDMA system is defined as the sum of the other users's interference form their main subcarrier and all the other inter-subcarriers. For any two synchronous transmissions at subcarriers $f_{s,v}$ and $f_{i,j}$ with the initial phase $\phi_{s,v}$ and $\phi_{i,j}$, respectively, the orthogonality requirement

$$\int_0^{T_c} \cos(2\pi f_{s,v}t + \phi_{s,v})\cos(2\pi f_{i,j}t + \phi_{i,j})dt = 0 \tag{5.7}$$

can be fulfilled if the following condition is sustained:

$$|f_{s,v} - f_{i,j}| = \frac{h}{T_c} , \tag{5.8}$$

where h is non-zero positive integer and T_c is the chip duration.

However, for asynchronous users, the orthogonality condition between subcarriers can not be held anymore. Assume that the reference user and the interfering user k in group $\mathbf{X}$ is misaligned by τ, where $0 < \tau < T_c$. As shown in Fig. 5.3, we consider the $(n+1)$-th chip of the reference user, during which the interfering user sends part of the $(m+1)$-th chip and part of the $(m+2)$-th chip. Recall that $g_o[n]$ denotes the $(n+1)$-th chip of the spreading code of the reference user and $g_k^{(\mathbf{X})}[m]$ denotes the $(m+1)$-th chip of the spreading code of the interfering user. Suppose that the reference and the interfering users transmit data at subcarriers $f_{s,v}$ and $f_{i,j}$, respectively, and define the unit step function $H(t)$ as

$$H(t) = \begin{cases} 1, & t \geq 0 \ , \\ 0, & t < 0 \ . \end{cases} \tag{5.9}$$

We can express the cross-correlation between the two subcarriers $f_{s,v}$ and $f_{i,j}$ during the $(n+1)$-th chip as

$$\int_{nT_c}^{(n+1)T_c} g_o[n]\cos(2\pi f_{s,v}t + \phi_{s,v}) \Big[g_k^{(\mathbf{X})}[m][H(nT_c)-$$

$$H(nT_c + \tau)] + g_k^{(\mathbf{X})}[m+1][H(nT_c + \tau) - H((n+1)T_c)]\Big]\cos(2\pi f_{i,j}(t-\tau) + \phi_{i,j})dt$$

$$= \ g_o[n]g_k^{(\mathbf{X})}[m] \int_{nT_c}^{nT_c+\tau} \cos(2\pi f_{s,v}t + \phi_{s,v})\cos(2\pi f_{i,j}t + \phi_{i,j} - 2\pi f_{i,j}\tau)dt \ +$$

$$g_o[n]g_k^{(\mathbf{X})}[m+1] \int_{nT_c+\tau}^{(n+1)T_c} \cos(2\pi f_{s,v}t + \phi_{s,v})\cos(2\pi f_{i,j}t + \phi_{i,j} - 2\pi f_{i,j}\tau)dt$$

$$= \begin{cases} \xi \neq 0 \,, & \text{when } g_o[n]g_k^{(\mathbf{X})}[m] \neq g_o[n]g_k^{(\mathbf{X})}[m+1], \\ 0 & , \text{otherwise,} \end{cases} \tag{5.10}$$

where ξ is a non-zero value. Clearly, the orthogonality between subcarriers of the two users can no longer be ensured for asynchronously transmitted data. Thus, in
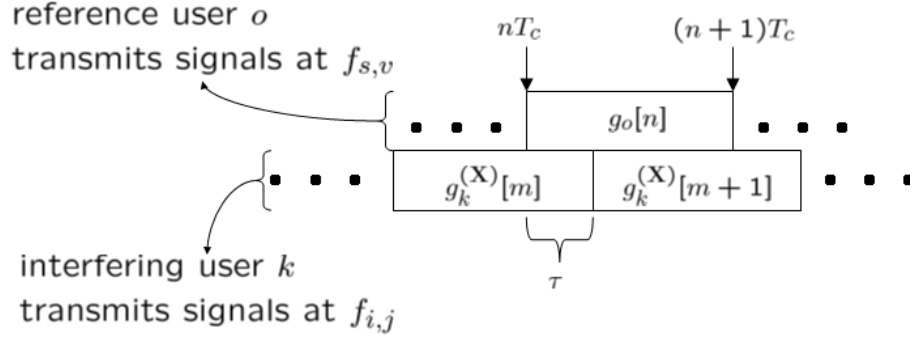
Fig. 5.3: An illustrative example of inter-subcarrier interference for asynchronous users, where the misalignment between the reference user o and the interfering user k in group $\mathbf{X}$ by τ.

addition to the MAI from the main subcarrier in an MC-DS-CDMA system, it is also important to evaluate this kind of other inter-subcarriers' MAI.

5.2.2   BER Performance

We denote the MAI from the main subcarrier by $I_{\mathbf{X},k}^{(1)}$ and the MAI from other inter-subcarriers, by $I_{\mathbf{X},k}^{(2)}$, respectively. As in [58, 69], both types of MAIs are modeled by a zero mean Gaussian random variable. Because $I_{\mathbf{X,k}}^{(1)}$ can be obtained from $I_{\mathbf{X,k}}^{(2)}$ by letting $f_{i,j} = f_{s,v}$, we first analyze $I_{\mathbf{X,k}}^{(2)}$. To analyze the MAI in the case of multi-rate transmissions, we further consider two scenarios according to the relationship between T_o (the bit duration of the reference user) and $T_k^{(\mathbf{X})}$ (bit duration of the interfering user).

Other Inter-Subcarriers' MAI from Low Data Rate Users

In this case $T_o \leq T_k^{(\mathbf{X})}$. Since $\tau_k^{(\mathbf{X})}$ is uniformly distributed in the interval $[0,\ T_k^{(\mathbf{X})})$, $\tau_k^{(\mathbf{X})}$ may fall into two possible regions: (a) $0 \leq \tau_k^{(\mathbf{X})} < T_o$ and (b) $T_o \leq \tau_k^{(\mathbf{X})} < T_k^{(\mathbf{X})}$.

Clearly, the probability of $\tau_k^{(\mathbf{X})}$ falling in region (a) is

$$P(0 \le \tau_k^{(\mathbf{X})} < T_o) \;=\; \frac{T_o}{T_k^{(\mathbf{X})}} \tag{5.11}$$

and that of $\tau_k^{(\mathbf{X})}$ falling in region (b) is

$$P(T_o \le \tau_k^{(\mathbf{X})} < T_k^{(\mathbf{X})}) \;=\; \frac{T_k^{(\mathbf{X})} - T_o}{T_k^{(\mathbf{X})}} \;. \tag{5.12}$$

Denote $I_{\mathbf{X},k}^{(2)'}$ and $I_{\mathbf{X},k}^{(2)''}$ the MAI from other inter-subcarriers in cases (a) and (b), respectively. Let $b_{o,s}[0]$ be the bit of interest. Referring to (5.3) and (5.10), the MAI from the j-th subcarrier of the i-th substream ($f_{i,j}$) to the desired v-th subcarrier of the s-th substream ($f_{s,v}$) can be expressed as follows:

$$
\begin{aligned}
I_{\mathbf{X},k}^{(2)'} &= \sqrt{\frac{\lambda_k^{(\mathbf{X})} P_k^{(\mathbf{X})}}{\lambda_o P_o}} \frac{\alpha_{k,i,j}^{(\mathbf{X})} \beta_{o,s,v} c_k^{(\mathbf{X})}[j] c_o[v]}{T_o} \int_0^{T_o} b_{k,i}^{(\mathbf{X})}(t - \tau_k^{(\mathbf{X})}) g_k^{(\mathbf{X})}(t - \tau_k^{(\mathbf{X})}) g_o(t) \times \\
&\qquad \cos(2\pi(f_{i,j} - f_{s,v})t + \theta_{k,i,j}^{(\mathbf{X})}) dt \\
&= \sqrt{\frac{\lambda_k^{(\mathbf{X})} P_k^{(\mathbf{X})}}{\lambda_o P_o}} \frac{\alpha_{k,i,j}^{(\mathbf{X})} \beta_{o,s,v} c_k^{(\mathbf{X})}[j] c_o[v]}{T_o} \left[b_{k,i}^{(\mathbf{X})}[-1] \times R(\tau_k^{(\mathbf{X})}, \theta_{k,i,j}^{(\mathbf{X})}) + b_{k,i}^{(\mathbf{X})}[0] \widetilde{R}(\tau_k^{(\mathbf{X})}, \theta_{k,i,j}^{(\mathbf{X})}) \right],
\end{aligned}
\tag{5.13}
$$

where $\theta_{k,i,j}^{(\mathbf{X})} = \phi_{k,i,j}^{(\mathbf{X})} - \phi_{o,s,v}$ is uniformly distributed in $[0,\ 2\pi)$;

$$R(\tau_k^{(\mathbf{X})}, \theta_{k,i,j}^{(\mathbf{X})}) \;=\; \int_0^{\tau_k^{(\mathbf{X})}} g_k^{(\mathbf{X})}(t - \tau_k^{(\mathbf{X})}) g_o(t) \cos(2\pi(f_{i,j} - f_{s,v})t + \theta_{k,i,j}^{(\mathbf{X})}) dt; \tag{5.14}$$

$$\widetilde{R}(\tau_k^{(\mathbf{X})}, \theta_{k,i,j}^{(\mathbf{X})}) \;=\; \int_{\tau_k^{(\mathbf{X})}}^{T_o} g_k^{(\mathbf{X})}(t - \tau_k^{(\mathbf{X})}) g_o(t) \cos(2\pi(f_{i,j} - f_{s,v})t + \theta_{k,i,j}^{(\mathbf{X})}) dt. \tag{5.15}$$

Similarly, we can express $I_{\mathbf{X},k}^{(2)''}$ as

$$I_{\mathbf{X},k}^{(2)''} \;=\; \sqrt{\frac{\lambda_k^{(\mathbf{X})} P_k^{(\mathbf{X})}}{\lambda_o P_o}} \frac{\alpha_{k,i,j}^{(\mathbf{X})} \beta_{o,s,v} c_k^{(\mathbf{X})}[j] c_o[v]}{T_o} \left[b_{k,i}^{(\mathbf{X})}[-1]\; R(T_o, \theta_{k,i,j}^{(\mathbf{X})}) \right], \tag{5.16}$$

where

$$R(T_o, \theta_{k,i,j}^{(\mathbf{X})}) = \int_0^{T_o} g_k^{(\mathbf{X})}(t - \tau_k^{(\mathbf{X})}) g_o(t) \cos(2\pi(f_{i,j} - f_{s,v})t + \theta_{k,i,j}^{(\mathbf{X})}) dt \quad . \quad (5.17)$$

Note that (5.16) only exists for the multi-rate transmissions, which is not seen in the single rate case. Because it is assumed that the MAI can be approximated by a Gaussian distributed random variable, we express the variance of $I_{\mathbf{X},k}^{(2)'}$ and $I_{\mathbf{X},k}^{(2)''}$ as follows:

$$Var[I_{\mathbf{X},k}^{(2)'}] = \frac{\bar{\lambda} P_k^{(\mathbf{X})}}{\lambda_o P_o} \frac{E[(\alpha_{k,i,j}^{(\mathbf{X})})^2] \beta_{o,s,v}^2}{T_o^2} \{Var[R(\tau_k^{(\mathbf{X})}, \theta_{k,i,j}^{(\mathbf{X})})] + Var[\tilde{R}(\tau_k^{(\mathbf{X})}, \theta_{k,i,j}^{(\mathbf{X})})]\}$$

$$(5.18)$$

and

$$Var[I_{\mathbf{X},k}^{(2)''}] = \frac{\bar{\lambda} P_k^{(\mathbf{X})}}{\lambda_o P_o} \frac{E[(\alpha_{k,i,j}^{(\mathbf{X})})^2] \beta_{o,s,v}^2}{T_o^2} \{Var[R(T_o, \theta_{k,i,j}^{(\mathbf{X})})]\} \quad . \quad (5.19)$$

The detail derivations of $R(\tau_k^{(\mathbf{X})}, \theta_{k,i,j}^{(\mathbf{X})})$, $\tilde{R}(\tau_k^{(\mathbf{X})}, \theta_{k,i,j}^{(\mathbf{X})})$, and $R(T_o, \theta_{k,i,j}^{(\mathbf{X})})$ can be found in Appendices A and B. Note that $E[(\alpha_{k,i,j}^{(\mathbf{X})})^2] = 1$ for the flat Rayleigh fading channel. The distributions of power control errors among all the users are assumed to be the same. Denote $\bar{\lambda} = E[\lambda_k^{(\mathbf{X})}]$ the average power control error. After some derivations, we can have

$$Var[I_{\mathbf{X},k}^{(2)'}] = Var[I_{\mathbf{X},k}^{(2)''}]$$

$$= \frac{\bar{\lambda} P_k^{(\mathbf{X})}}{\lambda_o P_o} \frac{\beta_{o,s,v}^2}{2G_o \pi^2 [(i-s) + (j-v)U]^2} \quad . \quad (5.20)$$

From (5.11), (5.12), (5.19), and (5.20), it is followed that

$$Var[I_{\mathbf{X},k}^{(2)}] = Var[I_{\mathbf{X},k}^{(2)'}] P(0 \le \tau_k^{(\mathbf{X})} < T_o) + Var[I_{\mathbf{X},k}^{(2)''}] P(T_o \le \tau_k^{(\mathbf{X})} < T_k^{(\mathbf{X})}) \,(5.21)$$

$$= \frac{\bar{\lambda} P_k^{(\mathbf{X})}}{\lambda_o P_o} \frac{\beta_{o,s,v}^2}{2G_o \pi^2 [(i-s) + (j-v)U]^2} \quad . \quad (5.22)$$

Other Inter-Subcarriers' MAI from High Data Rate Users

In this case $T_o > T_k^{(\mathbf{X})}$. Assume $T_o = LT_k^{(\mathbf{X})}$, where $L_k^{(\mathbf{X})}$ is a positive integer. Similarly, be referring to (5.3) and (5.10), we express the MAI from the j-th subcarrier of the i-th substream ($f_{i,j}$) to the desired v-th subcarrier of the s-th substream ($f_{s,v}$) as follows:

$$I_{\mathbf{X},k}^{(2)} = \sqrt{\frac{\lambda_k^{(\mathbf{X})} P_k^{(\mathbf{X})}}{\lambda_o P_o}} \frac{\alpha_{k,i,j}^{(\mathbf{X})} \beta_{o,s,v} c_k^{(\mathbf{X})}[j] c_o[v]}{T_o} \sum_{\ell=0}^{L_k^{(\mathbf{X})}-1} \int_{\ell T_k^{(\mathbf{X})}}^{(\ell+1)T_k^{(\mathbf{X})}} b_{k,i}^{(\mathbf{X})}(t - \tau_k^{(\mathbf{X})}) g_k^{(\mathbf{X})}(t - \tau_k^{(\mathbf{X})}) \times$$

$$g_o(t)\cos(2\pi(f_{i,j} - f_{s,v})t + \theta_{k,i,j}^{(\mathbf{X})})dt$$

$$= \sqrt{\frac{\lambda_k^{(\mathbf{X})} P_k^{(\mathbf{X})}}{\lambda_o P_o}} \frac{\alpha_{k,i,j}^{(\mathbf{X})} \beta_{o,s,v} c_k^{(\mathbf{X})}[j] c_o[v]}{T_o} \sum_{\ell=0}^{L_k^{(\mathbf{X})}-1} \{b_{k,i}^{(\mathbf{X})}[\ell - 1] R_\ell(\tau_k^{(\mathbf{X})}, \theta_{k,i,j}^{(\mathbf{X})}) +$$

$$b_{k,i}^{(\mathbf{X})}[\ell] \widetilde{R}_\ell(\tau_k^{(\mathbf{X})}, \theta_{k,i,j}^{(\mathbf{X})})\} \ , \tag{5.23}$$

where

$$R_\ell(\tau_k^{(\mathbf{X})}, \theta_{k,i,j}^{(\mathbf{X})}) = \int_{\ell T_k^{(\mathbf{X})}}^{\ell T_k^{(\mathbf{X})} + \tau_k^{(\mathbf{X})}} g_k^{(\mathbf{X})}(t - \tau_k^{(\mathbf{X})}) g_o(t)\cos(2\pi(f_{i,j} - f_{s,v})t + \theta_{k,i,j}^{(\mathbf{X})})dt \ ;$$

$$\widetilde{R}_\ell(\tau_k^{(\mathbf{X})}, \theta_{k,i,j}^{(\mathbf{X})}) = \int_{\ell T_k^{(\mathbf{X})} + \tau_k^{(\mathbf{X})}}^{(\ell+1)T_k^{(\mathbf{X})}} g_k^{(\mathbf{X})}(t - \tau_k^{(\mathbf{X})}) g_o(t)\cos(2\pi(f_{i,j} - f_{s,v})t + \theta_{k,i,j}^{(\mathbf{X})})dt \ .$$

$$\tag{5.24}$$

Note that (5.23) exists only for the multi-rate transmissions. Following the procedures of deriving (5.20), we obtain

$$Var[I_{\mathbf{X},k}^{(2)}] = \frac{\bar{\lambda} P_k^{(\mathbf{X})}}{\lambda_o P_o} \frac{\beta_{o,s,v}^2}{2G_o \pi^2[(i - s) + (j - v)U]^2} \ . \tag{5.25}$$

Main Subcarriers' MAI

Let $z = (i - s) + (j - v)U$ in (5.25). Referring to [69], we can obtain the variance of the main subcarriers' MAI from the low or high data rate users as

$$Var[I_{\mathbf{X},k}^{(1)}] = \lim_{z \to 0} Var[I_{\mathbf{X},k}^{(2)}] = \frac{\bar{\lambda}}{\lambda_o} \frac{P_k^{(\mathbf{X})}}{P_o} \frac{\beta_{o,s,v}^2}{3G_o} \quad . \tag{5.26}$$

Note that in (5.22), (5.25), and (5.26), the effects of multi-rate transmissions and PCE are included in $P_k^{(\mathbf{X})}/P_o$ and $\bar{\lambda}/\lambda_o$, respectively.

5.2.3 The Statistics of the Decision Variable $Y_{o,s}$

Consider the maximum ratio combining scheme and choose the weighting factor $(\beta_{o,s,v})$ as the complex conjugate of the channel response of the reference user $(\alpha_{o,s,v})$. The decision variable $Y_{o,s}$ is also a Gaussian distributed random variable since the MAI is modelled by a Gaussian distributed random variable. Combining (5.3), (5.4), (5.25), and (5.26) and averaging $Y_{o,s}$ over s and v, we can express the mean and the variance of $Y_{o,s}$ with a frequency domain spreading factor M as follows:

$$E[Y_{o,s}] = b_{o,s}[0] \sum_{v=1}^{M} |\alpha_{o,s,v}|^2 \tag{5.27}$$

and

$$Var[Y_{o,s}] = \left[\frac{1}{2\lambda_o} \left(\frac{E_o}{MN_0} \right)^{-1} + \sum_{\mathbf{X} \in \{\mathbf{A_u}, \mathbf{B_u}, \mathbf{C_u}\}} \sum_{k=1}^{K_\mathbf{X}} \frac{\bar{\lambda}}{\lambda_o} \frac{P_k^{(\mathbf{X})}}{P_o G_o} \left(\frac{1}{3} + (UM - 1)I_{oc} \right) \right] \sum_{v=1}^{M} |\alpha_{o,s,v}|^2 \quad , \tag{5.28}$$

where

$$I_{oc} = \frac{1}{UM} \sum_{s=1}^{U} \sum_{v=1}^{M} \left\{ \frac{1}{UM - 1} \underbrace{\sum_{i=1}^{U} \sum_{j=1}^{M}}_{j \neq v \ for \ i=s} \left[\frac{1}{2\pi^2 [(i - s) + (j - v)U]^2} \right] \right\} \quad . \tag{5.29}$$

Define the received signal to noise ratio (denoted by γ) as

$$\gamma = \frac{E^2[Y_{o,s}]}{2Var[Y_{o,s}]} \quad . \tag{5.30}$$

Substituting (5.27) and (5.28) into (5.30), we can have

$$\gamma = \lambda_o \gamma_c \gamma_M \; , \tag{5.31}$$

where

$$\gamma_c = \left[(\frac{E_o}{MN_0})^{-1} + \sum_{\mathbf{X} \in \{\mathbf{A_u}, \mathbf{B_u}, \mathbf{C_u}\}} \sum_{k=1}^{K_\mathbf{X}} \frac{2\bar{\lambda} P_k^{(\mathbf{X})}}{P_o G_o} \left(\frac{1}{3} + (UM - 1)I_{oc} \right) \right]^{-1} , \tag{5.32}$$

is a parameter to characterize the joint effects of the complete MAI and power control errors and

$$\gamma_M = \sum_{v=1}^{M} |\alpha_{o,s,v}|^2 \tag{5.33}$$

is the central chi-square distributed random variable with $2M$ degrees of freedom. From [87], the probability density function (*pdf*) of γ_M is given by

$$f(\gamma_M) = \frac{1}{(M-1)!} \gamma_M^{M-1} e^{-\gamma_M}, \quad \text{for} \; \gamma_M \geq 0 \; . \tag{5.34}$$

Like [70] and [88], we let $P_k^{(\mathbf{X})}/P_o = R_k^{(\mathbf{X})}/R_o$ in (5.28) and (5.32), where R_o and $R_k^{(\mathbf{X})}$ are the transmission rates of the reference user and user k in group $\mathbf{X}$, respectively. This implies that a user needs more power to support higher transmission rate.

For binary phase shift keying modulation with coherent detection, the conditional error probability for a given γ_M and λ_o is equal to

$$P(e|\gamma_M, \lambda_o) = Q(\sqrt{2\gamma}) = Q(\sqrt{2\lambda_o \gamma_c \gamma_M}) \; , \tag{5.35}$$

where $Q(x) = \frac{1}{\sqrt{2\pi}} \int_x^\infty e^{-t^2/2} dt$. Referring to [58, 72] and averaging (5.35) over the *pdf* of γ_M from (5.34), we can further simplify the conditional error probability for a

given PCE λ_o as

$$P(e|\lambda_o) = \int_0^\infty Q(\sqrt{2\lambda_o\gamma_c\gamma_M})f(\gamma_M)d\gamma_M$$

$$= \left[\frac{1}{2}\left(1 - \sqrt{\frac{\lambda_o\gamma_c}{1 + \lambda_o\gamma_c}}\right)\right]^M \sum_{n=0}^{M-1} \left(\begin{array}{c} M-1+n \\ n \end{array}\right) \times \left[\frac{1}{2}\left(1 + \sqrt{\frac{\lambda_o\gamma_c}{1 + \lambda_o\gamma_c}}\right)\right]^n .$$

$$(5.36)$$

5.3 Effect of PCE on BER Performance

Now we consider the effect of power control errors. According to [72,89], the open-loop PCE can be modelled as a log-normally distributed random variable with standard deviation σ_e in the dB domain and mean $\bar{\lambda} = \exp\left\{\frac{(b\sigma_e)^2}{2}\right\}$, where $b = \ln 10/10$. Let $\delta = 10\log_{10}\lambda_o$. Then δ becomes a normal distributed random variable with zero mean and standard deviation σ_e. Averaging $P(e|\lambda_o)$ of (5.36) over the *pdf* of λ_o, we can obtain the total error probability $P(e)$ as

$$P(e) = \frac{1}{\sqrt{2\pi\sigma_e^2}} \int_{-\infty}^\infty \left[\frac{(1 - \mu(\delta))}{2}\right]^M \sum_{n=0}^{M-1} \left(\begin{array}{c} M-1+n \\ n \end{array}\right) \left[\frac{(1 + \mu(\delta))}{2}\right]^n e^{-\delta^2/2\sigma_e^2}d\delta ,$$

$$(5.37)$$

where

$$\mu(\delta) = \sqrt{\frac{10^{\delta/10}\gamma_c}{1 + 10^{\delta/10}\gamma_c}} . \tag{5.38}$$

Based on the Hermite polynomial approach of [90], the integration for a function $q(y)e^{-y^2}$ can be computed by

$$\int_{-\infty}^\infty q(y)e^{-y^2}dy = \sum_{i=1}^{D_p} \omega_i q(y_i) , \tag{5.39}$$

where y_i and ω_i are the abscissas and the weight factor of the Hermite polynomials with order D_p, respectively. Letting $\delta = \sqrt{2}\sigma_e y$ in (5.37), we can further simplify the total error probability $P(e)$ to

$$P(e) \approx \frac{1}{\sqrt{\pi}} \sum_{i=1}^{D_p} \omega_i \left[\frac{(1 - \mu(\sqrt{2}\sigma_e y_i))}{2} \right]^M \sum_{n=0}^{M-1} \begin{pmatrix} M-1+n \\ n \end{pmatrix} \times \left[\frac{(1 + \mu(\sqrt{2}\sigma_e y_i))}{2} \right]^n .$$

(5.40)

For the single-carrier DS-CDMA, the influence of the PCE was investigated by means of the first order Taylor expansion method in [72]. However, this method is only suitable for a small PCE ($\sigma_e \leq 1$ dB) and small diversity order (≤ 3). Our approach can evaluate the effect of a larger PCE (i.e. $\sigma_e \geq 1$ dB) and a higher diversity order for the multi-carrier DS-CDMA system. Unlike that the diversity order in the single-carrier DS-CDMA system means path diversity, the diversity order in the MC-DS-CDMA system means the frequency-domain diversity.

5.4   Numerical Results

In this section, we apply the developed analytical models to evaluate the joint impact of the complete MAI and the PCE on the error probability and capacity performances of a multi-rate MC-DS-CDMA system. In order to have the complete frequency diversity gain, the frequency separations for the M subcarriers carrying the same data bit follow the assumption of (5.6). We adopt the following parameters in most examples unless they are defined again:

1. The total number of subcarriers is 512 ($UM = 512$), where M is the frequency domain spreading factor and U is the size of the serial-to-parallel process.

2. Variable data rates are achieved by changing the time-domain spreading factors

in a set of $\{\mathbf{max}(G_o), \mathbf{max}(G_o)/2, \mathbf{max}(G_o)/4\}$ for a fixed frequency domain spreading factor M.

3. There exist total 12 asynchronous users in the system, where three equal-numbered groups are formed. These three groups transmit data rates with frequency- and time-domain spreading factor $(M,\mathbf{max}(G_o))$, $(M,\mathbf{max}(G_o)/2)$, $(M,\mathbf{max}(G_o)/4)$, respectively.

4. The maximum total spreading gain is 256, i.e. $M \times \mathbf{max}(G_o) = 256$.

5. The Hermite polynomials order D_p used in (5.40) is 20.

5.4.1 Discussions

Here we first qualitatively discuss the the error probability by observing the received signal to noise and interference ratio (SINR) γ defined in (5.30). For the sake of convenience, we assume that the bit energy (E_o) and the E_o/N_0 is large enough to ignore the influence of noise on the error probability. Note that $E_o = P_o T_o = P_k^{(\mathbf{X})} T_k^{(\mathbf{X})}$ (i.e. $P_k^{(\mathbf{X})} G_k^{(\mathbf{X})} = P_o G_o$ is fixed). Thus, we can rewrite (5.30) as

$$\gamma \approx \frac{(\lambda_o/\bar{\lambda})G_o \sum_{v=1}^{M} |\alpha_{o,s,v}|^2}{\sum_{\mathbf{X}\in\{\mathbf{A},\mathbf{B},\mathbf{C}\}} \sum_{k=1}^{K_{\mathbf{X}}} 2\frac{P_k^{(\mathbf{X})}}{P_o}\left(\frac{1}{3} + (UM-1)I_{oc}\right)}. \tag{5.41}$$

In this chapter, variable data rates are achieved by changing the time-domain spreading factors in a set of $\{\mathbf{max}(G_o), \mathbf{max}(G_o)/2, \mathbf{max}(G_o)/4\}$ for a fixed frequency domain spreading factor M. Therefore, the ratio of different transmission power is fixed for various values of G_o, i.e. $P_k^{(\mathbf{X})}/P_o$ is fixed. Note that $P_k^{(\mathbf{X})}/P_o = R_k^{(\mathbf{X})}/R_o$ [70, 88]. According to (5.41), we summarize the impacts of the power control error ($\lambda_o/\bar{\lambda}$), the transmission powers (P_o and $P_k^{(\mathbf{X})}$), the frequency-domain spreading gain (M), and the time-domain spreading gain (G_o) on the error probability in the following.

1. With fixed M and $\lambda_o/\bar{\lambda}$, a high data rate user can have better error rate performance because the high data rate user experience small amount of interference produced by low data rate users transmitting at lower power, i.e. $P_k^{(\mathbf{X})}$ is smaller.

2. With the same conditions as above, a larger time-domain spreading factor (G_o) can lead to a lower error probability because of the larger spreading gain.

3. With fixed G_o and $\lambda_o/\bar{\lambda}$, increasing the frequency-domain spreading gain (M) can result in a better error rate performance because of the larger frequency-diversity gain.

4. With fixed M, a larger G_o can make error probability more sensitive to power control errors because the larger G_o can magnify a minor change of $\lambda_o/\bar{\lambda}$. Thus, a better error rate performance thanks to a larger G_o comes at the cost of being more sensitive to power control errors.

5. Similar to the above phenomenon, a large M can also raise the sensitivity of the error probability to power control errors, although larger frequency-domain spreading gain can result in a lower error probability.

6. With a fixed product of $M \times G_o$, frequency domain spreading (M) in the MC-DS-CDMA system is more sensitive to power control errors than time domain spreading (G_o). To compare $(M, G_o) = (4, 2)$ and $(8, 1)$, we let $\zeta = G_o \sum_{v=1}^{M} |\alpha_{o,s,v}|^2$. Fig. 5.4 shows the cumulative density functions of ζ for $(M, G_o) = (4, 2)$ and $(8, 1)$. From the figure, one can find the 90th percentile of ζ for $(M, G_o) = (8, 1)$ is 4.6 which is larger than 3.3 for $(M, G_o) = (4, 2)$. Thus, the case of $(M, G_o) = (8, 1)$ results in larger diversity gain than $(M, G_o) = (4, 2)$. That is, the case of $(M, G_o) = (8, 1)$ can amplify a small change of $\lambda_o/\bar{\lambda}$ more than the case of $(M, G_o) = (4, 2)$. Hence, $(M, G_o) = (8, 1)$ is also more sensitive to power control errors.
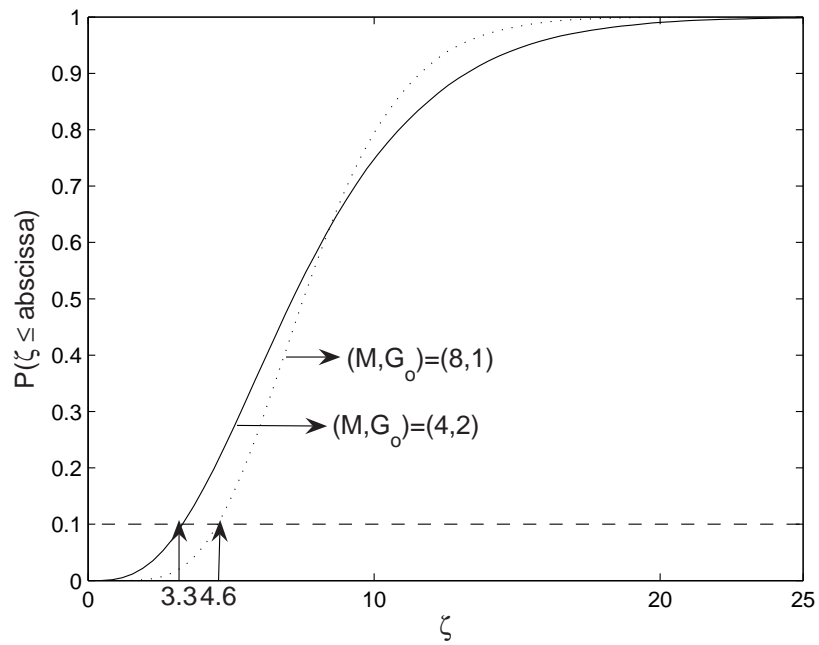
Fig. 5.4: Cumulative density functions of $\zeta = G_o \sum_{v=1}^{M} |\alpha_{o,s,v}|^2$ for $(M, G_o) = (4, 2)$ and $(M, G_o) = (8, 1)$.

5.4.2 Impact of Complete MAI and PCE on Bit Error Probability

Figure 5.5 shows the joint effect of complete MAI and PCE on the error rate performance of the MC-DS-CDMA system. Assume that 12 asynchronous users be equally partitioned into three groups with the frequency-domain and time-domain spreading factors $(M, G_o) = (8, 8)$, $(8, 16)$, and $(8, 32)$, respectively. First, without power control, we have following important observations:

- Compared to the effect of the main-subcarrier-only MAI, the complete MAI from all the inter-subcarriers significantly degrades the BER performance. For $P(e) = 1.5 \times 10^{-3}$ and $(M, G_o) = (8, 8)$, the required E_b/N_0 is 10 dB in the main-subcarrier-only MAI case, while the required E_b/N_0 is increased to 12 dB in the complete MAI case.

- High data rate users have better BER performance compared to low data rate users. This observation confirms the first point of qualitative analysis in Section 5.4.

- Note that both the main-subcarrier-only MAI and the complete MAI result in a floor of error probability in the region of high E_b/N_0. In the former case the error floor is about 1.95×10^{-5}, while in the latter case the error floor is increased to 1.47×10^{-4}.

Now we consider the impact of PCE. In the figure, the standard deviation of PCE $\sigma_e = 1.5$ dB. For comparison, we also show the case with the single user and perfect power control (the curve with the legend *"Neither complete MAI nor PCE"*) and the case with the single user and imperfect power control (the curve with the legend *"PCE only"*). We observe that PCE exacerbates the effect of the complete MAI.
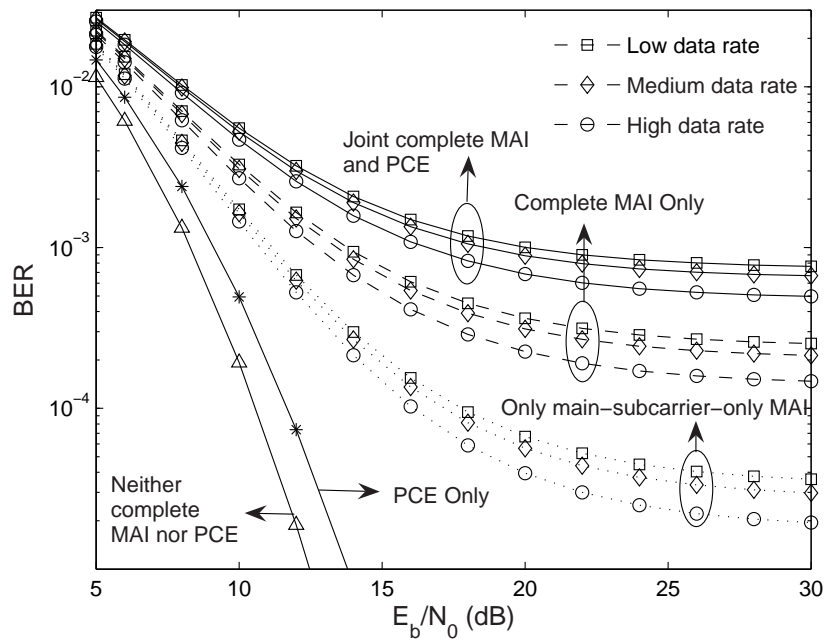
Fig. 5.5: The impact of the joint effect of complete MAI and PCE on the error rate performance of the MC-DS-CDMA system with $(M, G_o) = (8, 8)$, $(8,16)$, and $(8,32)$, where $M \times \max(G_o) = 256$ and the standard deviation of PCE $\sigma_e = 1.5$ dB.

That is, the increase of the required E_b/N_0 due to the joint PCE and complete MAI is indeed higher than the summation of those due to PCE only and complete MAI only individually. For $P(e) = 10^{-3}$, the required E_b/N_0 are 8.2, 9.1, 13.8, and 16.8 dB for the cases of "*Neither complete MAI nor PCE*", "*PCE only*", "*Complete MAI only*", and "*Joint complete MAI and PCE*", respectively. Compared to the based-line case of "*Neither complete MAI nor PCE*", the effect of power control errors increases the required E_b/N_o by 0.9 dB (i.e. the difference of 8.2 and 9.1 dB), while the effect of the complete MAI increases the required E_b/N_o by 5.6 dB (i.e. the difference of 8.2 to 13.8dB). However, the joint effect of the complete MAI and PCE increases the required E_b/N_o by 8.6 dB (i.e. the difference of 16.8 and 8.2 dB). As a result, the joint effect of complete MAI and PCE further degrades the performance by 2.1 dB compared to the sum of the degradation from complete MAI only and PCE only individually.

5.4.3   Impact of Various Time-domain and Frequency-domain Spreading Factors

Figure 5.6 shows the impact of various time domain spreading factors and PCE on the multi-rate MC-DS-CDMA system when frequency domain spreading factor $M = 8$ and $E_b/N_0 = 25$ dB. The error rate performances of three groups of spreading factors for $M \times \mathbf{max}(G_o) = 256$, 512, and 1024 are compared. To ease illustration, we only show the performances with the highest data rate in each group, i.e. (8,8), (8,16), and (8,32). In general, we find that a larger maximum total spreading gain by increasing the time domain spreading factor can improve the performance. This is mainly because users transmit lower power in a group of a larger maximum total spreading gain, thereby yielding fewer interference. Note that the product of the frequency-domain spreading gain and the time-domain spreading gain is not the only

factor to determine the system performance. It is also influenced by various levels of transmission power from surrounding multi-rate users. In Fig. 5.6, the group with $M \times \mathbf{max}(G_o) = 256$ means that four users are allocated with the rates $(M, G_o) = (8, 8), (8, 16), (8, 32)$, respectively. Thus, the user with $(M, G_o) = (8, 32)$ in this group belongs to the low rate user and will experience the interference from 3 low-rate users with $(M, G_o) = (8, 32)$, 4 medium-rate users with $(M, G_o) = (8, 16)$ and 4 high rate user with $(M, G_o) = (8, 8)$. Similarly, a user with $(M, G_o) = (8, 32)$ in the group with $M \times \mathbf{max}(G_o) = 1024$ is classified to a high rate user, who will be interfered by 3 other high-rate users with $(M, G_o) = (8, 32)$, 4 medium-rate users with $(M, G_o) = (8, 64)$ and 4 low rate users with $(M, G_o) = (8, 128)$. Due to less interference, a user with $(M, G_o) = (8, 32)$ in the group of $M \times \mathbf{max}(G_o) = 1024$ indeed outperforms the user with $(M, G_o) = (8, 32)$ in the group of $M \times \mathbf{max}(G_o) = 256$. Our developed analytical model (i.e. (34)) can accurately calculate the MAI in the multi-rate MS-DS-CDMA system. Furthermore, due to the reason of the second point of the qualitatively analysis in Section 5.4, the high rate user with $(M, G_o) = (8, 32)$ in the group of $M \times \mathbf{max}(G_o) = 1024$ can outperform the high rate user with $(M, G_o) = (8, 8)$ in the group of $M \times \mathbf{max}(G_o) = 256$, as shown in Fig. 5.

However, an MC-DS-CDMA system with a larger time domain spreading factor also becomes more sensitive to PCE. When $(M, G_o) = (8, 8)$ and σ_e increasing from 0 dB to 4 dB, the error probability is increased by about an order of 10^2 (i.e. from 2.77×10^{-4} to 1.16×10^{-2}). For $(M, G_o) = (8, 32)$ in the same range of σ_e, the error probability is increased by about an order of 10^3 (i.e. from 1.88×10^{-7} to 7.49×10^{-4}). This phenomenon can be explained by the forth point of the qualitative analysis in Section 5.4. Thus, power control errors can reduce the performance benefits resulting from a larger time-domain spreading factor.

In Fig. 5.7, the impact of PCE on the multi-rate MC-DS-CDMA system is evaluated for a fixed time domain spreading factor ($G_o = 16$) and changing the
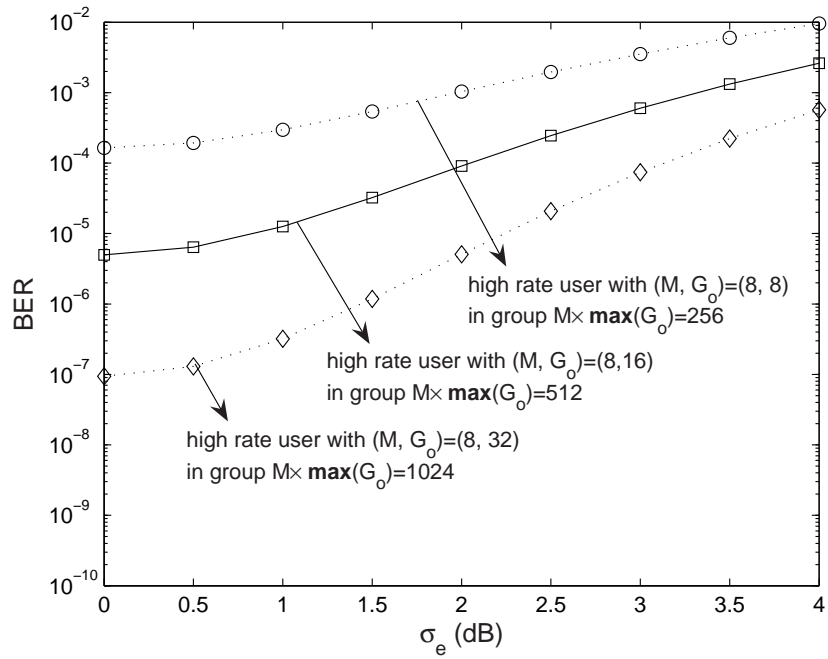
Fig. 5.6: The impact of PCE on the error rate performance of the MC-DS-CDMA system with a fixed frequency domain spreading factors $(M = 8)$ and various time domain spreading factors $G_o = 8, 16$ and 32 for $M \times \mathbf{max}(G_o) = 256$, 512, and 1024, respectively, when $E_b/N_0 = 25$ dB.

frequency domain spreading factors when $E_b/N_0 = 25$ dB. Consider three sets of spreading factors for $M \times \mathbf{max}(G_o) = 256$, 512, and 1024. Here we only show the performance with $(M, G_o) = (4, 16)$ for $M \times \mathbf{max}(G_o) = 256$, $(8, 16)$ for $M \times \mathbf{max}(G_o) = 512$, and $(16, 16)$ for $M \times \mathbf{max}(G_o) = 1024$. In the figure, as stated in the third and fifth points of the qualitative analysis in Section 5.4, a larger maximum total spreading gain by increasing the frequency domain spreading factor results in better performance due to a larger frequency domain diversity gain but the sensitivity of the system to PCE also becomes higher. For example, when $M = 4$ and σ_e increases from 0 dB to 4 dB, the error probability changes from the order of 10^{-4} to 10^{-2}, whereas for $M = 16$ the error probability changes from the order of 10^{-10} to 10^{-4}. When the frequency domain spreading factor (M) increases, the aggregated PCEs among M subcarriers become quite significant and therefore reduce the advantage of frequency diversity over the system with a smaller frequency domain spreading factor.

Interestingly, by comparing Figs. 5.6 and 5.7, one can find that frequency domain spreading (M) in the MC-DS-CDMA system is more sensitive to power control errors than time domain spreading (G_o). This phenomena can be explained by the sixth point of the qualitative analysis. To further confirm the above interesting observation, we perform simulations and evaluate the BER of MC-DS-CDMA systems according to (5.37) to illustrate the impact of PCE (σ_e) with various combinations of frequency domain and time domain spreading factors, as shown in Fig. 5.8. We let the maximum total spreading gain $M \times \max(G_o) = 256$ in this example. First, it is shown that the Hermite approach can accurately match both the analytical integration results and the simulation results. Second and more importantly, comparing the result of $(M, G_o) = (16, 4)$ with $(M, G_o) = (4, 16)$, we find that the performance improvement thanks to a larger frequency spreading factor is reduced as σ_e increases. For $\sigma_e = 0$ dB, changing the spreading factor from $(M, G_o) = (4, 16)$ to $(M, G_o) = (16, 4)$ can improve the bit error rate $P(e) = 9.3 \times 10^{-4}$ to $P(e) = 3.7 \times 10^{-5}$. However, in
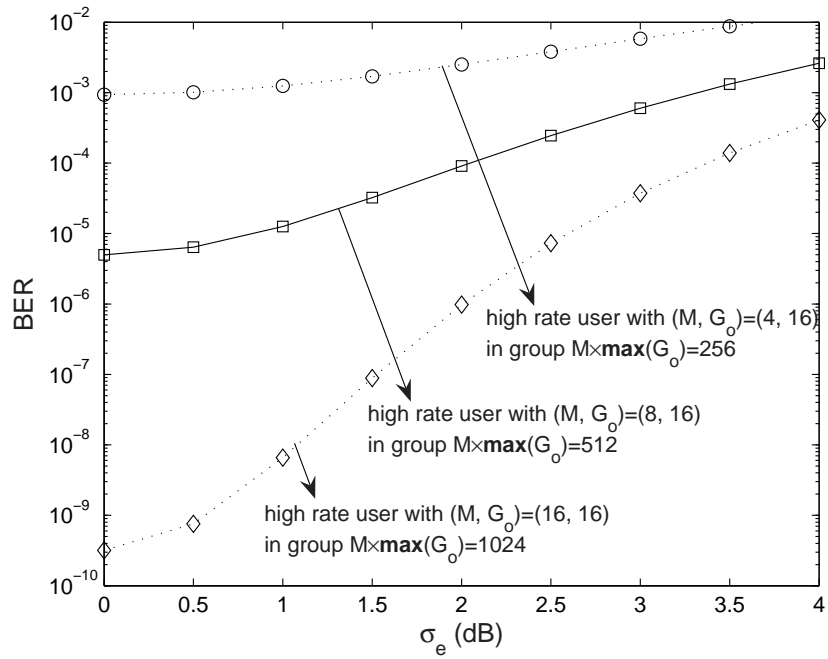
Fig. 5.7: The impact of PCE on the error rate performance of the MC-DS-CDMA system with a fixed time domain spreading factors ($G_o = 16$) and various frequency domain spreading factors $M = 4, 8$ and 16 for $M \times \mathbf{max}(G_o) = 256$, 512 and 1024, respectively, when $E_b/N_0 = 25$ dB.
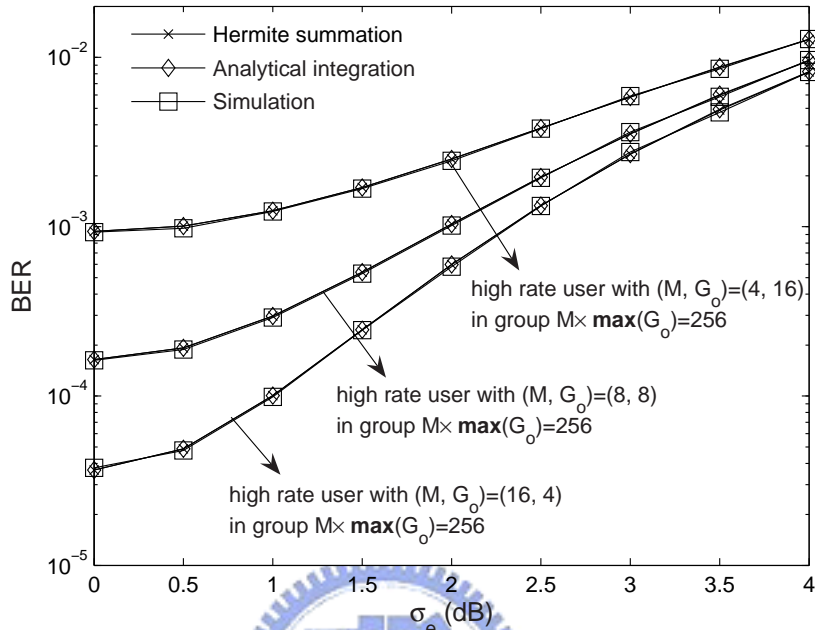
Fig. 5.8: The impact of PCE on the error rate performance of the MC-DS-CDMA system with various combinations of $(M, G_o) = (4, 16)$, (8,8), and (16,4), where $M \times \max(G_o) = 256$ and $E_b/N_0 = 25$ dB.

the case of $\sigma_e = 4$ dB, $P(e) = 9.5 \times 10^{-3}$ for $(M, G_o) = (4, 16)$ and $P(e) = 8.2 \times 10^{-3}$ for $(M, G_o) = (16, 4)$. Although the system with a larger frequency domain spreading factor still performs better than that with a smaller frequency spreading factor, the difference between the two becomes quite insignificant in the presence of a large power control error.

5.4.4 Impact of Complete MAI and PCE on Capacity

Figure 5.9 shows the impact of the complete MAI and PCE on the capacity of the multi-rate MC-DS-CDMA system with time-domain and frequency-domain spread-

ing factors in the group of $M \times \mathbf{max}(G_o) = 256$, $M = 8$ and $E_b/N_0 = 25$ dB. In the figure, the total number of users is three times the abscissa and the only the curve of $(M, G_o) = (8, 32)$ is drawn for each case. For a given $P(e) = 10^{-3}$ requirement and $\sigma_e = 0$ dB, the numbers of acceptable users in each group are 8 and 5 for the main-subcarrier-only MAI and the complete MAI, respectively. The capacity decreases by 37.5 %. However, for PCE $\sigma_e = 3$ dB and the complete MAI, is the number of acceptable users becomes 2. That is, the joint effect of the PCE and the complete MAI can further decrease the capacity by 60 % (from 5 to 2). Clearly, the effect of PCE worsens the impact of the complete MAI on the capacity of the multi-rate MC-DS-CDMA system. This phenomenon can be explained by observing the parameter $\bar{\lambda}$ (denoting the average power control error) in γ_c of (5.32), where the joint effect of PCE and complete MAI is analytically modelled by the term $\sum_{\mathbf{X} \in \{\mathbf{A}, \mathbf{B}, \mathbf{C}\}} \sum_{k=1}^{K_{\mathbf{X}}} [2\bar{\lambda} P_k^{(\mathbf{X})} (1/3 + (UM - 1)I_{oc})]/(P_o G_o)$.

5.5 Chapter Summary

In this chapter, we have developed an analytical model to quantitatively evaluate the performance of multi-rate MC-DS-CDMA systems using time and frequency domain spreading codes subject to the PCE and the complete MAI from all subcarriers. Applying the developed analytical model, we have obtained the following observations:

- When both PCE and the complete MAI are jointly considered, the effect of PCE can exacerbate the impact of complete MAI on the MC-DS-CDMA system, or vice versa.

- A larger maximum total spreading gain either by increasing frequency or time domain spreading factors can enhance the performance of the multi-rate MC-DS-CDMA system. However, the sensitivity of these performance gains to
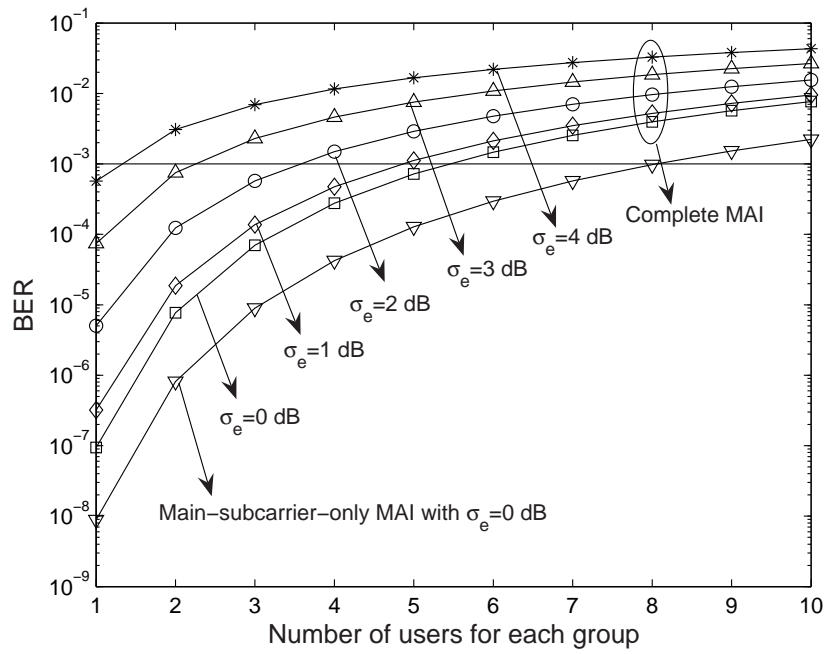
Fig. 5.9: The impact of complete MAI and PCE on the capacity of the multi-rate MC-DS-CDMA system with $\{(M, G_o)\} = \{(8, 8), (8, 16), (8, 32)\}$.

power control errors cannot be ignored.

- A larger PCE (σ_e) can possibly make the frequency domain diversity gain diminish faster than the gain obtained from the time-domain spreading. Thus, although for the same maximum total time and frequency spreading gain, the MC-DS-CDMA system with a larger frequency domain spreading factor results in better performance than that with a larger time domain spreading factor, the performance difference between the two become less significant as power control errors increase.

The developed analytical model and the above observations can provide some important insights into the performance issues of multi-rate MC-DS-CDMA systems.

Chapter 6

Interference Avoidance Code Assignment for Downlink MC-DS-CDMA

This chapter investigates the code assignment problem for the downlink multi-rate multi-carrier direct sequence code division multiple access (MC-DS-CDMA) system with time- and frequency-domain (TF-domain) spreading. In the MC-DS-CDMA system, each user is assigned a set of time-domain and frequency-domain spreading code. However, in the frequency-selective fading channel, the orthogonality of the frequency-domain spreading code may be damaged. In this situation, even two users with orthogonal time-domain spreading code, they may interfere with each other by different amount of MAI in the multi-rate MC-DS-CDMA system. Thus, how to design an effective radio resource management strategy for the MC-DS-CDMA systems subject to different levels of MAIs becomes a new and important issue. In this chapter, based on the error rate analysis in the physical layer, we observe and define a new performance metric, called the *MAI coefficient*, which can quantitatively predict the MAI effect imposed on a particular code in a multi-rate MC-DS-CDMA system. Furthermore, from the radio resource management perspective, we develop an interference avoidance code assignment scheme based on the MAI coefficient.

6.1   Problem Formulation

Consider a scenario when a code with time-domain spreading factor $SF = 8$ is requested. Clearly, the candidate codes for this request are $\left\{ C_{8,8}^{(1)}, C_{8,1}^{(3)}, C_{8,2}^{(3)}, C_{8,3}^{(3)}, C_{8,4}^{(3)} \right.$ $, C_{8,1}^{(4)}, C_{8,2}^{(4)}, C_{8,3}^{(4)}, C_{8,4}^{(4)}, C_{8,5}^{(4)}, C_{8,6}^{(4)}, C_{8,7}^{(4)}, C_{8,8}^{(4)} \right\}$. According to the interferers of the allocated

codes by observing the grid representation in Fig. 2.7, these candidate codes can be roughly classified into four groups as shown in Fig. 2.6. Specifically, Groups 1 to 4 are affected by the interference from the users with the allocated codes $\left\{C_{2,2}^{(2)}, C_{2,2}^{(3)}\right\}$, $\left\{C_{2,1}^{(1)}, C_{2,1}^{(2)}\right\}$, $\left\{C_{4,3}^{(1)}, C_{2,2}^{(2)}, C_{2,2}^{(3)}\right\}$, and $\left\{C_{8,7}^{(1)}, C_{2,2}^{(2)}, C_{2,2}^{(3)}\right\}$, respectively.

Then, an interesting question arise: how can an MC-CDMA system pick a code from a 2D code tree with less MAI, while maintaining good call admission probability? More importantly, the *potential* impact on the existing used codes should be taken into account for evaluating the candidature of a code. The challenges lie in two folds. First, the impact of the incurred MAI for a candidate code should be *predicted* before transmitting a signal. This MAI prediction scheme should not only be accurate but simple. Second, multi-rate users make the code assignment problem nontrivial since some high-rate users may request more channel resources. Thus, a 2D code tree structure should be considered in the code assignment problem aiming to increase call admission rate for multi-rate users.

Hence, we are motivated to propose a new performance metric, called as the *MAI coefficient*, to quantitatively estimate the amount of the possible incurred MAI for the candidate codes. Moreover, based on the newly defined *MAI coefficient*, we propose a novel interference avoidance code assignment strategy for MC-DS-CDMA with time- and frequency-domain spreading, which can effectively reduce the impact of MAI and achieve high call admission performance.

6.2 System Model

6.2.1 Transmitted Signal

The transmitter structure in the MC-DS-CDMA system using both time- and frequency-domain spreading codes is shown in Fig. 5.1. First, the serial-to-parallel process

reduces the subcarrier data rate by converting data streams with bit duration $T_{b,k}^{(\mathbf{X})}$ into U reduced-rate parallel substreams with new bit duration $T_k^{(\mathbf{X})} = UT_{b,k}^{(\mathbf{X})}$ for user k in group $\mathbf{X} \in \{\mathbf{A_o}, \mathbf{B_o}, \mathbf{C_o}\}$, where each substream experiences a frequency flat (or non-dispersive) fading. Then the data in each substream are spread by a time domain spreading code $g_k^{(\mathbf{X})}(t)$. After being copied to M subcarriers, the data in each substream is multiplied by a frequency domain spreading code $\{c_k^{(\mathbf{X})}[j]\}$. Note that in this case the frequency-domain spreading gain is M. The user group $\mathbf{X}$ is defined as follows. Let $g_o(t)$ and $c_o[j]$ be the time domain spreading code and the frequency domain spreading code of the reference user, respectively. As in [68], we categorize the interfering users into three groups:

1. group $\mathbf{A_o}$: $\dfrac{1}{T_o} \displaystyle\int_0^{T_o} g_k^{(\mathbf{A_o})}(t)g_o(t)dt \neq 0$ and $\dfrac{1}{M} \displaystyle\sum_{j=1}^{M} c_k^{(\mathbf{A_o})}[j]c_o[j] = 0$.

2. group $\mathbf{B_o}$: $\dfrac{1}{T_o} \displaystyle\int_0^{T_o} g_k^{(\mathbf{B_o})}(t)g_o(t)dt = 0$ and $\dfrac{1}{M} \displaystyle\sum_{j=1}^{M} c_k^{(\mathbf{B_o})}[j]c_o[j] \neq 0$.

3. group $\mathbf{C_o}$: $\dfrac{1}{T_o} \displaystyle\int_0^{T_o} g_k^{(\mathbf{C_o})}(t)g_o(t)dt = 0$ and $\dfrac{1}{M} \displaystyle\sum_{j=1}^{M} c_k^{(\mathbf{C_o})}[j]c_o[j] = 0$.

Note the above grouping of users is only valid for the downlink MC-DS-CDMA system. Also, group A will disappear and groups B and C will be blended into one group when using a single frequency-domain spreading code with all chips equal to one for all users. In that case, the system capacity will be largely reduced.

The transmitted signal of user k in group $\mathbf{X} \in \{\mathbf{A_o}, \mathbf{B_o}, \mathbf{C_o}\}$ can be expressed as

$$s_k^{(\mathbf{X})}(t) = \sum_{i=1}^{U} \sum_{j=1}^{M} \sqrt{\frac{2P_k^{(\mathbf{X})}}{M}} b_{k,i}^{(\mathbf{X})}(t)g_k^{(\mathbf{X})}(t)c_k^{(\mathbf{X})}[j]\cos(2\pi f_{i,j}t + \varphi_{k,i,j}^{(\mathbf{X})}) , \quad (6.1)$$

where $P_k^{(\mathbf{X})}$, $\{f_{i,j}\}$ and $\{\varphi_{k,i,j}^{(\mathbf{X})}\}$ represent the transmitted power, the j-th subcarrier frequency and the initial phase in the i-th substream, respectively. Note that as

in [91], the spectrum of the considered MC-DS-CDMA system is overlapped and any two adjacent subcarriers are separated by a minimum distance to preserve the orthogonality in the frequency domain. The waveform of the i-th substream $b_{k,i}^{(\mathbf{X})}(t) = \sum_{h=-\infty}^{\infty} b_{k,i}^{(\mathbf{X})}[h] P_{T_k^{(\mathbf{X})}}(t - hT_k^{(\mathbf{X})})$ contains a rectangular pulses of duration $T_k^{(\mathbf{X})}$, where $b_{k,i}^{(\mathbf{X})}[h] = \pm 1$ with equal probability. The time domain spreading code $g_k^{(\mathbf{X})}(t) = \sum_{\ell=-\infty}^{\infty} g_k^{(\mathbf{X})}[\ell] P_{T_c}(t - \ell T_c)$ represents the chip sequence of the rectangular pulses of duration T_c, where $g_k^{(\mathbf{X})}[\ell] = \pm 1$ with equal probability. Note that the time domain spreading factor of user k in the group $\mathbf{X}$ is $G_k^{(\mathbf{X})} = T_k^{(\mathbf{X})}/T_c$.

6.2.2 Received Signal

In this chapter, we consider a single cell in downlink transmissions with subcarrier experiencing the flat Rayleigh fading. In the considered environment, the received signal of the reference user (denoted by r_o) can be expressed as:

$$
\begin{aligned}
r_o(t) = & \sum_{i=1}^{U} \sum_{j=1}^{M} \sqrt{\frac{2P_o}{M}} \alpha_{o,i,j} b_{o,i}(t) g_o(t) c_o[j] \cos(2\pi f_{i,j} t + \alpha_{o,i,j}) + \\
& \sum_{\mathbf{X} \in \{\mathbf{A_o}, \mathbf{B_o}, \mathbf{C_o}\}} \sum_{k=1}^{K_{\mathbf{X}}} \sum_{i=1}^{U} \sum_{j=1}^{M} \sqrt{\frac{2P_k^{(\mathbf{X})}}{M}} \alpha_{o,i,j} b_{k,i}^{(\mathbf{X})}(t) g_k^{(\mathbf{X})}(t) c_k^{(\mathbf{X})}[j] \cos(2\pi f_{i,j} t + \alpha_{o,i,j}) \\
& + n(t) \ ,
\end{aligned}
\tag{6.2}
$$

where $\alpha_{o,i,j}$ is the channel amplitude for the j-th subcarrier of the i-th substream; $K_{\mathbf{X}}$ is the number of users in the group $\mathbf{X}$; and $n(t)$ is the white Gaussian noise with double-sided power spectrum density of $N_0/2$. In (6.2), $\phi_{o,i,j} = \varphi_{o,i,j} + \psi_{o,i,j}$ is uniformly distributed in $[0, 2\pi)$, where $\psi_{o,i,j}$ is the channel's phase of the j-th subcarrier in the i-th substream. Note that as in [42, 91], the subcarriers carrying the same data bit $(\alpha_{o,i,1} \sim \alpha_{o,i,M})$ are assumed to experience independent flat Rayleigh fading channels.

The receiver structure of the MC-DS-CDMA using time-domain and frequency-domain spreading codes is shown in Fig. 5.2. Without loss of generality, let the bit of interest be the first bit in the s-th substream of the reference user (denoted by $b_{o,s}[0]$). After time domain despreading, the output signal for the reference user in the v-th subcarrier of the s-th substream can be expressed as:

$$Y_{o,s,v} = \int_0^{T_o} r_o(t)\beta_{o,s,v}g_o(t)c_o[v]\cos(2\pi f_{s,v}t + \phi_{s,v})dt$$

$$= \sqrt{\frac{P_o}{2M}}T_o\left\{b_{o,s}[0]\alpha_{o,s,v}\beta_{o,s,v} + \sum_{\mathbf{X}\in\{\mathbf{A_o},\mathbf{B_o},\mathbf{C_o}\}}\sum_{k=1}^{K_{\mathbf{X}}} I_{k,s,v}^{(\mathbf{X})} + n_{s,v}\right\} , \quad (6.3)$$

where P_o and T_o are the transmitted power and the bit duration of the reference user, respectively; $\beta_{o,s,v}$ is the weights for a certain combining scheme; $I_{k,s,v}^{(\mathbf{X})}$ denotes the MAI induced from user k of group $\mathbf{X}$ to the v-th subcarrier of the s-th substream of the reference user; and $n_{s,v}$ is the white Gaussian noise with zero mean and variance of $\frac{|\beta_{o,s,v}|^2}{2}(\frac{E_o}{MN_0})^{-1}$, where $E_o = P_oT_o$ is the bit energy of the reference user. The MAI terms $I_{k,s,v}^{(\mathbf{X})}$ in (6.3) can be expressed as

$$I_{k,s,v}^{(\mathbf{X})} = \sqrt{\frac{P_k^{(\mathbf{X})}}{P_o}}\frac{\alpha_{o,s,v}\beta_{o,s,v}c_k^{(\mathbf{X})}[v]c_o[v]}{T_o}\int_0^{T_o} b_{k,s}^{(\mathbf{X})}(t)g_k^{(\mathbf{X})}(t)g_o(t)dt . \quad (6.4)$$

Then combining M subcarriers, the decision variable of $b_{o,s}[0]$ for the reference user becomes

$$Y_{o,s} = \sum_{v=1}^{M} Y_{o,s,v} , \quad (6.5)$$

where $Y_{o,s,v}$ is given in (6.3).

6.3 Impact of MAI

In this section, we analyze the effect of MAI in the multi-rate MC-DS-CDMA system. To calculate $I_{k,s,v}^{(\mathbf{X})}$, we need to further consider two scenarios according to the relation

between T_o (the bit duration of the reference user) and $T_k^{(\mathbf{X})}$ (the bit duration of the interfering user k in group $\mathbf{X}$).

6.3.1 MAI from High Data Rate Users $(T_o > T_k^{(\mathbf{X})})$:

In this case, we let $L_k^{(\mathbf{X})} = T_o/T_k^{(\mathbf{X})}$ be the ratio of bit duration of the desired users to the interfering user of group $\mathbf{X} \in \{\mathbf{A_o}, \mathbf{B_o}, \mathbf{C_o}\}$, where $L_k^{(\mathbf{X})}$ is a positive integer. Then we can rewrite (6.4) as

$$
\begin{aligned}
I_{k,s,v}^{(\mathbf{X})} &= \sqrt{\frac{P_k^{(\mathbf{X})}}{P_o}} \frac{\alpha_{o,s,v}\beta_{o,s,v}c_k^{(\mathbf{X})}[v]c_o[v]}{T_o} \int_0^{T_o} b_{k,s}^{(\mathbf{X})}(t)g_k^{(\mathbf{X})}(t)g_o(t)dt \\
&= \sqrt{\frac{P_k^{(\mathbf{X})}}{P_o}} \frac{\alpha_{o,s,v}\beta_{o,s,v}c_k^{(\mathbf{X})}[v]c_o[v]}{L_k^{(\mathbf{X})}T_k^{(\mathbf{X})}} \sum_{\ell=0}^{L_k^{(\mathbf{X})}-1} b_{k,s}^{(\mathbf{X})}[\ell] \int_0^{T_k^{(\mathbf{X})}} g_k^{(\mathbf{X})}(t)g_o(t)dt \ . \quad (6.6)
\end{aligned}
$$

According to the definition of user group in Section 6.2.1, the time-domain spreading codes of users in groups $\mathbf{B_o}$ and $\mathbf{C_o}$ are orthogonal to the reference user, i.e. $\int_0^{T_k^{(\mathbf{B_o})}} g_k^{(\mathbf{B_o})}(t)g_o(t)dt = 0$ and $\int_0^{T_k^{(\mathbf{C_o})}} g_k^{(\mathbf{C_o})}(t)g_o(t)dt = 0$. Hence, we have $I_{k,s,v}^{(\mathbf{B_o})} = I_{k,s,v}^{(\mathbf{C_o})} = 0$. Recall that $b_{k,s}^{(\mathbf{C_o})}[\ell] = \pm 1$ with equal probability. Thus, for OVSF codes, we can have

$$
\frac{b_{k,s}^{(\mathbf{C_o})}[\ell]}{T_k^{(\mathbf{A_o})}} \int_0^{T_k^{(\mathbf{A_o})}} g_k^{(\mathbf{A_o})}(t)g_o(t)dt = \pm 1 \tag{6.7}
$$

with equal probability. Consequently, (6.6) can be expressed as

$$
I_{k,s,v}^{(\mathbf{A_o})} = \sqrt{\frac{P_k^{(\mathbf{A_o})}}{P_o}} \frac{\alpha_{o,s,v}\beta_{o,s,v}c_k^{(\mathbf{A_o})}[v]c_o[v]}{L_k^{(\mathbf{A_o})}} \sum_{\ell=0}^{L_k^{(\mathbf{A_o})}-1} \Delta[\ell] \ , \tag{6.8}
$$

where $\Delta[\ell] = \pm 1$ with equal probability.

6.3.2 MAI from Low Data Rate Users $(T_o \leq T_k^{(\mathbf{X})})$:

In this case, we express $I_{k,s,v}^{(\mathbf{X})}$ as

$$
\begin{aligned}
I_{k,s,v}^{(\mathbf{X})} &= \sqrt{\frac{P_k^{(\mathbf{X})}}{P_o}} \frac{\alpha_{o,s,v}\beta_{o,s,v}c_k^{(\mathbf{X})}[v]c_o[v]}{T_o} \int_0^{T_o} b_{k,s}^{(\mathbf{X})}(t)g_k^{(\mathbf{X})}(t)g_o(t)dt \\
&= \sqrt{\frac{P_k^{(\mathbf{X})}}{P_o}} \frac{\alpha_{o,s,v}\beta_{o,s,v}c_k^{(\mathbf{X})}[v]c_o[v]}{T_o} b_{k,s}^{(\mathbf{X})}[0] \int_0^{T_o} g_k^{(\mathbf{X})}(t)g_o(t)dt \ . \qquad (6.9)
\end{aligned}
$$

Similar to the case of MAI from high data rate users, we have $I_{k,v}^{(\mathbf{B_o})} = I_{k,v}^{(\mathbf{C_o})} = 0$ and

$$
\frac{b_{k,s}^{(\mathbf{X})}[0]}{T_o} \int_0^{T_o} g_k^{(\mathbf{A_o})}(t)g_o(t)dt = \pm 1 \ . \qquad (6.10)
$$

Then it is followed that

$$
I_{k,s,v}^{(\mathbf{A_o})} = \sqrt{\frac{P_k^{(\mathbf{A_o})}}{P_o}} \alpha_{o,s,v}\beta_{o,s,v}c_k^{(\mathbf{A_o})}[v]c_o[v]\Delta[0] \ , \qquad (6.11)
$$

where $\Delta[0]$ is defined in (6.8). Note that (6.11) is the special case of (6.8). Specifically, we can obtain (6.11) by letting $L_k^{(\mathbf{A_o})} = 1$ in (6.8).

Consider the maximum ratio combining scheme. Then it is followed $\beta_{o,s,v} = \alpha_{o,s,v}^*$. Substituting (6.3), (6.8), and (6.11) into (6.5), we obtain

$$
\begin{aligned}
Y_{o,s} &= \sum_{v=1}^{M} Y_{o,s,v} \\
&= \sqrt{\frac{P_o}{2M}}T_o \left\{ b_{o,s}[0] \sum_{v=1}^{M} |\alpha_{o,s,v}|^2 + \sum_{v=1}^{M}\sum_{k=1}^{K_{\mathbf{A_o}}}\sum_{\ell=0}^{L_k^{(\mathbf{A_o})}-1} \sqrt{\frac{P_k^{(\mathbf{A_o})}}{P_o}} \frac{|\alpha_{o,s,v}|^2 c_k^{(\mathbf{A_o})}[v]c_o[v]}{L_k^{(\mathbf{A_o})}}\Delta[\ell] \right. \\
&\left. + \sum_{v=1}^{M} n_{s,v} \right\} \ . \qquad (6.12)
\end{aligned}
$$

Assume that the MAI can be approximated by a zero mean Gaussian distributed random variable. Then the normalized decision variable $Y_{o,s}$ is modelled by a Gaussian

random variable with mean

$$E[Y_{o,s}] = b_{o,s}[0] \sum_{v=1}^{M} |\alpha_{o,s,v}|^2 \qquad (6.13)$$

and variance

$$Var[Y_{o,s}] = \sum_{v=1}^{M} \sum_{k=1}^{K_{\mathbf{A_o}}} \sum_{\ell=0}^{L_k^{(\mathbf{A_o})}-1} Var\left[\sqrt{\frac{P_k^{(\mathbf{A_o})}}{P_o}} \frac{|\alpha_{o,s,v}|^2 c_k^{(\mathbf{A_o})}[v] c_o[v]}{L_k^{(\mathbf{A_o})}} \Delta[\ell]\right] +$$

$$\frac{1}{2}(\frac{E_o}{MN_0})^{-1} \sum_{v=1}^{M} |\alpha_{o,s,v}|^2$$

$$= \sum_{v=1}^{M} \sum_{k=1}^{K_{\mathbf{A_o}}} \sum_{\ell=0}^{L_k^{(\mathbf{A_o})}-1} \frac{P_k^{(\mathbf{A_o})}}{P_o} \frac{|\alpha_{o,s,v}|^4}{(L_k^{(\mathbf{A_o})})^2} + \frac{1}{2}(\frac{E_o}{MN_0})^{-1} \sum_{v=1}^{M} |\alpha_{o,s,v}|^2 \quad . \ (6.14)$$

Define the received E_b/N_0 (denoted by γ) as

$$\gamma = \frac{E^2[Y_{o,s}]}{2Var[Y_{o,s}]}$$

$$= \frac{(\sum_{v=1}^{M} |\alpha_{o,s,v}|^2)^2}{2\sum_{v=1}^{M} \sum_{k=1}^{K_{\mathbf{A_o}}} \sum_{\ell=0}^{L_k^{(\mathbf{A_o})}-1} \frac{P_k^{(\mathbf{A_o})}}{P_o} \frac{|\alpha_{o,s,v}|^4}{(L_k^{(\mathbf{A_o})})^2} + (\frac{E_o}{MN_0})^{-1} \sum_{v=1}^{M} |\alpha_{o,s,v}|^2}$$

$$= \frac{P_o G_o (\sum_{v=1}^{M} |\alpha_{o,s,v}|^2)^2}{\underbrace{2\sum_{v=1}^{M} \sum_{k=1}^{K_{\mathbf{A_o}}} \sum_{\ell=0}^{L_k^{(\mathbf{A_o})}-1} \frac{P_k^{(\mathbf{A_o})}}{P_o} \frac{|\alpha_{o,s,v}|^4}{(L_k^{(\mathbf{A_o})})^2} P_o G_o}_{MAI} + \underbrace{MP_N \sum_{v=1}^{M} |\alpha_{o,s,v}|^2}_{noise}} \quad , \qquad (6.15)$$

where R_o and $R_k^{(\mathbf{A_o})}$ are the transmission rates of the reference user and user k in group $\mathbf{A_o}$, respectively. Note that E_o/N_0 denotes the reference user's transmitting signal-to-noise ratio per bit. $E_o = P_o T_o$ and $N_0 = P_N T_c$, where P_o and P_N are the transmission power of the reference user and the noise power. In [70, 88], $R_k^{(\mathbf{A_o})}/R_o = P_k^{(\mathbf{A_o})}/P_o$. That is, a high-rate user needs more power.

6.3.3 MAI Coefficient

In order to quantize the MAI imposed on each code channel, we define a new performance metric — *MAI coefficient.* In the considered single cell in downlink transmissions all the interferers experience the same fading channel as the reference user. The only difference between these interferers are the volumes of interference they produce. In other words, the effects of the channel can be ignored in evaluating the impact of MAI on the reference user. Now, lets rewrite the MAI term of γ in (6.15) as

$$\sum_{k=1}^{K_{\mathbf{A_o}}} \sum_{\ell=0}^{L_k^{(\mathbf{A_o})}-1} \frac{R_k^{(\mathbf{A_o})}}{R_o(L_k^{(\mathbf{A_o})})^2} \left[2P_oG_o \sum_{v=1}^{M} |\alpha_{o,s,v}|^4 \right] . \tag{6.16}$$

Since the downlink MAI is resulted from the sub-carriers of reusing time-domain spreading codes in different frequency-domain code trees, we assume that the fading parameters in (6.16) are independent. With respect to the target user, the term $2P_oG_o \sum_{v=1}^{M} |\alpha_{o,s,v}|^4$ in (6.16) is common to all the $K_{\mathbf{A_o}}$ interfering users. As a result, we can just use $\sum_{k=1}^{K_{\mathbf{A_o}}} \sum_{\ell=0}^{L_k^{(\mathbf{A_o})}-1} R_k^{(\mathbf{A_o})}/(R_o(L_k^{(\mathbf{A_o})})^2)$ to characterize the downlink MAI in the MC-DS-CDMA system. There are two possible scenarios as described below.

1. **MAI from High Data Rate Users:** In this case $R_k^{(\mathbf{A_o})}/R_o = T_o/T_k^{(\mathbf{A_o})} = L_k^{(\mathbf{A_o})} > 1$. Then it is followed that

$$\sum_{k=1}^{K_{\mathbf{A_o}}} \sum_{\ell=0}^{L_k^{(\mathbf{A_o})}-1} \frac{R_k^{(\mathbf{A_o})}}{R_o(L_k^{(\mathbf{A_o})})^2} = \sum_{k=1}^{K_{\mathbf{A_o}}} \sum_{\ell=0}^{L_k^{(\mathbf{A_o})}-1} \frac{1}{L_k^{(\mathbf{A_o})}}$$

$$= \sum_{k=1}^{K_{\mathbf{A_o}}} 1 . \tag{6.17}$$

2. **MAI from Low Data Rate Users:** By letting $L_k^{(\mathbf{A_o})} = 1$ in (6.16), we can obtain the MAI from low data rate users as

$$\sum_{k=1}^{K_{\mathbf{A_o}}} \sum_{\ell=0}^{L_k^{(\mathbf{A_o})}-1} \frac{R_k^{(\mathbf{A_o})}}{R_o(L_k^{(\mathbf{A_o})})^2} = \sum_{k=1}^{K_{\mathbf{A_o}}} \frac{R_k^{(\mathbf{A_o})}}{R_o} . \tag{6.18}$$

Note that $R_k^{(\mathbf{A_o})}/R_o < 1$ in this case.

Combining (6.17) and (6.18), we define the downlink *MAI COEFFICIENT* in the MC-DS-CDMA system with TF-domain spreading as

$$\kappa = \sum_{k=1}^{K_{\mathbf{A_o}}} \mathbf{min}(1, \frac{R_k^{(\mathbf{A_o})}}{R_o}) \ . \tag{6.19}$$

According to the grip representation in Section 2.2.5, (6.19) can also be expressed as

$$\kappa = \sum_{k=1}^{K_{\mathbf{A_o}}} \mathbf{min}(1, \frac{\sigma_k^{(\mathbf{A_o})}}{\sigma_o}) \ , \tag{6.20}$$

where $\sigma_k^{(\mathbf{A_o})}$ and σ_o represent the areas of the rectangles in Fig. 2.7 for codes with transmission rates $R_k^{(\mathbf{A_o})}$ and R_o, respectively.

6.4 Interference Avoidance Code Assignment Strategy

6.4.1 Principles

Now we propose an MAI-coefficient-based interference avoidance code assignment strategy. With the aid of the MAI coefficient, the proposed interference avoidance code assignment strategy can quickly and easily evaluate the candidacy of each spreading code and pick one which incurs less MAI. The objective of the interference avoidance code assignment strategy is to reduce the MAI effect in the MC-DS-CDMA system, while keeping the code tree compact to maintain high call admission performance for users with various data rates. In principle, the proposed interference avoidance code assignment strategy consists of three stages. As shown in Fig. 6.1, the first stage is to check the sum of the incremental MAI coefficients of the candidate

codes. If some candidate codes tie in the first stage, the sum of the MAI coefficients are compared. At last, the crowded-first code assignment in [75, 76] is applied for the candidate codes who tie in the second stage. The detail rules of the interference code assignment strategy are summarized as follows.

Let $\{C_{SF,j}^{(i)}\}$ be the set of candidate codes with frequency- and time-domain spreading factors M and SF, respectively, where $1 \leq i \leq M$ and $1 \leq j \leq SF$. Denote $\mathbf{R_c}(C_{SF,j}^{(i)})$ the set of the codes related to $C_{SF,j}^{(i)}$. The candidature of each code $C_{SF,j}^{(i)}$ is evaluated in the following three stages.

1. **In the first stage**, the the incurred MAI of using code $C_{SF,j}^{(i)}$ is estimated by the sum of the increment of the MAI coefficients of codes in $\mathbf{R_c}(C_{SF,j}^{(i)})$. If any two candidate codes lead to the same amount of incremental MAI coefficients in $\mathbf{R_c}(C_{SF,j}^{(i)})$, go to the second stage. Otherwise, the smallest sum of incremental MAI coefficients in the set of $\mathbf{R_c}(C_{SF,j}^{(i)})$ is selected. We detail the rules in the first stage as follows:

    (a) For the n-th code in $\mathbf{R_c}(C_{SF,j}^{(i)})$, denoted by $C_n \in \mathbf{R_c}(C_{SF,j}^{(i)})$, we calculate its increments of the MAI coefficient $(\Delta_\kappa(C_n))$ if $C_{SF,j}^{(i)}$ is chosen.

    (b) Denote $\Delta_\kappa(\mathbf{R_c}(C_{SF,j}^{(i)}))$ the sum of $\Delta_\kappa(C_n)$ for $C_n \in \mathbf{R_c}(C_{SF,j}^{(i)})$. Then we can have

    $$\Delta_\kappa(\mathbf{R_c}(C_{SF,j}^{(i)})) = \sum_{C_n \in \mathbf{R_c}(C_{SF,j}^{(i)})} \Delta_\kappa(C_n) \ . \qquad (6.21)$$

    (c) Select the codes with $\mathbf{min}\left\{\Delta_\kappa(\mathbf{R_c}(C_{SF,j}^{(i)}))\right\}$.

    (d) If there is only one code with $\mathbf{min}\left\{\Delta_\kappa(\mathbf{R_c}(C_{SF,j}^{(i)}))\right\}$, the code assignment process ends, or go to the next stage.

2. **In the second stage**, the sum of the MAI coefficients of the codes in $\mathbf{R_c}(C_{SF,\beta}^{(\alpha)})$ are compared, where $\{C_{SF,\beta}^{(\alpha)}\}$ is the code set with the same sum of increment

of MAI coefficients. In this stage, we assign the code with the smallest sum of MAI coefficients. If two candidates tie, go to the the third stage. The details of the rules in the second stage is as follows:

(a) Similar to the first step, we calculate the MAI coefficient of the n-th codes in $\mathbf{R_c}(C_{SF,\beta}^{(\alpha)})$, which is denoted by $\kappa(C_n)$.

(b) Denote $\kappa(\mathbf{R_c}(C_{SF,\beta}^{(\alpha)}))$ the sum of $\kappa(C_n)$, where $C_n \in \mathbf{R_c}(C_{SF,\beta}^{(\alpha)})$. Then we can have

$$\kappa(\mathbf{R_c}(C_{SF,\beta}^{(\alpha)})) = \sum_{C_n \in \mathbf{R_c}(C_{SF,\beta}^{(\alpha)})} \kappa(C_n) \ . \tag{6.22}$$

(c) Pick the codes with $\mathbf{min}\left\{\kappa(\mathbf{R_c}(C_{SF,\beta}^{(\alpha)}))\right\}$.

(d) If there is only one code with $\mathbf{min}\left\{\kappa(\mathbf{R_c}(C_{SF,\beta}^{(\alpha)}))\right\}$, the code assignment process ends, or go to the last step.

3. **In the third stage**, a code in $\left\{C_{SF,\delta}^{(\gamma)}\right\}$ is selected according to the crowded-first-code principle as suggested in [76], where $\left\{C_{SF,\delta}^{(\gamma)}\right\}$ is the code set with the same sum of MAI coefficients in the second stage. This assignment strategy selects a code of which ancestor code has the fewest free codes, thereby leaving more space for future high-rate users and so increasing the call admission rate.

6.4.2   Example

Now we give an example to illustrate the interference avoidance code assignment strategy. Consider codes $\left\{C_{8,8}^{(1)}, C_{8,1}^{(3)}, C_{8,5}^{(4)}, C_{8,7}^{(4)}\right\}$ in the four groups of the 2D code tree in Fig. 2.6.

1. <u>Compare the increment of the MAI coefficient $(\sum \Delta_\kappa(\cdot))$</u>: First, we compare the increment of the MAI coefficient $\sum \Delta_\kappa(\cdot)$. Referring to Fig. 2.7 and the definition of (2.1), one can easily find that the related codes for code $C_{8,8}^{(1)}$ are $C_{2,2}^{(2)}$

Check the candidate codes $\{C_{SF,j}^{(i)}\}$

In the first stage: check the sum of the incremental MAI coefficients.

If more than two codes tie

No

Yes

In the second stage: check the sum of MAI coefficients.

Assign $C_{SF,j}^{(i)}$ and code assignment process ends

If more than two codes tie

No

Yes

In the third stage: select a code by the crowded-first-code method.
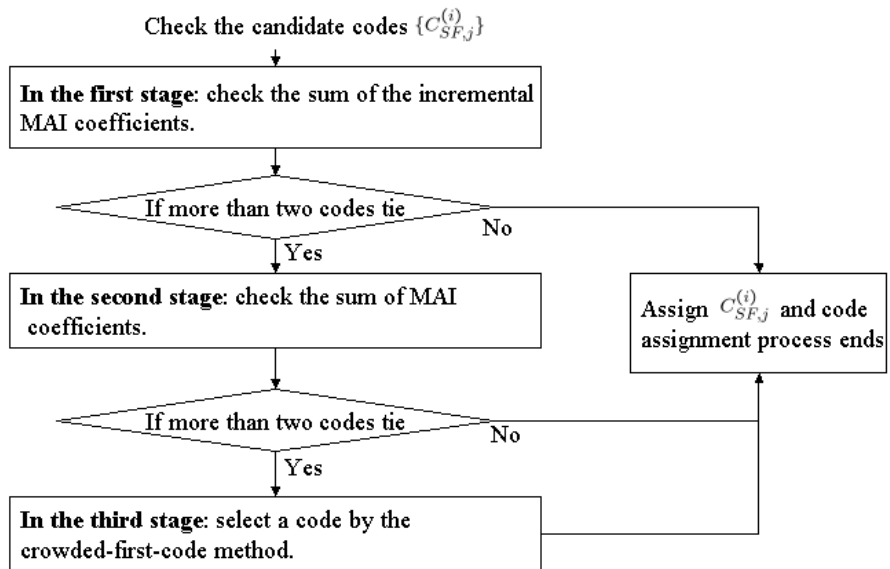
Fig. 6.1: Flow chart of the interference avoidance code assignment strategy.

and $C_{2,2}^{(3)}$ because they are in the same column. Thus, we have

$$\mathbf{R}_c(C_{8,8}^{(1)}) = \left\{ C_{8,8}^{(1)}, C_{2,2}^{(2)}, C_{2,2}^{(3)} \right\} \quad . \tag{6.23}$$

Based on (6.20), the incurred MAI coefficient $\Delta_\kappa(\mathbf{R}_c(C_{8,8}^{(1)}))$ after allocating code $C_{8,8}^{(1)}$ is equal to

$$\begin{aligned}
\Delta_\kappa(\mathbf{R}_c(C_{8,8}^{(1)})) &= \sum_{C_n \in \mathbf{R}_c(C_{8,8}^{(1)})} \Delta_\kappa(C_n) \\
&= \Delta_\kappa(C_{8,8}^{(1)}) + \Delta_\kappa(C_{2,2}^{(2)}) + \Delta_\kappa(C_{2,2}^{(3)}) = 2.5 \quad , \tag{6.24}
\end{aligned}$$

where

$$\begin{aligned}
\Delta_\kappa(C_{8,8}^{(1)}) &= \min(1, \frac{\sigma_{2,2}^{(2)}}{\sigma_{8,8}^{(1)}}) + \min(1, \frac{\sigma_{2,2}^{(3)}}{\sigma_{8,8}^{(1)}}) \\
&= \min(1, \frac{4}{1}) + \min(1, \frac{4}{1}) = 2 \quad , \tag{6.25}
\end{aligned}$$

$$\Delta_\kappa(C_{2,2}^{(2)}) = \min(1, \frac{\sigma_{8,8}^{(1)}}{\sigma_{2,2}^{(2)}}) = \frac{1}{4} \tag{6.26}$$

and

$$\Delta_\kappa(C_{2,2}^{(3)}) = \min(1, \frac{\sigma_{8,8}^{(1)}}{\sigma_{2,2}^{(3)}}) = \frac{1}{4} \quad . \tag{6.27}$$

Similarly, we can obtain $\Delta_\kappa(\mathbf{R}_c(C_{8,1}^{(3)})) = 2.5$, $\Delta_\kappa(\mathbf{R}_c(C_{8,5}^{(4)})) = 4$, and $\Delta_\kappa(\mathbf{R}_c(C_{8,7}^{(4)})) = 4.25$. Since $\Delta_\kappa(\mathbf{R}_c(C_{8,8}^{(1)})) = \Delta_\kappa(\mathbf{R}_c(C_{8,1}^{(3)})) = 2.5$, the code assignment enters the second stage to compares codes $C_{8,8}^{(1)}$ and $C_{8,1}^{(3)}$.

2. <u>Compare the sum of MAI coefficient $(\sum \kappa(\cdot))$</u>: In this stage, the sum of MAI coefficients of related codes $\sum \kappa(\cdot)$ for codes $C_{8,8}^{(1)}$ and $C_{8,1}^{(3)}$ are compared.

(a) <u>Calculate $\kappa(\mathbf{R}_c(C_{8,8}^{(1)}))$</u>: Recall (6.23) that $\mathbf{R}_c(C_{8,8}^{(1)}) = \left\{ C_{8,8}^{(1)}, C_{2,2}^{(2)}, C_{2,2}^{(3)} \right\}$.

As shown in Fig. 2.7, $C_{4,3}^{(1)}$, $C_{8,7}^{(1)}$, $C_{8,8}^{(1)}$, and $C_{2,2}^{(3)}$ are positioned in the same

column as $C_{2,2}^{(2)}$. Thus, we have $\mathbf{R}_c(C_{2,2}^{(2)}) = \left\{ C_{2,2}^{(2)}, C_{4,3}^{(1)}, C_{8,7}^{(1)}, C_{8,8}^{(1)}, C_{2,2}^{(3)} \right\}$.

Similarly, we can obtain $\mathbf{R}_c(C_{2,2}^{(3)}) = \mathbf{R}_c(C_{2,2}^{(2)})$. Then, it follows that

$$
\begin{aligned}
\kappa(\mathbf{R}_c(C_{8,8}^{(1)})) &= \sum_{C_n \in \mathbf{R}_c(C_{8,8}^{(1)})} \kappa(C_n) \\
&= \kappa(C_{8,8}^{(1)}) + \kappa(C_{2,2}^{(2)}) + \kappa(C_{2,2}^{(3)}) = 6 \ , \quad (6.28)
\end{aligned}
$$

where $\kappa(C_{8,8}^{(1)})) = \Delta_\kappa(C_{8,8}^{(1)})) = 2$ from (6.24) and

$$
\begin{aligned}
\kappa(C_{2,2}^{(2)}) &= \kappa(C_{2,2}^{(3)}) \\
&= \mathbf{min}(1, \frac{\sigma_{4,3}^{(1)}}{\sigma_{2,2}^{(2)}}) + \mathbf{min}(1, \frac{\sigma_{8,7}^{(1)}}{\sigma_{2,2}^{(2)}}) + \mathbf{min}(1, \frac{\sigma_{8,8}^{(1)}}{\sigma_{2,2}^{(2)}}) + \mathbf{min}(1, \frac{\sigma_{2,2}^{(3)}}{\sigma_{2,2}^{(2)}}) \\
&= \mathbf{min}(1, \frac{2}{4}) + \mathbf{min}(1, \frac{1}{4}) + \mathbf{min}(1, \frac{1}{4}) + \mathbf{min}(1, \frac{4}{4}) = 2 \quad (6.29)
\end{aligned}
$$

(b) <u>Calculate $\kappa(\mathbf{R}_c(C_{8,1}^{(3)}))$</u>:

Referring to Fig. 2.7, it is clearly that

$$
\mathbf{R}_c(C_{2,1}^{(2)}) = \mathbf{R}_c(C_{2,1}^{(1)}) = \mathbf{R}_c(C_{8,1}^{(3)}) = \left\{ C_{8,1}^{(3)}, C_{2,1}^{(1)}, C_{2,1}^{(2)} \right\} \ . \quad (6.30)
$$

By the same approach of obtaining (6.28), we have

$$
\begin{aligned}
\kappa(\mathbf{R}_c(C_{8,1}^{(3)})) &= \sum_{C_n \in \mathbf{R}_c(C_{8,1}^{(3)})} \kappa(C_n) \\
&= \kappa(C_{8,1}^{(3)}) + \kappa(C_{2,1}^{(1)}) + \kappa(C_{2,1}^{(2)}) = 4.5 \ , \quad (6.31)
\end{aligned}
$$

where $\kappa(C_{8,1}^{(3)})) = \Delta_\kappa(C_{8,1}^{(3)})) = 2$ and

$$
\begin{aligned}
\kappa(C_{2,1}^{(2)}) &= \kappa(C_{2,1}^{(1)}) \\
&= \min(1, \frac{\sigma_{8,1}^{(3)}}{\sigma_{2,1}^{(1)}}) + \min(1, \frac{\sigma_{2,1}^{(2)}}{\sigma_{2,1}^{(1)}}) \\
&= \min(1, \frac{1}{4}) + \min(1, \frac{4}{4}) = 1.25 \ . \qquad (6.32)
\end{aligned}
$$

Since code $C_{8,1}^{(3)}$ will have less total MAI in the set of its related codes than code $C_{8,8}^{(1)}$, it is chosen for serve the requested call.

6.5   Simulation Results

In this section, we illustrate the effectiveness of the proposed MAI-coefficient-based interference avoidance code assignment for the MC-DS-CDMA system. We first validate the correctness of Gaussian approximation of MAI. Then, we compare various code assignment strategies: random assignment (RM), pure crowded-first-code assignment (CF) without considering MAI, and the proposed interference avoidance assignment (IA+CF) methods.

6.5.1   Simulation Setup

Simulation Environment

In the simulation, we consider downlink MC-DS-CDMA in a single cell environment with the parameters listed in Table 6.1. Based on the assumptions in [42, 91], the subcarriers carrying the same data bits are assumed to experience independent flat Rayleigh fading. The background noise is modelled by white Gaussian noise with double-sided power spectrum density of $N_0/2$ and the transmitting $E_b/N_0 = 12$ dB.

A new call is modelled by a Poisson arrival process with the arrival rate (λ_c) of $1/2$ per time unit and the departure rate (μ_c) selecting from the set $\{1/24, 1/32, 1/40, 1/48, 1/56, 1/64, 1/80, 1/96, 1/112, 1/128, 1/144, 1/160, 1/176\}$. Thus, there are $\lambda_c/\mu_c = 12 \sim 88$ active calls in the system on average. With $U = 128$ parallel substreams, the frequency domain spreading factor (M) is 8 and the time domain spreading factor (SF) are 4, 8, 16, or 32. Each call requests a code of $8R_L$ ($SF = 4$), $4R_L$ ($SF = 8$), $2R_L$ ($SF = 16$), or R_L ($SF = 32$) with a probability according to the code traffic pattern [$a\ b\ c\ d$], where R_L is the basic data rate and the code traffic pattern of [$a\ b\ c\ d$] means that the times of requesting data rates $8R_L$, $4R_L$, $2R_L$, and R_L are proportional to $a : b : c : d$, respectively. It is assumed that the data rate of each user is fixed during his call holding time. To quantify the total traffic load carried by the active calls with different data rates, we define an effective traffic load (ρ) as follows:

$$\rho = \frac{\lambda_c}{\mu_c} \times \frac{8R_L \times a + 4R_L \times b + 2R_L \times c + R_L \times d}{a + b + c + d} \times \frac{1}{32R_L} \ . \tag{6.33}$$

where the time-domain spreading factor is selected from $SF = [\ 4\ 8\ 16\ 32\ ]$ and the code traffic pattern of [$a\ b\ c\ d$] is already defined. For example, when $\lambda_c = 1/2$ and $\mu_c = 1/40$ and the code traffic pattern [1 1 2 8], the effective traffic load ρ is 125% of the utilization of the time-domain resources.

Call Admission Control Principle

For call admission control, we consider the average received E_b/N_0. For an MAI coefficient (κ), the average received E_b/N_0 can be calculated by taking the average of (C.1) over M subcarriers' fading channels. A new coming call is blocked if accepting this new call will decrease the signal quality of any active calls below the required received $E_b/N_o = 5$ dB. We simulate 10,000 incoming calls for each combination of λ_c and μ_c.

Tab. 6.1: The Simulation Parameters

Call arrival rate (λ_c)	1/2
Departure rate (μ_c)	{1/24, 1/32, 1/40, 1/48, 1/56, 1/64, 1/80, 1/112, 1/128, 1/144, 1/160, 1/176}
Frequency-domain spreading factor (M)	8
Time-domain spreading factor (SF)	[4 8 16 32]
Code traffic pattern	[1 1 2 8]
Transmitting E_b/N_0	12 dB
Required received E_b/N_0	5 dB

Code Assignment Strategy

When a user requests a code with rate $2^k R_L$, a code assignment strategy should pick a free candidate code with rate $2^k R_L$ and ensure that its ancestor/decent codes are not used. In this paper, we compare our proposed IA+CF method with two other code assignment methods:

Random Assignment(RM) If there is one or more candidate codes in the 2D code tree, the RM method randomly selects a code without considering the code tree structure and impact of MAI.

Crowded-First(CF) If there is one or more candidate codes in the 2D code tree, the CF method picks a code whose ancestor code has the fewest free codes, thereby leaving more space for future high-rate users and so lowering the call blocking rate [76]. Note that the CF method considers the code tree structure but ignoring the impact of MAI.

6.5.2 Gaussian Approximation of MAI

To check the correctness of the Gaussian approximation of MAI, we simulate the MAI term $\sum_{v=1}^{M} \sum_{k=1}^{K_{\mathbf{A_o}}} \sum_{\ell=0}^{L_k^{(\mathbf{A_o})}-1} \sqrt{\frac{P_k^{(\mathbf{A_o})}}{P_o}} \frac{|\alpha_{o,s,v}|^2 c_k^{(\mathbf{A_o})}[v]c_o[v]}{L_k^{(\mathbf{A_o})}} \Delta[\ell]$ in (6.12). Figure 6.2 presents an example of Gaussian approximation of MAI for the frequency-domain spreading factor $M = 8$. Let the time-domain spreading factor of both the reference user and single interferer be $SF = 16$. The statistics of the MAI are obtained from 10,000 simulations. As shown in the figure, the MAI in the MC-DS-CDMA system is close to a Gaussian distributed random variable because the decision variable of a desired signal is a combination of $M = 8$ subcarriers' signals and these eight subcarriers experience independent flat fading. This can justify the assumption used in our model for the MAI coefficient.

6.5.3 Comparison of Code Assignment Strategies

Figures 6.3(a) and 6.3(b) show the received E_b/N_0 and the call admission rate of the RM, CM, and IA+CF code assignment strategies with various effective traffic loads. We have following observations. First, comparing to RM, the IA+CF method has better received E_b/N_0 when $0.75 \leq \rho \leq 2.25$. However for $\rho \geq 2.5$, IA+CF has lower received E_b/N_0 due to the increasing MAI by accommodating more users than RM. Second, comparing to CF, the IA+CF method has better E_b/N_0 at the cost of a slightly lower call admission rate. For $\rho = 2$, the E_b/N_0 improvement of the IA+CF method over the CF method is 1.9 dB, while the call admission of IA+CF is 1.6% lower than CF. The reason why the call admission rate for the IA+CF method is slightly lower than that of the CF method can be explained as follows. The CF method can make the tree structure of the allocated codes more compact, gather more larger code resources for higher-rate users, thereby increasing the admission rate. The IA+CF method aims to avoid MAI first before executing the CF principle. Third, one can
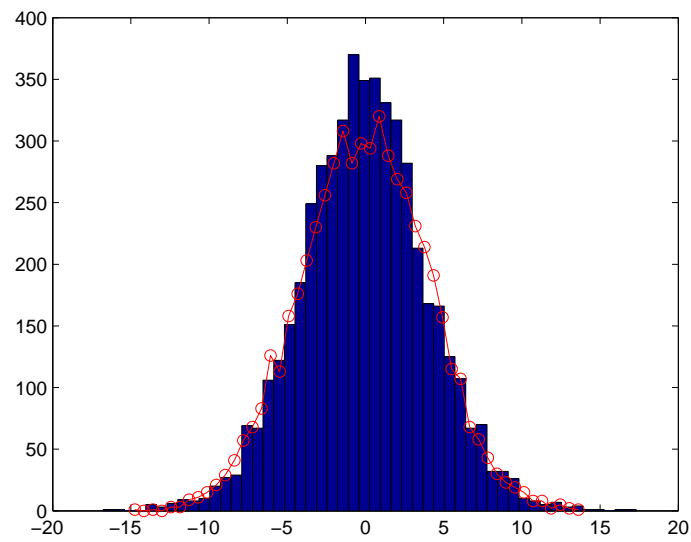
Fig. 6.2: An illustration example of approximating MAI by Gaussian distributed random variable. The time- and frequency-domain spreading factors of the reference and single interfering users are $SF = 16$ and $M = 8$, respectively.

also find that for $1 \leq \rho \leq 2.25$ the IA+CF method has highest received E_b/N_0, the RM method ranks second, and the CF method has the lowest E_b/N_0. Fourth, as the traffic load increases, the difference between the IA+CF and CF methods, in terms of both the received E_b/N_0 and call admission rate, becomes smaller. For example, the difference of E_b/N_0 between the two methods decreases from 1.9 dB to 0.1 dB as ρ changes from 2 to 5.5; the call admission rate appears to be the same at $\rho = 5.5$. This is because when there are more active users in the system, the IA+CF method can not easily find a good code with low interference for a new coming user. In this situation, the IA+CF method picks a code according to the CF principle.

6.6   Chapter Summary

In this chapter, we have proposed a novel interference avoidance code assignment strategy for multi-rate MC-DS-CDMA with TF-domain spreading. We analyze the error rate performance and defined new performance metric — *MAI coefficient* — to estimate the quantity of MAI imposed on each code channel. By simulations and analysis, we demonstrate that the proposed interference avoidance code assignment method can effectively reduce the MAI for multi-rate users in an MC-DS-CDMA system with time- and frequency-domain spreading, while maintaining the high call admission rate.
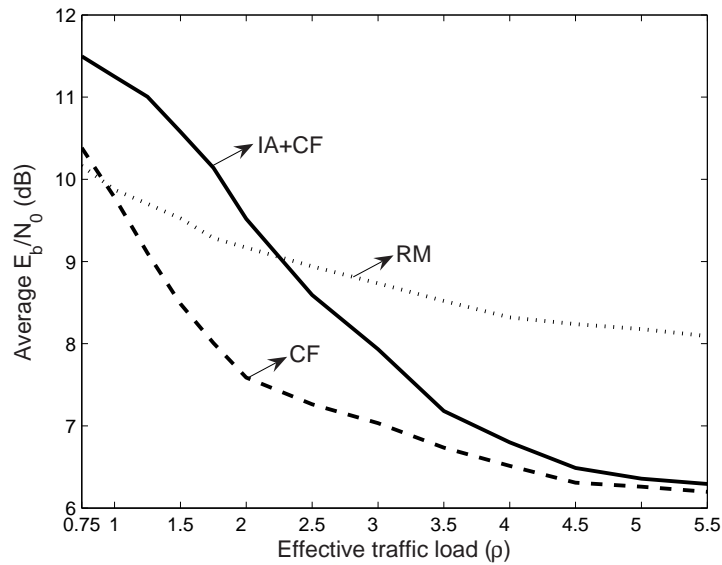
(a) Average received E_b/N_0 (dB)
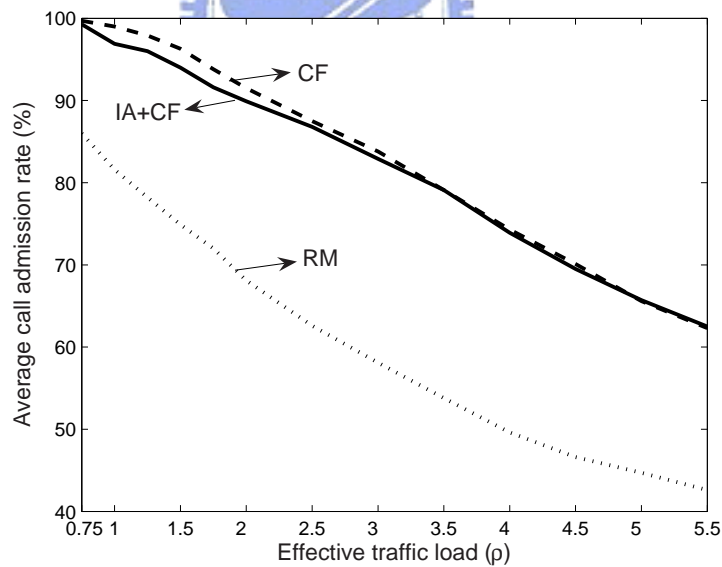
(b) Average admission rate

Fig. 6.3: Comparison of the average received E_b/N_0 and call admission rate against the effective traffic load for the RM, CF, and the IA+CF code assignment strategies, where the code pattern is [1 1 2 8], $E_b/N_0 = 12$ dB at the transmitter, and the required received $E_b/N_0 = 5$ dB.

Chapter 7

Joint Subcarrier Power Allocation and Interference Avoidance Code Assignment for Downlink MC-DS-CDMA

In this chapter, we cooperate a subcarrier power allocation and the interference avoidance code assignment in Chapter 6 to solve the challenging problem — how to maximally benefit from a particular subcarrier power allocation, while simultaneously controlling the MAI at an acceptable level and maintaining a high call admission rate in the downlink multi-rate multi-carrier direct sequence code division multiple access (MC-DS-CDMA) system with time- and frequency-domain (TF-domain) spreading. To achieve this goal, a subcarrier power allocation is first proposed to optimize the received signal power. By analyzing the error rate performance in the presence of the subcarrier power allocation, we can define the same MAI coefficient as that in Chapter 6. This means the interference code assignment method proposed in Chapter 6 can also be applied together with the subcarrier power allocation. Thus, in the proposed joint scheme, the interference avoidance code assignment plays the role to eliminate MAI and the subcarrier power allocation is to optimize the received signal power.

7.1 System Model

7.1.1 Transmitted Signal

The transmitter structure in the MC-DS-CDMA system with time- and frequency-domain spreading is shown in Fig. 5.1. A serial-to-parallel converter is applied to reduce the subcarrier data rate by converting data streams with bit duration $T_{b,k}^{(\mathbf{X})}$ into U reduced-rate parallel substreams with new bit duration $T_k^{(\mathbf{X})} = U T_{b,k}^{(\mathbf{X})}$ for user k in group $\mathbf{X} \in \{\mathbf{A_o}, \mathbf{B_o}, \mathbf{C_o}\}$. Each substream experiences a frequency flat (or non-dispersive) fading. Then, for each substream, a spreading code $g_k^{(\mathbf{X})}(t)$ is used to spread data signal in the time domain. After being copied to M subcarriers, the data in each substream is multiplied by a frequency domain spreading code $\{c_k^{(\mathbf{X})}[j]\}$. In this case, the frequency-domain spreading gain is M. The user group $\mathbf{X}$ is defined as follows. Let $g_o(t)$ and $c_o[j]$ be the time domain spreading code and the frequency domain spreading code of the reference user, respectively. Following [44], we categorize the interfering users into three groups:

1. group $\mathbf{A_o}$: $\dfrac{1}{T_o} \displaystyle\int_0^{T_o} g_k^{(\mathbf{A_o})}(t) g_o(t) dt \neq 0$ and $\dfrac{1}{M} \displaystyle\sum_{j=1}^M c_k^{(\mathbf{A_o})}[j] c_o[j] = 0$.

2. group $\mathbf{B_o}$: $\dfrac{1}{T_o} \displaystyle\int_0^{T_o} g_k^{(\mathbf{B_o})}(t) g_o(t) dt = 0$ and $\dfrac{1}{M} \displaystyle\sum_{j=1}^M c_k^{(\mathbf{B_o})}[j] c_o[j] \neq 0$.

3. group $\mathbf{C_o}$: $\dfrac{1}{T_o} \displaystyle\int_0^{T_o} g_k^{(\mathbf{C_o})}(t) g_o(t) dt = 0$ and $\dfrac{1}{M} \displaystyle\sum_{j=1}^M c_k^{(\mathbf{C_o})}[j] c_o[j] = 0$.

The transmitted signal of user k in group $\mathbf{X} \in \{\mathbf{A_o}, \mathbf{B_o}, \mathbf{C_o}\}$ can be expressed as

$$s_k^{(\mathbf{X})}(t) \;=\; \sum_{i=1}^U \sum_{j=1}^M \sqrt{2 P_{k,i,j}^{(\mathbf{X})}} b_{k,i}^{(\mathbf{X})}(t) g_k^{(\mathbf{X})}(t) c_k^{(\mathbf{X})}[j] \cos(2\pi f_{i,j} t + \varphi_{k,i,j}^{(\mathbf{X})}) \;, \qquad (7.1)$$

where $P_{k,i,j}^{(\mathbf{X})}$, $\{f_{i,j}\}$ and $\{\varphi_{k,i,j}^{(\mathbf{X})}\}$ represent the transmitted power, the j-th subcarrier frequency and the initial phase in the i-th substream, respectively. The waveform of

the i-th substream $b_{k,i}^{(\mathbf{X})}(t) = \sum_{h=-\infty}^{\infty} b_{k,i}^{(\mathbf{X})}[h] P_{T_k^{(\mathbf{X})}}(t - hT_k^{(\mathbf{X})})$ contains a rectangular pulses of duration $T_k^{(\mathbf{X})}$, where $b_{k,i}^{(\mathbf{X})}[h] = \pm 1$ with equal probability. The time domain spreading code $g_k^{(\mathbf{X})}(t) = \sum_{\ell=-\infty}^{\infty} g_k^{(\mathbf{X})}[\ell] P_{T_c}(t - \ell T_c)$ represents the chip sequence of the rectangular pulses of duration T_c, where $g_k^{(\mathbf{X})}[\ell] = \pm 1$ with equal probability. Note that the time domain spreading factor of user k in the group $\mathbf{X}$ is $G_k^{(\mathbf{X})} = T_k^{(\mathbf{X})}/T_c$.

7.1.2 Received Signal

The receiver structure of the MC-DS-CDMA using time-domain and frequency-domain spreading codes is shown in Fig. 5.2. Recall that each substream experiences the flat Rayleigh fading. Then, the received signal of the reference user (denoted by r_o) in the synchronous transmission can be expressed as:

$$
\begin{aligned}
r_o(t) &= \sum_{i=1}^{U}\sum_{j=1}^{M}\sqrt{2P_{o,i,j}}\,\alpha_{o,i,j}b_{o,i}(t)g_o(t)c_o[j]\cos(2\pi f_{i,j}t + \phi_{o,i,j}) + \\
&\quad \sum_{\mathbf{X}\in\{\mathbf{A_o},\mathbf{B_o},\mathbf{C_o}\}}\sum_{k=1}^{K_{\mathbf{X}}}\sum_{i=1}^{U}\sum_{j=1}^{M}\sqrt{2P_{k,i,j}^{(\mathbf{X})}}\,\alpha_{o,i,j}b_{k,i}^{(\mathbf{X})}(t)g_k^{(\mathbf{X})}(t)c_k^{(\mathbf{X})}[j]\cos(2\pi f_{i,j}t + \phi_{o,i,j}) \\
&\quad +n(t) \ ,
\end{aligned} \tag{7.2}
$$

where $P_{o,i,j}$ and $\alpha_{o,i,j}$ are the reference user's transmission power and the channel amplitude for the i-th subcarrier of the j-th substream; $K_{\mathbf{X}}$ is the number of users in the group $\mathbf{X}$; and $n(t)$ is the white Gaussian noise with double-sided power spectrum density of $N_0/2$. In (7.2), $\phi_{o,i,j} = \varphi_{o,i,j} + \psi_{o,i,j}$ is uniformly distributed in $[0, 2\pi)$, where $\psi_{o,i,j}$ is the channel's phase of the i-th subcarrier in the j-th substream.

Without loss of generality, let the bit of interest be $b_{o,s}[0]$, i.e. the first bit in the s-th substream from the reference user. After time domain despreading, the output signal for the reference user in the v-th subcarrier of the s-th substream can

be expressed as:

$$Y_{o,s,v} = \int_0^{T_o} r_o(t)\beta_{o,s,v}g_o(t)c_o[v]\cos(2\pi f_{s,v}t + \phi_{s,v})dt$$

$$= \frac{T_o}{\sqrt{2}}\left\{b_{o,s}[0]\sqrt{P_{o,s,v}}\alpha_{o,s,v}\beta_{o,s,v} + \sum_{\mathbf{X}\in\{\mathbf{A_o},\mathbf{B_o},\mathbf{C_o}\}}\sum_{k=1}^{K_{\mathbf{X}}}I_{k,s,v}^{(\mathbf{X})} + n_{s,v}\right\} \quad, \quad (7.3)$$

where T_o is the bit duration of the reference user; $\beta_{o,s,v}$ is the weights for a certain combining scheme; $I_{k,s,v}^{(\mathbf{X})}$ denotes the MAI induced from user k of group $\mathbf{X}$ to the v-th subcarrier of the s-th substream of the reference user; and $n_{s,v}$ is the white Gaussian noise with zero mean and variance of $\frac{|\beta_{o,s,v}|^2}{2}\frac{N_o}{T_0}$. The MAI terms $I_{k,s,v}^{(\mathbf{X})}$ in (7.3) can be expressed as

$$I_{k,s,v}^{(\mathbf{X})} = \sqrt{P_{k,s,v}^{(\mathbf{X})}}\frac{\alpha_{o,s,v}\beta_{o,s,v}c_k^{(\mathbf{X})}[v]c_o[v]}{T_o}\int_0^{T_o}b_{k,s}^{(\mathbf{X})}(t)g_k^{(\mathbf{X})}(t)g_o(t)dt \quad. \quad (7.4)$$

Then combining M subcarriers, the decision variable of $b_{o,s}[0]$ for the reference user becomes

$$Y_{o,s} = \sum_{v=1}^{M}Y_{o,s,v}$$

$$= \frac{T_o}{\sqrt{2}}\left\{\underbrace{b_{o,s}[0]\sum_{v=1}^{M}\sqrt{P_{o,s,v}}\alpha_{o,s,v}\beta_{o,s,v}}_{desired\ signal} + \underbrace{\sum_{\mathbf{X}\in\{\mathbf{A_o},\mathbf{B_o},\mathbf{C_o}\}}\sum_{k=1}^{K_{\mathbf{X}}}\sum_{v=1}^{M}I_{k,s,v}^{(\mathbf{X})}}_{MAI} + \sum_{v=1}^{M}n_{s,v}\right\},$$

$$(7.5)$$

where $Y_{o,s,v}$ is given in (7.3).

In (7.5), we face the problem to simultaneously maximize the desired signal's power and eliminate the MAI. One should note that as a user maximizes its received signal power by a particular subcarrier power allocation, it may result in excessive MAI to other users. The MAI occrus when user k adjusts $P_{k,s,v}^{(\mathbf{X})}$ according to $\alpha_{k,s,v}^{(\mathbf{X})}$. It

is difficult to please each user just by this particular subcarrier power allocation. One of the goals in this chapter is to find a method to improve the desired signal quality and control MAI.

7.2 Subcarrier Power Allocation and Interference Analysis

7.2.1 Subcarrier Power Allocation

The goal of this subsection is to propose a subcarrier power allocation to optimize the signal of the desired user in (7.5). The transmission power is constrained to avoid the so-called party effect in CDMA system. The party effect is a situation where all users continuously increase transmission power but indeed the signal quality is not improved due to increasing interference. The transmission power constraint on the reference user can be expressed as:

$$\sum_{v=1}^{M} P_{o,s,v} = P_o \ , \tag{7.6}$$

where P_o is assumed to be proportional to the reference user's transmission rate as in [70] and [88]. From (7.5), the subcarrier power allocation to maximize the desired signal can be formulated as follows:

$$\text{maximize} \quad \sum_{v=1}^{M} \sqrt{P_{o,s,v}} \alpha_{o,s,v} \beta_{o,s,v}$$

$$\text{subject to} \quad \sum_{v=1}^{M} P_{o,s,v} = P_o \ . \tag{7.7}$$

According to the maximal ratio combine (MRC) criteria, the subcarrier's signal is maximized when $\beta_{o,s,v} = \alpha_{o,s,v}^*$. Applying the Lagrange multiplier method, we obtain

the Lagrange function as

$$J(P_{o,s,1}, ..., P_{o,s,M}) = \sum_{v=1}^{M} \sqrt{P_{o,s,v}} |\alpha_{o,s,v}|^2 + \lambda_L \left(\sum_{v=1}^{M} P_{o,s,v} - P_o \right) , \quad (7.8)$$

where λ_L is the Lagrange multiplier. Differentiating (7.8) with respect to $P_{o,s,v}$ and setting it to zero, it is followed that

$$\frac{1}{2\sqrt{P_{o,s,v}}} |\alpha_{o,s,v}|^2 + \lambda_L = 0, \quad v = 1 \sim M . \quad (7.9)$$

Solving (7.6) and (7.9), we can obtain the optimal $P_{o,s,v}$

$$P_{o,s,v} = \frac{|\alpha_{o,s,v}|^4}{\sum_{v=1}^{M} |\alpha_{o,s,v}|^4} P_o , \quad (7.10)$$

which can maximize the desired signal in (7.5). Similarly, we can also have

$$P_{k,s,v}^{(\mathbf{X})} = \frac{|\alpha_{k,s,v}^{(\mathbf{X})}|^4}{\sum_{v=1}^{M} |\alpha_{k,s,v}^{(\mathbf{X})}|^4} P_k^{(\mathbf{X})} , \quad (7.11)$$

where $\alpha_{k,s,v}^{(\mathbf{X})}$ is the channel amplitude for the s-th subcarrier of the v-th substream of the interfering user. Note that $P_k^{(\mathbf{X})}/P_o = R_k^{(\mathbf{X})}/R_o$, where R_o and $R_k^{(\mathbf{X})}$ are the transmission rates of the reference user and user k in group $\mathbf{X}$, respectively.

7.2.2 Interference Analysis

Now, we analyze the effect of MAI in the multi-rate MC-DS-CDMA system with TF-domain spreading when applying the subcarrier power allocation. To facilitate the calculation of $I_{k,s,v}^{(\mathbf{X})}$, we consider two scenarios according to the relation between T_o (the bit duration of the reference user) and $T_k^{(\mathbf{X})}$ (the bit duration of the interfering user k in group $\mathbf{X}$).

1. MAI from High Data Rate Users $(T_o > T_k^{(\mathbf{X})})$ In this case, the ratio of bit duration of the desired users to the interfering user of group $\mathbf{X} \in \{\mathbf{A_o}, \mathbf{B_o}, \mathbf{C_o}\}$ can

be written as $L_k^{(\mathbf{X})} = T_o/T_k^{(\mathbf{X})}$, where $L_k^{(\mathbf{X})}$ is a positive integer. Rewrite (7.4) as

$$
\begin{aligned}
I_{k,s,v}^{(\mathbf{X})} &= \sqrt{P_{k,s,v}^{(\mathbf{X})}} \frac{\alpha_{o,s,v}\beta_{o,s,v}c_k^{(\mathbf{X})}[v]c_o[v]}{T_o} \int_0^{T_o} b_{k,s}^{(\mathbf{X})}(t)g_k^{(\mathbf{X})}(t)g_o(t)dt \\
&= \sqrt{P_{k,s,v}^{(\mathbf{X})}} \frac{\alpha_{o,s,v}\beta_{o,s,v}c_k^{(\mathbf{X})}[v]c_o[v]}{L_k^{(\mathbf{X})}T_k^{(\mathbf{X})}} \sum_{\ell=0}^{L_k^{(\mathbf{X})}-1} b_{k,s}^{(\mathbf{X})}[\ell] \int_0^{T_k^{(\mathbf{X})}} g_k^{(\mathbf{X})}(t)g_o(t)dt \ .
\end{aligned}
$$

$$(7.12)$$

Based on the definition of user group in Section 7.1.1, we can have $I_{k,s,v}^{(\mathbf{B_o})} = I_{k,s,v}^{(\mathbf{C_o})} = 0$ because $\int_0^{T_k^{(\mathbf{B_o})}} g_k^{(\mathbf{B_o})}(t)g_o(t)dt = 0$ and $\int_0^{T_k^{(\mathbf{C_o})}} g_k^{(\mathbf{C_o})}(t)g_o(t)dt = 0$. That is, the time-domain spreading codes of users in groups $\mathbf{B_o}$ and $\mathbf{C_o}$ are orthogonal to the reference user. Recall that $b_{k,s}^{(\mathbf{C_o})}[\ell] = \pm 1$ with equal probability. Thus, it is followed that

$$
\frac{b_{k,s}^{(\mathbf{C_o})}[\ell]}{T_k^{(\mathbf{A_o})}} \int_0^{T_k^{(\mathbf{A_o})}} g_k^{(\mathbf{A_o})}(t)g_o(t)dt = \pm 1 \tag{7.13}
$$

with equal probability. Consequently, (7.12) can be simplified to

$$
I_{k,s,v}^{(\mathbf{A_o})} = \sqrt{P_{k,s,v}^{(\mathbf{X})}} \frac{\alpha_{o,s,v}\beta_{o,s,v}c_k^{(\mathbf{A_o})}[v]c_o[v]}{L_k^{(\mathbf{A_o})}} \sum_{\ell=0}^{L_k^{(\mathbf{A_o})}-1} \Delta[\ell] \ , \tag{7.14}
$$

where $\Delta[\ell] = \pm 1$ with equal probability.

2. <u>MAI from Low Data Rate Users $(T_o \leq T_k^{(\mathbf{X})})$</u> In this case, we express $I_{k,s,v}^{(\mathbf{X})}$ as

$$
\begin{aligned}
I_{k,s,v}^{(\mathbf{X})} &= \sqrt{P_{k,s,v}^{(\mathbf{X})}} \frac{\alpha_{o,s,v}\beta_{o,s,v}c_k^{(\mathbf{X})}[v]c_o[v]}{T_o} \int_0^{T_o} b_{k,s}^{(\mathbf{X})}(t)g_k^{(\mathbf{X})}(t)g_o(t)dt \\
&= \sqrt{P_{k,s,v}^{(\mathbf{X})}} \frac{\alpha_{o,s,v}\beta_{o,s,v}c_k^{(\mathbf{X})}[v]c_o[v]}{T_o} b_{k,s}^{(\mathbf{X})}[0] \int_0^{T_o} g_k^{(\mathbf{X})}(t)g_o(t)dt \ . \quad (7.15)
\end{aligned}
$$

Similar to the case of MAI from high data rate users, we have $I_{k,v}^{(\mathbf{B_o})} = I_{k,v}^{(\mathbf{C_o})} = 0$ and

$$
\frac{b_{k,s}^{(\mathbf{X})}[0]}{T_o} \int_0^{T_o} g_k^{(\mathbf{A_o})}(t)g_o(t)dt = \pm 1 \ . \tag{7.16}
$$

Thus, we have

$$I_{k,s,v}^{(\mathbf{A_o})} = \sqrt{P_{k,s,v}^{(\mathbf{X})}} \alpha_{o,s,v} \beta_{o,s,v} c_k^{(\mathbf{A_o})}[v] c_o[v] \Delta[0] \ , \tag{7.17}$$

where $\Delta[0]$ is defined in (7.14). Note that (7.17) is the special case of (7.14). Specifically, we can obtain (7.17) by letting $L_k^{(\mathbf{A_o})} = 1$ in (7.14).

Let $\beta_{o,s,v} = \alpha_{o,s,v}^*$ for the maximum ratio combining scheme. With $I_{k,v}^{(\mathbf{B_o})} = I_{k,v}^{(\mathbf{C_o})} = 0$, we substitute (7.10), (7.11), (7.14) and (7.17) into (7.5) and obtain

$$Y_{o,s} = \sqrt{\frac{P_o}{2}} T_o \left\{ b_{o,s}[0] \frac{\sum_{v=1}^{M} |\alpha_{o,s,v}|^4}{\sqrt{\sum_{i=1}^{M} |\alpha_{o,s,i}|^4}} + \right.$$
$$\left. \sum_{k=1}^{K_{\mathbf{A_o}}} \sum_{v=1}^{M} \sum_{\ell=0}^{L_k^{(\mathbf{A_o})}-1} \sqrt{\frac{P_k^{(\mathbf{X})}}{P_o}} \frac{|\alpha_{k,s,v}^{(\mathbf{A_o})}|^2 |\alpha_{o,s,v}|^2 c_k^{(\mathbf{A_o})}[v] c_o[v]}{\sqrt{\sum_{i=1}^{M} |\alpha_{k,s,i}^{(\mathbf{A_o})}|^4} L_k^{(\mathbf{A_o})}} \Delta[\ell] + \frac{1}{\sqrt{P_o}} \sum_{v=1}^{M} n_{s,v} \right\} . \tag{7.18}$$

Following [62], we assume that the MAI can be approximated by a zero mean Gaussian distributed random variable. Thus, the normalized decision variable $Y_{o,s}$ can be modelled by a Gaussian random variable with mean

$$E[Y_{o,s}] = b_{o,s}[0] \sqrt{\sum_{v=1}^{M} |\alpha_{o,s,v}|^4} \tag{7.19}$$

and variance

$$
Var[Y_{o,s}] = \sum_{v=1}^{M}\sum_{k=1}^{K_{\mathbf{A_o}}}\sum_{\ell=0}^{L_k^{(\mathbf{A_o})}-1} Var\left[\sqrt{\frac{P_k^{(\mathbf{A_o})}}{P_o}}\frac{|\alpha_{k,s,v}^{(\mathbf{A_o})}|^2|\alpha_{o,s,v}|^2 c_k^{(\mathbf{A_o})}[v]c_o[v]}{\sqrt{\sum_{i=1}^{M}|\alpha_{k,s,i}^{(\mathbf{A_o})}|^4 L_k^{(\mathbf{A_o})}}}\Delta[\ell]\right] +
$$

$$
\frac{1}{2}(\frac{E_o}{N_0})^{-1}\sum_{v=1}^{M}|\alpha_{o,s,v}|^2
$$

$$
= \sum_{v=1}^{M}\sum_{k=1}^{K_{\mathbf{A_o}}}\sum_{\ell=0}^{L_k^{(\mathbf{A_o})}-1}\frac{P_k^{(\mathbf{A_o})}}{P_o}\frac{|\alpha_{o,s,v}|^4}{(L_k^{(\mathbf{A_o})})^2}\mathrm{E}\left[\frac{|\alpha_{k,s,v}^{(\mathbf{A_o})}|^4}{\sum_{i=1}^{M}|\alpha_{k,s,i}^{(\mathbf{A_o})}|^4}\right] + \frac{1}{2}(\frac{E_o}{N_0})^{-1}\sum_{v=1}^{M}|\alpha_{o,s,v}|^2 \ .
$$

$$(7.20)$$

Define the received E_b/N_0 (denoted by γ) as

$$
\gamma = \frac{E^2[Y_{o,s}]}{2Var[Y_{o,s}]}
$$

$$
= \frac{\sum_{v=1}^{M}|\alpha_{o,s,v}|^4}{2\sum_{v=1}^{M}\sum_{k=1}^{K_{\mathbf{A_o}}}\sum_{\ell=0}^{L_k^{(\mathbf{A_o})}-1}\frac{P_k^{(\mathbf{A_o})}}{P_o}\frac{|\alpha_{o,s,v}|^4}{(L_k^{(\mathbf{A_o})})^2}\mathrm{E}\left[\frac{|\alpha_{k,s,v}^{(\mathbf{A_o})}|^4}{\sum_{i=1}^{M}|\alpha_{k,s,i}^{(\mathbf{A_o})}|^4}\right] + (\frac{E_o}{N_0})^{-1}\sum_{v=1}^{M}|\alpha_{o,s,v}|^2}
$$

$$
= \frac{P_oG_o\sum_{v=1}^{M}|\alpha_{o,s,v}|^4}{\underbrace{2\sum_{v=1}^{M}\sum_{k=1}^{K_{\mathbf{A_o}}}\sum_{\ell=0}^{L_k^{(\mathbf{A_o})}-1}\frac{R_k^{(\mathbf{A_o})}}{R_o}\frac{|\alpha_{o,s,v}|^4}{(L_k^{(\mathbf{A_o})})^2}\mathrm{E}\left[\frac{|\alpha_{k,s,v}^{(\mathbf{A_o})}|^4}{\sum_{i=1}^{M}|\alpha_{k,s,i}^{(\mathbf{A_o})}|^4}\right]P_oG_o}_{MAI} + \underbrace{P_N\sum_{v=1}^{M}|\alpha_{s,v}|^2}_{noise}} \ ,
$$

$$(7.21)$$

where R_o and $R_k^{(\mathbf{A_o})}$ are the transmission rates of the reference user and user k in group $\mathbf{A_o}$, respectively. Note that $E_o = P_oT_o$ and $N_0 = P_NT_c$, where P_o and P_N are the transmission power of the reference user and the noise power. As in [70, 88], $R_k^{(\mathbf{A_o})}/R_o = P_k^{(\mathbf{A_o})}/P_o$ means a high-rate user needs more power.

7.2.3   MAI Coefficient

In order to quantize the effect of MAI imposed on each code channel, we define a performance metric — *MAI coefficient*. Assume that the fading parameters in the MAI term of (7.21) are independent because the downlink MAI is resulted from the sub-carriers of reusing time-domain spreading codes in different frequency-domain code trees. Now, we observe the MAI term of γ in (7.21) and find that the term $2P_oG_o\sum_{v=1}^{M}|\alpha_{o,s,v}|^4\mathrm{E}\left[|\alpha_{k,s,v}^{(\mathbf{A_o})}|^4 \Big/ \sum_{i=1}^{M}|\alpha_{k,s,i}^{(\mathbf{A_o})}|^4\right]$ is common to all the $K_{\mathbf{A_o}}$ interfering users. As a result, we can just use $\sum_{k=1}^{K_{\mathbf{A_o}}}\sum_{\ell=0}^{L_k^{(\mathbf{A_o})}-1} R_k^{(\mathbf{A_o})}/(R_o(L_k^{(\mathbf{A_o})})^2)$ to characterize the downlink MAI in the MC-DS-CDMA system. There are two possible scenarios as described below.

1. **MAI from High Data Rate Users:** In this case $R_k^{(\mathbf{A_o})}/R_o = T_o/T_k^{(\mathbf{A_o})} = L_k^{(\mathbf{A_o})} > 1$. Subsequently, we can obtain

$$\sum_{k=1}^{K_{\mathbf{A_o}}}\sum_{\ell=0}^{L_k^{(\mathbf{A_o})}-1}\frac{R_k^{(\mathbf{A_o})}}{R_o(L_k^{(\mathbf{A_o})})^2} = \sum_{k=1}^{K_{\mathbf{A_o}}}\sum_{\ell=0}^{L_k^{(\mathbf{A_o})}-1}\frac{1}{L_k^{(\mathbf{A_o})}}$$

$$= \sum_{k=1}^{K_{\mathbf{A_o}}}1 \ . \tag{7.22}$$

2. **MAI from Low Data Rate Users:** Let $L_k^{(\mathbf{A_o})} = 1$ in the MAI term of (7.21). Then it is followed that

$$\sum_{k=1}^{K_{\mathbf{A_o}}}\sum_{\ell=0}^{L_k^{(\mathbf{A_o})}-1}\frac{R_k^{(\mathbf{A_o})}}{R_o(L_k^{(\mathbf{A_o})})^2} = \sum_{k=1}^{K_{\mathbf{A_o}}}\frac{R_k^{(\mathbf{A_o})}}{R_o} \ . \tag{7.23}$$

Note that $R_k^{(\mathbf{A_o})}/R_o < 1$ in this case.

Observing (7.22) and (7.23), we can define the downlink *MAI coefficient* in the MC-DS-CDMA system with TF-domain spreading as

$$\kappa = \sum_{k=1}^{K_{\mathbf{A_o}}}\mathbf{min}(1, \frac{R_k^{(\mathbf{A_o})}}{R_o}) \ . \tag{7.24}$$

According to the grip representation in Section 2.2.5, (7.24) can also be expressed as

$$\kappa = \sum_{k=1}^{K_{\mathbf{A_o}}} \mathbf{min}(1, \frac{\sigma_k^{(\mathbf{A_o})}}{\sigma_o}) \ , \tag{7.25}$$

where $\sigma_k^{(\mathbf{A_o})}$ and σ_o represent the areas of the rectangles in Fig. 2.7 for codes with transmission rates $R_k^{(\mathbf{A_o})}$ and R_o, respectively.

7.3 Joint Subcarrier Power Allocation and Interference Avoidance Code Assignment Strategy

7.3.1 Principles

In this section, we propose to integrate the subcarrier power allocation and the interference avoidance code assignment strategy to optimize the received signal power and eliminate the MAI simultaneously. In principle, as shown in Fig. 7.1, the joint scheme consists of two steps: the subcarrier power allocation and code assignment. In the first step, each user apply the subcarrier power allocation greedily to maximize his own received signal power. In the second step, the interference avoidance code assignment is used to pick spreading codes which produce less MAI. Let $\{C_{SF,j}^{(i)}\}$ be the set of candidate codes with frequency domain and time domain spreading factors M and SF, respectively, where $1 \leq i \leq M$ and $1 \leq j \leq SF$. Denote $\mathbf{R_c}(C_{SF,j}^{(i)})$ the set of the codes related to $C_{SF,j}^{(i)}$. The joint subcarrier power allocation and code assignment strategy is summarized as follows.

1. **In the first step**: Each user implements the subcarrier power allocation according to (7.10) and (7.11).

2. ***In the second step***: With the aid of the MAI coefficient, we apply the interference avoidance code assignment strategy proposed in Chapter 6. The principles of the interference avoidance code assignment strategy are also summarized in the following.

   (a) ***In the first stage***, the incurred MAI of using code $C_{SF,j}^{(i)}$ is estimated by the sum of the increment of the MAI coefficients of codes in $\mathbf{R_c}(C_{SF,j}^{(i)})$. If any two candidate codes lead to the same amount of incremental MAI coefficients in $\mathbf{R_c}(C_{SF,j}^{(i)})$, go to the second stage. Otherwise, the smallest sum of incremental MAI coefficients in the set of $\mathbf{R_c}(C_{SF,j}^{(i)})$ is selected.

   (b) ***In the second stage***, the sum of the MAI coefficients of the codes in $\mathbf{R_c}(C_{SF,j}^{(i)})$ is compared and the one with the smallest sum of MAI coefficients. If two candidates tie, go to the the third stage.

   (c) ***In the third stage***, a code in $\left\{ C_{SF,j}^{(i)} \right\}$ is selected according to the crowded-first principle as suggested in [76]. This assignment strategy selects a code of which ancestor code has the fewest free codes, thereby leaving more space for future high-rate users and so increasing the call admission rate.

7.4 Simulation Results

In this section, we demonstrate that the effectiveness of the proposed joint subcarrier power allocation and code assignment strategy. We first show the advantages of using the proposed subcarrier power allocation. Then, with the subcarrier power allocation (SPA), we illustrate the impact of MAI-coefficient-based interference code assignment strategy by comparing the various code assignment strategies: random assignment (RM), pure crowded-first-code assignment (CF) without considering MAI, and the

A new call arrives

In step 1: implement the subcarrier power allocation to maximize the coming user's received signal power.

In step 2: implement the MAI-coefficient based interference code assignment strategy to pick a code which produces less MAI to the system.
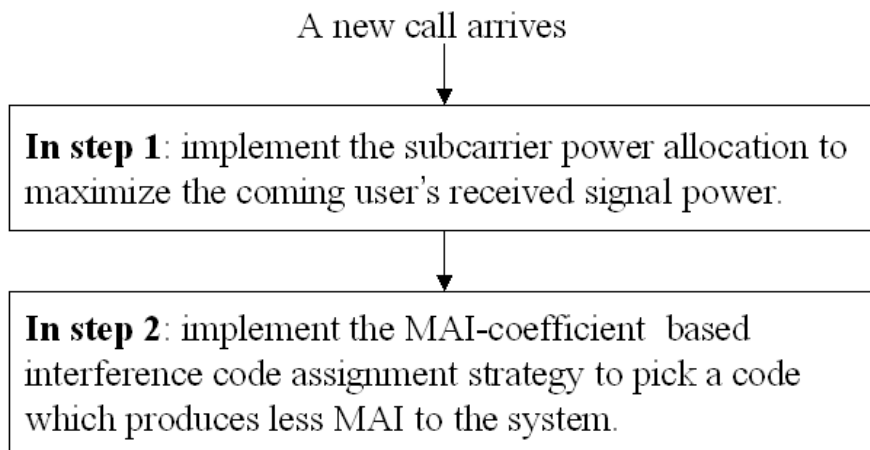
Fig. 7.1: Flow chart of the joint subcarrier power allocation and interference avoidance code assignment strategy.

interference avoidance assignment (IA+CF) methods in terms of the received E_b/N_0 and call admission rate.

7.4.1 Simulation Setup

Simulation Environment

In the simulation, we consider downlink MC-DS-CDMA in a single cell environment. Following the assumptions in [42,91], the subcarriers carrying the same data bits are assumed to experience independent flat Rayleigh fading. The background noise is modelled by white Gaussian noise with double-sided power spectrum density of $N_0/2$ and the transmitting $E_b/N_0 = 12$ dB. A new call is modelled by a Poisson arrival process with the arrival rate (λ_c) of 1/2 per time unit and the departure rate (μ_c) selecting from the set 1/32, 1/48, 1/64, 1/80, 1/96, 1/112,1/144,1/176}. Thus, there are averagely $\lambda/\mu = 16 \sim 56$ active calls in the system. With $U = 128$ parallel substreams, the frequency domain spreading factor (M) is 8 and the time domain spreading factor (SF) are 4, 8, 16, or 32. Each call requests a code of $8R_L$ ($SF = 4$), $4R_L$ ($SF = 8$), $2R_L$ ($SF = 16$), or R_L ($SF = 32$) with a probability according to the code traffic pattern [1 1 2 8], where R_L is the basic data rate. A code traffic pattern of [$a\ b\ c\ d$] means that the times of requesting data rates $8R_L$, $4R_L$, $2R_L$, and R_L are proportional to $a : b : c : d$, respectively. The data rate of each user is fixed during his lifetime. To clearly indicate the traffic load brought by the active calls with different data rates, we define an effective traffic load in the following. With the time domain spreading factor selecting from $SF=$[4 8 16 32] and the code traffic pattern of [$a\ b\ c\ d$], the effective traffic load (ρ) is defined as

$$\rho = \frac{\lambda}{\mu} \times \frac{8R_L \times a + 4R_L \times b + 2R_L \times c + R_L \times d}{a+b+c+d} \times \frac{1}{32R_L} \quad . \qquad (7.26)$$

For $\lambda_c = 1/2$ and $\mu_c = 1/80$ and the code traffic pattern [1 1 2 8], the effective traffic load ρ is 250% of the utilization of the time-domain resources.

Call Admission Control

In the call admission control, we consider the average received E_b/N_0. For an MAI coefficient (κ), the average received E_b/N_0 can be calculated by taking the average of (D.1) over M subcarriers' fading channels. A new coming call is blocked if accepting this new call decreases the signal quality of any active calls in the system below the required received $E_b/N_o = 5$ dB. We simulate 10,000 incoming calls for each combination of λ_c and μ_c.

Code Assignment Strategy

Consider a call request for a code with rate $2^k R_L$, where k is an integer ranging from 0 to 3. Then, a code assignment strategy should be implemented to pick a candidate code to accommodate this new coming call. A candidate code is defined as a free code with rate $2^k R_L$ and its ancestor codes and descent codes are not used. In this chapter, we consider three code assignment methods, including RM, CF, and IA+CF. Now, we introduce RM and CF methods.

Random Assignment(RM)   If there is one or more candidate codes in the 2D code tree, the RM method randomly selects a code without considering the code tree structure and impact of MAI.

Crowded-First(CF)   If there is one or more candidate codes in the 2D code tree, the CF method picks a code whose ancestor code has the fewest free codes, thereby leaving more space for future high-rate users and so increasing the call admission

rate [76]. Note that the CF method considers the code tree structure but the impact of MAI.

7.4.2 Effect of Subcarrier Power Allocation

Figure 7.2 compares the proposed joint subcarrier power allocation and code assignment strategy (IA+CF+SPA) with the pure interference avoidance code assignment strategy (IA+CF) in terms of the (a) average received E_b/N_0, (b) average call admission rate, and (c) standard deviation (STD) of the received E_b/N_0 with various effective traffic loads. One can see that with the help of SPA, the proposed IA+CF+SPA method performs much better than the pure IA+CF method both in terms of the average received E_b/N_0 and the average call admission rate. Furthermore, the advantage of using SPA grows as the traffic load increases. Referring to Fig. 7.2(a), from the average received E_b/N_0 aspect, the improvement by using SPA increases from 0.3 dB to 1.9 dB for $\rho = 1.5$ and 3.5, respectively. As shown in Fig. 7.2(b) as well, the improvement of the call admission raises from 4% to 10% for $\rho = 1.5$ and 3.5, respectively. Moreover, thanks to SPA, the standard deviation of the received E_b/N_0 can be significantly reduced, as shown in Fig. 7.2(c). At $\rho = 1.5$, the STD of the received E_b/N_0 reduces from 2.6 to 1.4 in the dB domain. This is because SPA can make the received signal quality more robust against the fading channel. One should note that STD of the received E_b/N_0 for both IA+CF and IA+CF+SPA increases in the range of $1 \leq \rho \leq 1.5$ and begins to decrease as ρ increases. When the traffic load is light at $\rho = 1$, the interference avoidance code assignment strategy can efficiently select codes for all users without producing extra MAI. However, as the traffic load increases to $\rho = 1.5$, some users may use codes experiencing few interferers while some other users may not. As the traffic load continues to grow, all the active codes may have similar amount of interference.
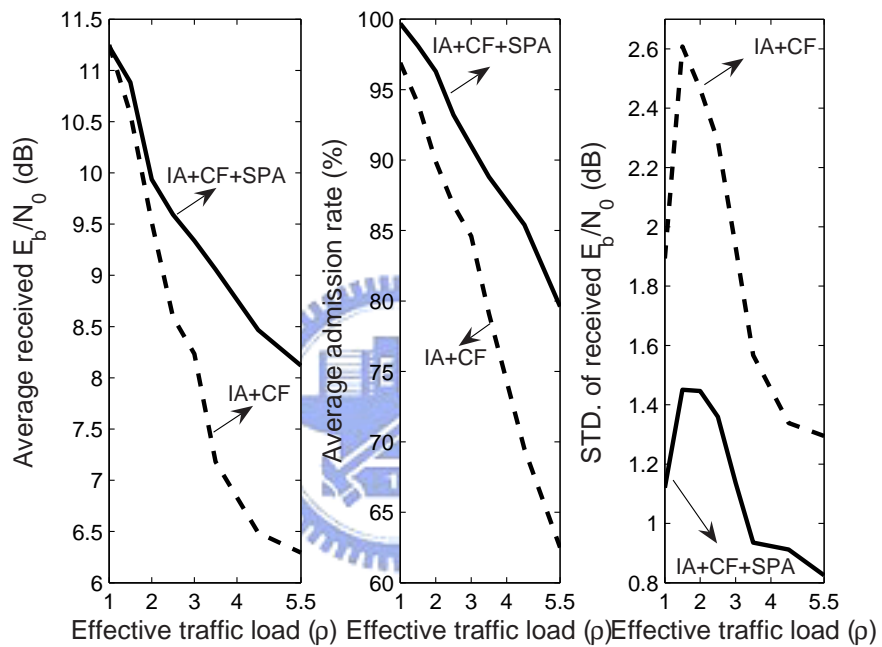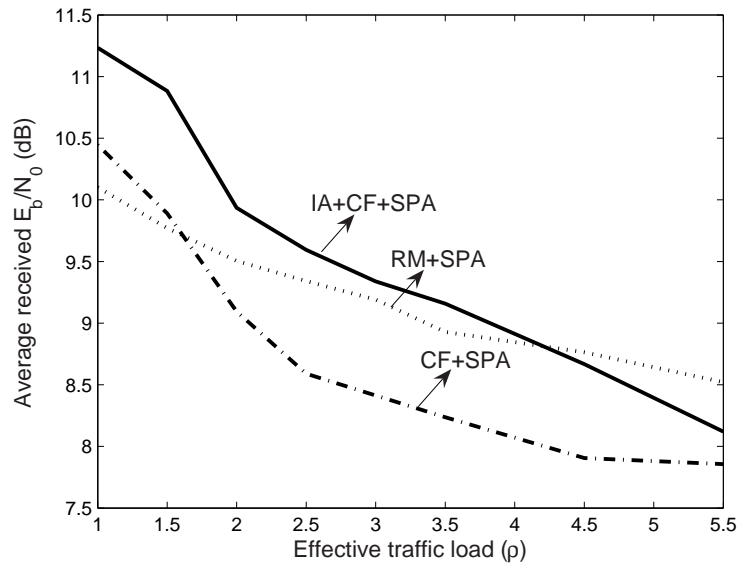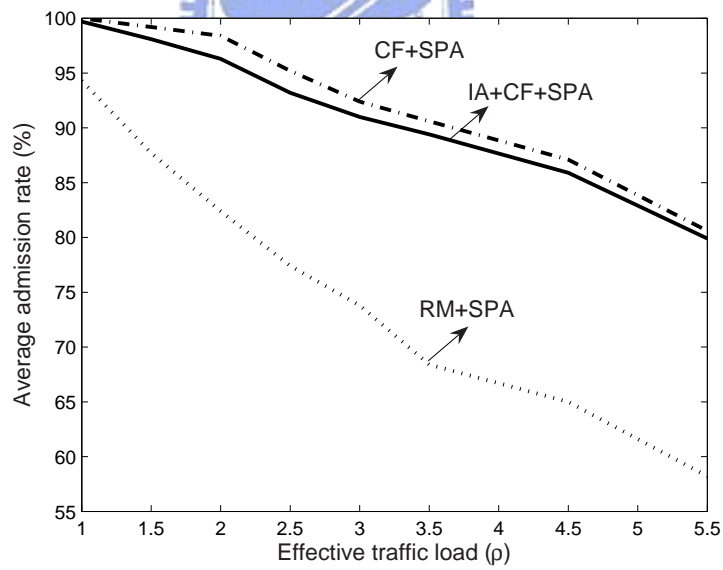
Fig. 7.2: Comparison between the proposed joint subcarrier power allocation and code assignment strategy and the pure interference avoidance code assignment strategy in terms of the (a) average received E_b/N_0; (b) call admission rate; and (c) standard deviation (STD) of the received E_b/N_0 with various effective traffic loads.

7.4.3 Effect of Interference Code Assignment Strategy

Figure 7.3(a) and 7.3(b) compare the average received E_b/N_0 and call admission rate against the effective traffic load for the proposed joint subcarrier power allocation and code assignment (IA+CF+SPA), SPA-aided crowded-first assignment (CF+SPA), and SPA-aided random assignment (RM+SPA) strategies. First, in terms of received E_b/N_0, IA+CF+SPA performs better than RM+SPA for $1 \leq \rho < 4.5$ while in the higher traffic load region of $\rho \geq 4.5$, the received E_b/N_0 of the IA+CF+SPA is lower than that of RM+SPA owing to the increasing MAI for accommodating more user than RM+SPA. Second, for the same reason, the received E_b/N_0 of the CF+SPA method becomes lower than RM+SPA in the region of $\rho > 1.5$. Third, the RM+SPA method performs the worse in terms of the call admission rate because it randomly assigns codes without considering the code tree structure or MAI. Fourth, comparing IA+CF+SPA and CF+SPA, the IA+CF+SPA method can have higher received E_b/N_0 than the CF+SPA method whereas the call admission rate of the IA+CF+SPA is slightly lower than the CF+SPA method. For example, the average received E_b/N_0 at $\rho = 2.5$ are 8.6 and 9.6 dB for CF+SPA and IA+CF+SPA, respectively. However, the call admission rate of the IA+CF+SPA is 2% lower than CF+SPA. Note that the CF+SPA method can make the tree structure of the allocated codes more compact, thereby gathering more larger code resources for higher-rate users and having higher admission rate. However, the IA+CF+SPA method aims to avoid MAI first before applying the CF method. Moreover, for the region of $1.5 \leq \rho \leq 4.5$, the CF+SPA method has the poorest E_b/N_0 performance even compared to the RA+SPA method. This also justifies the advantages of the IA+CF+SPA method.

(a) Average received E_b/N_0 (dB)

(b) Call admission rate

Fig. 7.3: Comparison of (a) the average received E_b/N_0 and (b) the call admission rate against the effective traffic load for the proposed joint subcarrier power allocation and code assignment (IA+CF+SPA), SPA-aided crowded-first-code assignment (CF+SPA), and SPA-aided random assignment (RM+SPA) strategies.

7.5 Chapter Summary

In this chapter, we have proposed a joint subcarrier power allocation and code assignment strategy for multi-rate synchronous MC-DS-CDMA with TF-domain spreading. In the proposed joint scheme, we first optimize the received signal power by a subcarrier power allocation. Then, an MAI coefficient aided interference avoidance code assignment strategy is applied to eliminate MAI. The MAI coefficient is used to predict to the quantity of MAI imposed on each code channel. By simulations and analysis, we demonstrate that the proposed joint subcarrier power allocation and code assignment method can effectively enhance the received E_b/N_0 and maintain a high call admission rate simultaneously.

Chapter 8

Concluding Remarks

In this dissertation, we have investigated several important radio resource management (RRM) issues for high speed downlink packet access (HSDPA) and multi-carrier code division multiple access (MC-DS-CDMA). In the HSDPA aspect, we have studied the stall issue of the media access control (MAC) layer's fast retransmission scheme using the multi-process stop-and-wait (SAW) hybrid auto-request request (HARQ) technique. In the MC-DS-CDMA aspect, we have looked into the effect of multiple access interference (MAI) on top of the power control errors (PCEs), the code assignment strategy, and the joint subcarrier power allocations and code assignment scheme. This dissertation includes the following research topics.

1. Analysis of Stall Avoidance Mechanisms for HSDPA in the WCDMA Systems.

2. Analysis of a Stall Avoidance Mechanism with Scheduling for HSDPA in the WCDMA Systems.

3. Effects of Power Control Errors and Complete Multiple Access Interference on Uplink MC-DS-CDMA.

4. Interference Avoidance Code Assignment for Downlink MC-DS-CDMA.

5. Joint Subcarrier Power Allocation and Interference Avoidance Code Assignment for Downlink MC-DS-CDMA.

The contributions from these research works are listed as follows.

For the HSDPA system:

1. Developed three closed-form expressions of the gap processing time for the timer-based, the window-based, and the indicator-based stall avoidance mechanisms in (3.4), (3.13), and (3.21), respectively.

2. Constructed the probability mass functions of the gap processing time in (3.6), (3.9), (3.16), (3.35), and (3.43).

3. Derived the gap processing time formula for the indicator-based stall avoidance scheme in (4.11) for the case with interleaving scheduling.

For the MC-DS-CDMA system:

1. Developed an analytical model in (5.40) to evaluate the error rate performance of the uplink multi-rate MC-DS-CDMA system with TF-domain spreading under the impacts of the PCEs and the complete MAI.

2. The error probabilities for the downlink MC-DS-CDMA with and without subcarrier power allocations was derived in (D.10) and (C.7), respectively.

3. An interference avoidance code assignment strategy was proposed to eliminate MAI for the downlink MC-DS-CMDA.

4. A hybrid of subcarrier power allocation and code assignment method was proposed to further enhance the signal quality in the downlink transmissions.

The following summarizes the results from the above contributions.

8.1 Gap Processing Time Analysis of Stall Avoidance Mechanisms for HSDPA

Chapter 3 and [92] investigated three stall avoidance mechanisms to enhance the performance of the fast retransmission scheme in the MAC layer by a parallel SAW HARQ technique adopted in HSDPA. To evaluate the performance of the stall avoidance mechanisms, we defined a new performance metric, the *gap processing time*. The gap processing time is the duration beginning when a non-recoverable gap appears in the sequence of MAC layer data due to a NACK-to-ACK error until the receiver recognizes that this gap cannot be recovered by the MAC layer retransmission scheme. In order to characterize the stall avoidance mechanisms, we developed the closed-form expressions of the average gap processing time and the corresponding probability mass functions for the timer-based, the window-based, and the indicator-based schemes. Simulation and analysis results have shown that (1) the indicator-based stall avoidance scheme significantly reduces the gap processing time compared to the timer-based and the window-based schemes; (2) under a gap processing time constraint, the number of the acceptable full-loaded users of the indicator-based schemes is much larger than that of two other considered schemes; (3) the gap processing time for the timer-based and the indicator-based schemes are centralized while that of the window-based scheme is widely spread. The proposed analytic model can also provide some important insights about the proper size in the reordering buffer in the MAC layer, the window size in the RLC layers, and the RLC timeout period.

8.2 Performance of an Indicator-based Stall Avoidance Mechanism for HSDPA with Interleaving Scheduling

Chapter 4 and [93] studied the characteristics of the indicator-based stall avoidance mechanism when applying an interleaving scheduling in HSDPA. For this purpose, we derived the gap processing time formula for the indicator-based scheme in the multi-user case. The gap processing time formula is a function of packet error rates, the numbers of allowable users, and the numbers of parallel processes in the SAW HARQ mechanism. Through simulation and analysis results, we found that the throughput enhancement by increasing the number of parallel processes in the SAW HARQ technique brings about a side effect of the longer gap processing time. Under a constraint of gap processing time 50 TTIs, 5 users can be allowed to stay in a 8-process SAW HARQ system, whereas 11 users can be supported in a system with 4 parallel SAW HARQ processes. The sharply increasing gap processing time can not be ignored when packet error requirement is stringent because the average gap processing time almost exponentially increases when the number of parallel SAW HARQ processes increases. Note that for moderate packet error rates, the gap processing time is linearly proportional to the number of users and the number of the parallel HARQ processes. From the higher layer user's perspective, the proposed analytical model can facilitate the evaluation of the overall performance of the HSDPA system, while considering the lower physical layer impact.
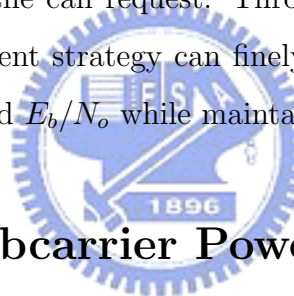
8.3 The Impact of Power Control Errors and Complete Multiple Access Interference on Uplink MC-DS-CDMA

Chapter 5 and [94] developed an analytical model to quantize the impact of open-loop power control errors and the complete MAI on the uplink multi-rate MC-DS-CDMA system with TF-domain spreading. Through the simulation and analysis, we have several interesting observations. First, the effect of PCEs can exacerbate the impact of complete MAI on MC-DS-CDMA, or vice versa because the joint effect of the complete MAI and PCEs is actually more serious than the summation of the performance degradation from the complete MAI and PCEs individually. Second, intuitionally, increasing the frequency or time domain spreading factor to have a larger total spreading gain can enhance the error rate performance. However, a higher sensitivity to power control errors should pay for this behavior. Third, for a fixed total time and frequency spreading gain, a larger frequency domain spreading can result in a better error rate performance but performance differences between the two are shrunk as power control errors increase.

8.4 An Interference Avoidance Code Assignment Strategy for Downlink MC-DS-CDMA

Chapter 6 and [95] aimed to design a code assignment strategy for downlink MC-DS-CDMA system to attain a better performance in the received E_b/N_0 while maintaining a high call admission rate. To achieve this, we first define an MAI coefficient by analyzing the error rate performance of the multi-rate MC-DS-CDMA with TF-domain

spreading for the downlink case. The MAI coefficient is a simple calculated index to quantitatively predict the incurred MAI before assigning a candidate code to the call request. With the aid of the MAI coefficient, we proposed a novel interference avoidance (IA) code assignment strategy to eliminate the MAI by choosing a code which produces the less amount of MAI. In principle, the proposed IA code assignment method possesses three stages to evaluate the candidature of each available code. The first stage is to select a code by limiting the newly generated MAI. The objective of the second stage is to average the interferers over all active users. If the first two stages can not pick a winner, the code selection procedure goes into the third stage. In the last stage, the conventional crowded-first-code method is applied to elect a single code for the call request. Through simulations, we found that the proposed IA code assignment strategy can finely achieve the goal: to have a better performance in the received E_b/N_o while maintaining a high call admission rate.

8.5 A Joint Subcarrier Power Allocation and Interference Avoidance Code Assignment Strategy for Downlink MC-DS-CDMA

Chapter 7 and [96] was devoted to solve a challenging issue in the multi-rate MC-DS-CDMA system with TF-domain spreading. The challenging issue is how to maximally benefit from a particular subcarrier power allocation while controlling the MAI at an acceptable level and maintaining a high call admission rate simultaneously? From the results in Chapter 6, we known that the novel IA code assignment method can eliminate MAI for the downlink MC-DS-CDMA. Thus, we were motivated to proposed a joint subcarrier power allocation and the code assignment scheme to solve the above challenging issue. In the proposed scheme, a subcarrier power allocation

is first implemented to maximize each user's received signal power. Then, the IA code assignment method is applied to eliminate MAI. The simulation results have shown that this corporation of the subcarrier power allocation and the IA code assignment can obviously improved the received E_b/N_0 compared with that of the pure IA method. Furthermore, the proposed hybrid of the subcarrier power allocation and IA code assignment scheme can approximate the call admission rate of the corporation of the crowded-first-code method and the subcarrier power allocation.

8.6 Suggestions for Future Research

Possible interesting research topics that can be extended from this dissertation include:

For the HSDPA system:

- Joint design of the MAC and RLC retransmission mechanism.
- Investigation of the effect of Chase combining on the gap processing time and its related upper protocol layers.
- Evaluation of the effect of incremental redundancy on the gap processing time for the multiple parallel HARQ mechanism.
- Development of an efficient admission control and scheduling algorithms subject to the gap processing time constraint.

For the MC-DS-CDMA system:

- Performance analysis for other types of fading channels [69, 97] and other distortion [98] subject to power control errors and complete MAI.
- Development of a resource allocation mechanisms including the scheduling [99] and the power control schemes [100].

- Application of the MAI coefficients' concept when combining power control mechanisms [101] or the multiple-input-multiple-out technology [102].

APPENDIX A

Derivation of $Var[R(\tau_k^{(\mathbf{X})}, \theta_{k,i,j}^{(\mathbf{X})})]$ in (5.18)

In this appendix, we derive $Var[R(\tau_k^{(\mathbf{X})}, \theta_{k,i,j}^{(\mathbf{X})})]$ in (5.18). To ease the notation, let $\tau_k^{(\mathbf{X})} = \tau$ and $\theta_{k,i,j}^{(\mathbf{X})} = \theta$. Then we can calculate $Var[R(\tau_k^{(\mathbf{X})}, \theta_{k,i,j}^{(\mathbf{X})})]$ by

$$Var[R(\tau,\theta)] = E_\tau[E_\theta[R^2(\tau,\theta)]] \ . \tag{A.1}$$

Recall that in the case of $(0 \le \tau_k^{(\mathbf{X})} < T_o)$, τ is uniformly distributed in $[0, \ T_o)$. Hence, we assume that $hT_c \le \tau < (h+1)T_c$, where $0 \le h \le G_o - 1$ and G_o is the time-domain spreading factor of the reference user. Following the same procedure as [58], we can have

$$E_\theta[R^2(\tau,\theta)] = \frac{1}{2} \int_{hT_c}^{(h+1)T_c} \{(\tau - hT_c)^2 \mathrm{sinc}^2(\frac{\pi z(\tau - hT_c)}{T_c})(h+1) + ((h+1)T_c - \tau)^2$$

$$\times \mathrm{sinc}^2(\frac{\pi z((h+1)T_c - \tau)}{T_c})h\}d\tau \ . \tag{A.2}$$

Then the expectation of (A.2) with respective to τ over $[0, \ T_o)$ can be obtained by calculating

$$Var[R(\tau,\theta)] = \frac{1}{2T_o} \sum_{h=0}^{G_o-1} \int_{hT_c}^{(h+1)T_c} \{(\tau - hT_c)^2 \mathrm{sinc}^2(\frac{\pi z(\tau - hT_c)}{T_c})(h+1)+$$

$$((h+1)T_c - \tau)^2 \mathrm{sinc}^2(\frac{\pi z((h+1)T_c - \tau)}{T_c})h\}d\tau$$

$$= \frac{G_o T_c^2}{4\pi^2[(i-s) + (j-v)U]^2} \ . \tag{A.3}$$

Similarly, we can obtain

$$Var[\widetilde{R}(\tau, \theta)] = Var[R(\tau, \theta)]$$

$$= \frac{G_o T_c^2}{4\pi^2[(i - s) + (j - v)U]^2} \quad . \tag{A.4}$$

APPENDIX B

Derivation of $Var[R(T_o, \theta_{k,i,j}^{(\mathbf{X})})]$ in (5.19)

Here we derive $Var[R(T_o, \theta_{k,i,j}^{(\mathbf{X})})]$ in (5.19). Let $\tau_k^{(\mathbf{X})} = \tau$ and $\theta_{k,i,j}^{(\mathbf{X})} = \theta$ without loss of generality. Then $Var[R(T_o, \theta_{k,i,j}^{(\mathbf{X})})]$ can be calculated as

$$Var[R(T_o, \theta)] = E_\tau[E_\theta[R^2(T_o, \theta)]] \ . \tag{B.1}$$

Recall that τ and θ are uniformly distributed in $[T_o, \ T_k^{(\mathbf{X})})$ and $[0, \ 2\pi)$, respectively. Assume $hT_c \le \tau < (h+1)T_c$, where $G_o \le h \le G_k^{(\mathbf{X})} - 1$; G_o and $G_k^{(\mathbf{X})}$ are the time domain spreading factors of the reference user and the interfering user, respectively. Then, referring to (5.10), we can express $R(T_o, \theta)$ as

$$R(T_o, \theta) = \sum_{j=0}^{G_o-1} g_o[j] g_k^{(\mathbf{X})} [G_k^{(\mathbf{X})} - h - 1 + j] \int_{jT_c}^{jT_c+\tau-hT_c} \cos(\frac{2\pi z t}{T_c} + \theta) dt +$$

$$\sum_{j=0}^{G_o-1} g_o[j] g_k^{(\mathbf{X})} [G_k^{(\mathbf{X})} - h + j] \int_{jT_c+\tau-hT_c}^{(j+1)T_c} \cos(\frac{2\pi z t}{T_c} + \theta) dt \ , \tag{B.2}$$

where

$$z = (i - s) + (j - v)U \ . \tag{B.3}$$

After some deductions, we obtain

$$R(T_o, \theta) = (\tau - hT_c)\text{sinc}(\frac{\pi z}{T_c}(\tau - hT_c)) \sum_{j=0}^{G_o-1} g_o[j]g_k^{(\mathbf{X})}[G_k^{(\mathbf{X})} - h - 1 + j]\cos\Phi_{j,\tau}^{(1)} +$$

$$[(h+1)T_c - \tau]\text{sinc}(\frac{\pi z}{T_c}((h+1)T_c - \tau)) \sum_{j=0}^{G_o-1} g_o[j]g_k^{(\mathbf{X})}[G_k^{(\mathbf{X})} - h + j]\cos\Phi_{j,\tau}^{(2)} \ ,$$

$$(\text{B.4})$$

where

$$\Phi_{j,\tau}^{(1)} = \frac{\pi z}{T_c}(2jT_c + \tau - hT_c) + \theta \ ; \tag{B.5}$$

$$\Phi_{j,\tau}^{(2)} = \frac{\pi z}{T_c}((2j+1)T_c + \tau - hT_c) + \theta \ . \tag{B.6}$$

Taking the expectation of $R^2(T_o, \theta)$ respective to θ over $[0, \ 2\pi)$, $g_o[j]$, and $g_k^{(\mathbf{X})}[j]$, where $g_o[j]$ and $g_k^{(\mathbf{X})}[j]$ are assumed to be ± 1 with equal probability, we can have

$$E_\theta[R^2(T_o, \theta)] = \frac{G_o}{2}[(\tau - hT_c)^2\text{sinc}^2(\frac{\pi z}{T_c}(\tau - hT_c)) +$$

$$[(h+1)T_c - \tau]^2\text{sinc}^2(\frac{\pi z}{T_c}((h+1)T_c - \tau))] \ . \tag{B.7}$$

Finally, substituting (B.7) into (B.1), we can get $Var[R(T_o, \theta)]$ by calculating

$$Var[R(T_o, \theta)] = \frac{G_o}{2(T_k^{(\mathbf{X})} - T_o)} \sum_{h=G_o}^{G_k^{(\mathbf{X})}-1} \int_{hT_c}^{(h+1)T_c} (\tau - hT_c)^2\text{sinc}^2(\frac{\pi z}{T_c}(\tau - hT_c)) +$$

$$[(h+1)T_c - \tau]^2\text{sinc}^2(\frac{\pi z}{T_c}((h+1)T_c - \tau))d\tau$$

$$= \frac{G_o T_c^2}{2\pi^2[(i-s) + (j-v)U]^2} \ . \tag{B.8}$$

APPENDIX C

Performance of Downlink MC-DS-CDMA

In this Appendix, we use the Laguerre integration to evaluate the error rate performance of the synchronous multi-rate MC-DS-CDMA system with TF-domain spreading. Now, substituting the MAI coefficient κ of (6.19) into the received E_b/N_0 of (6.15), we obtain

$$\gamma = \left[\frac{2 \sum_{v=1}^{M} |\alpha_{o,s,v}|^4}{(\sum_{v=1}^{M} |\alpha_{o,s,v}|^2)^2} \kappa + \frac{[E_o/(MN_o)]^{-1}}{\sum_{v=1}^{M} |\alpha_{o,s,v}|^2} \right]^{-1} . \tag{C.1}$$

For binary phase shift keying modulation with coherent detection, the conditional error probability for a given $\alpha_{o,s,v}$ is equal to

$$P(e|\alpha_{o,s,1}, \cdots, \alpha_{o,s,M}) = Q(\sqrt{2\gamma}) , \tag{C.2}$$

where $Q(x) = \frac{1}{\sqrt{2\pi}} \int_x^\infty e^{-t^2/2} dt$. Since $|\alpha_{o,s,v}|$ is the amplitude of the Rayleigh fading channel, $|\alpha_{o,s,v}|^2$ is an exponentially distributed random variable with mean $E[|\alpha_{o,s,v}|^2] = 1$. To ease the notation, we denote $z_v = |\alpha_{o,s,v}|^2$. Then the probability density function (*pdf*) of z_v is expressed as

$$f_{z_v}(z_v) = e^{-z_v} H(z_v), \tag{C.3}$$

where

$$H(t) = \begin{cases} 1, & t \geq 0 , \\ 0, & t < 0 . \end{cases} \tag{C.4}$$

Hence, the total error probability can be expressed as

$$P(e) = \int_0^\infty \cdots \int_0^\infty Q(\sqrt{2\gamma}|z_1, \cdots, z_M) f_{z_1}(z_1) \cdots f_M(z_M) dz_1 \cdots dz_M$$

$$= \int_0^\infty \cdots \int_0^\infty Q(\sqrt{2\gamma}|z_1, \cdots, z_M) e^{-z_1} \cdots e^{-z_M} dz_1 \cdots dz_M \ . \qquad (C.5)$$

Based on the Laguerre polynomial approach of [90], the integration for a function $q(y)e^{-y}$ can be computed by

$$\int_0^\infty q(y)e^{-y} dy = \sum_{i=1}^{D_p} \omega_i q(y_i) \ , \qquad (C.6)$$

where y_i and ω_i are the abscissas and the weight factor of the Laguerre polynomials with order D_p, respectively. Applying the Laguerre integration into (D.9), we can further simplify the total error probability $P(e)$ to

$$P(e) = \sum_{i_1=1}^{D_p} \cdots \sum_{i_M=1}^{D_p} w_{1,i_1} \times \cdots \times w_{M,i_M} Q(\sqrt{2\gamma}|z_{1,i_1}, \cdots, z_{M,i_M}) \ . \qquad (C.7)$$

APPENDIX D

Performance of Downlink MC-DS-CDMA with Subcarrier Power Allocation

In this Appendix, we use the Laguerre integration to evaluate the error rate performance of the synchronous multi-rate MC-DS-CDMA system with TF-domain spreading when the subcarrier power allocation is applied. Recall the received signal to noise ratio in (7.21) as

$$\gamma = \frac{\displaystyle\sum_{v=1}^{M} |\alpha_{o,s,v}|^4}{2\kappa \mathrm{E}\left[\dfrac{|\alpha_{k,s,v}^{(\mathbf{A})}|^4}{\sum_{i=1}^{M} |\alpha_{k,s,i}^{(\mathbf{A})}|^4}\right] \displaystyle\sum_{v=1}^{M} |\alpha_{o,s,v}|^4 + (\dfrac{E_o}{N_0})^{-1} \displaystyle\sum_{v=1}^{M} |\alpha_{o,s,v}|^2} \quad . \tag{D.1}$$

Since $|\alpha_{o,s,v}|$ and $|\alpha_{k,s,i}^{(\mathbf{A_o})}|$ are the amplitudes of the Rayleigh fading channel, $|\alpha_{o,s,v}|^2$ and $|\alpha_{k,s,i}^{(\mathbf{A_o})}|^2$ are the exponentially distributed random variable with mean $E[|\alpha_{o,s,v}|^2] = E[|\alpha_{k,s,i}^{(\mathbf{A_o})}|^2] = 1$. To ease the notation, we denote $z_v = |\alpha_{o,s,v}|^2$ and $z_{kv} = |\alpha_{k,s,i}^{(\mathbf{A_o})}|^2$. Then the probability density function (*pdf*) of z_v and z_{kv} are expressed as

$$f_{z_v}(z_v) = e^{-z_v} H(z_v) \tag{D.2}$$

and

$$f_{z_{kv}}(z_{kv}) = e^{-z_{kv}} H(z_{kv}) \ , \tag{D.3}$$

where

$$H(t) = \begin{cases} 1, & t \geq 0 \ , \\ 0, & t < 0 \ . \end{cases} \tag{D.4}$$

Then, $\mathrm{E}\left[|\alpha_{k,s,v}^{(\mathbf{A_o})}|^4 / \sum_{i=1}^{M} |\alpha_{k,s,i}^{(\mathbf{A_o})}|^4\right]$ of (7.21) can be expressed as

$$
\mathrm{E}\left[\frac{|\alpha_{k,s,v}^{(\mathbf{A_o})}|^4}{\sum_{i=1}^{M} |\alpha_{k,s,i}^{(\mathbf{A_o})}|^4}\right] = \mathrm{E}\left[\frac{|z_{kv}|^2}{\sum_{i=1}^{M} |z_{ki}|^2}\right]
$$

$$
= \int_0^\infty \cdots \int_0^\infty \frac{|z_{kv}|^2}{\sum_{i=1}^{M} |z_{ki}|^2} f_{z_{k1}}(z_{k1}) \cdots f_{z_{kM}}(z_{kM}) d_{z_{k1}} \cdots d_{z_{kM}}
$$

$$
= \int_0^\infty \cdots \int_0^\infty \frac{|z_{kv}|^2}{\sum_{i=1}^{M} |z_{ki}|^2} e^{-z_{k1}} \cdots e^{-z_{kM}} d_{z_{k1}} \cdots d_{z_{kM}} \ . \tag{D.5}
$$

Due to the tediousness and complexity, we suggest to apply the Laguerre polynomial approach of [90] to calculate (D.5). Based on the Laguerre polynomial approach, the integration for a function $q(y)e^{-y}$ can be computed by

$$\int_0^\infty q(y)e^{-y} dy = \sum_{i=1}^{D_p} \omega_i q(y_i) \ , \tag{D.6}$$

where y_i and ω_i are the abscissas and the weight factor of the Laguerre polynomials with order D_p, respectively. Applying the Laguerre integration into (D.5), we can calculate $\mathrm{E}\left[|\alpha_{k,s,v}^{(\mathbf{A_o})}|^4 / \sum_{i=1}^{M} |\alpha_{k,s,i}^{(\mathbf{A_o})}|^4\right]$ as

$$
\mathrm{E}\left[\frac{|\alpha_{k,s,v}^{(\mathbf{A_o})}|^4}{\sum_{i=1}^{M} |\alpha_{k,s,i}^{(\mathbf{A_o})}|^4}\right] = \sum_{i_1=1}^{H} \cdots \sum_{i_M=1}^{H} w_{k1,i_1} \times \cdots \times w_{kM,i_M} \frac{|z_{kv,i_v}|^2}{\sum_{j=1}^{M} |z_{kj,i_j}|^2} \ . \tag{D.7}
$$

For binary phase shift keying modulation with coherent detection, the conditional error probability for the given $\alpha_{o,s,v}$ is equal to

$$P(e|\alpha_{o,s,1}, \cdots, \alpha_{o,s,M}) = Q(\sqrt{2\gamma}) \ , \tag{D.8}$$

where $Q(x) = \frac{1}{\sqrt{2\pi}} \int_x^\infty e^{-t^2/2} dt$. Recall that $z_v = |\alpha_{o,s,v}|^2$. Hence, the total error probability can be expressed as

$$P(e) = \int_0^\infty \cdots \int_0^\infty Q(\sqrt{2\gamma}|z_1, \cdots, z_M) f_{z_1}(z_1) \cdots f_{z_M}(z_M) dz_1 \cdots dz_M$$

$$= \int_0^\infty \cdots \int_0^\infty Q(\sqrt{2\gamma}|z_1, \cdots, z_M) e^{-z_1} \cdots e^{-z_M} dz_1 \cdots dz_M \ . \qquad \text{(D.9)}$$

Applying the Laguerre integration into (D.9), we can further simplify the total error probability $P(e)$ to

$$P(e) = \sum_{i_1=1}^{D_p} \cdots \sum_{i_M=1}^{D_p} w_{1,i_1} \times \cdots \times w_{M,i_M} Q(\sqrt{2\gamma}|z_{1,i_1}, \cdots, z_{M,i_M}) \ . \qquad \text{(D.10)}$$

Bibliography

[1] S. Abedi, "Efficient radio resource management for wireless multimedia communications a multidimensional QoS-based packet scheduler," *IEEE Trans. on Communications*, vol. 4, no. 6, pp. 2811–2822, Nov. 2005.

[2] R. Ferrus, L. Alonso, A. Umbert, X. Reves, J. Perez-Romero, and F. Casadevall, "Cross-layer scheduling strategy for UMTS downlink enhancement," *IEEE Communications Magazine*, vol. 43, no. 6, pp. S24–S28, June. 2005.

[3] A. Hills and B. Friday, "Radio resource management in wireless LANs," *IEEE Communications Magazine*, vol. 42, no. 12, pp. S9–14, Dec. 2004.

[4] L. Jorguseski, E. Fledderus, J. Farserotu, and R. Prasad, "Radio resource allocation in third generation mobile communication systems," *IEEE Communications Magazine*, vol. 39, no. 2, pp. 117–123, Feb. 2001.

[5] S. Baey, M. Dumas, and M.-C. Dumas, "QoS tuning and resource sharing for UMTS WCDMA multiservice mobile," *IEEE Trans. on Mobile Computing*, vol. 1, no. 3, pp. 221–235, July-Sept. 2002.

[6] K. Kim, Y. Han, and S.-L. Kim, "Joint subcarrier and power allocation in uplink OFDMA systems," *IEEE Communications Letters*, vol. 9, no. 6, pp. 526–528, Jan. 2005.

[7] Y. Yao and G. Giannakis, "Rate-maximizing power allocation in OFDM based on partial channel knowledge," *IEEE Transaction on Wireless Communications*, vol. 4, no. 3, pp. 1073–1083, May 2005.

[8] A. Abrardo, G. Giambene, and D. Sennati, "Performance analysis of SIR-based closed-loop power control with feedback errors," *IEICE Transcation on Communication*, vol. E85-B, no. 5, pp. 872–881, May 2002.

[9] J. M. Romero-Jerez, M. Ruiz-Garcia, and A. Diaz-Estrella, "Effects of multipath fading on BER statistics in cellular CDMA networks with fast power control," vol. 4, no. 11, pp. 349–351, Nov. 2000.

[10] J. Hou, J. Yang, and S. Papavassiliou, "Integration of pricing with call admission control to meet QoS requirements in cellular networks," *IEEE Trans. on Parallel and Distributed Systems*, vol. 13, no. 9, pp. 898–910, Spet. 2002.

[11] D. Liu, Y. Zhang, and H. Zhang, "A self-learning call admission control scheme for CDMA cellular networks," *IEEE Trans. on Neural Networks*, vol. 16, no. 5, pp. 1219–1228, Spet. 2005.

[12] K. Wang and L.-S. Lee, "Design and analysis of QoS supported frequent handover schemes in microcellular ATM networks," *IEEE Trans. on Vehicular Technology*, vol. 50, no. 4, pp. 942–953, July 2001.

[13] A. Das, F. Khan, A. Sampath, and H.-J. Su, "Adaptive, asynchronous incremental redundancy A^{2}IR with fixed transmission time intervals (TTI) for HS-DPA," *IEEE International Symposium on Personal, Indoor and Mobile Radio Communications*, vol. 3, pp. 1083–1087, Spet. 2002.

[14] J. Zhang, W. Cao, M. Peng, and W. Wang, "Investigation of hybrid ARQ per-

formance for TDD CDMA HSDPA," *IEEE Vehicular Technology Conference*, vol. 4, pp. 2721–2724, Apr. 2003.

[15] F. Frederiksen and T. Kolding, "Performance and modeling of WCDMA/HSDPA transmission/H-ARQ schemes," *IEEE Vehicular Technology Conference*, vol. 1, pp. 472–476, Spet. 2002.

[16] M. Dell'Amico, F. Maffioli, and M. Merani, "A tree partitioning dynamic policy for OVSF codes assignment in wideband CDMA," *IEEE Transaction on Wireless Communications*, vol. 3, no. 4, pp. 1013–1017, July 2004.

[17] Y. Yang and T.-S. Yum, "Maximally flexible assignment of orthogonal variable spreading factor codes for multirate traffic," *IEEE Transaction on Wireless Communications*, vol. 3, no. 3, pp. 781–792, May 2004.

[18] P. Lin, C.-H. Gan, and C.-C. Hsu, "OVSF code channel assignment with dynamic code set and buffering adjustment for UMTS," *IEEE Trans. on Vehicular Technology*, vol. 54, no. 2, pp. 591–602, March 2005.

[19] 3GPP TR 25.950 V4.0.0, "UTRA high speed downlink packet access," March 2001.

[20] S. Parkvall, E. Dahlman, P. Frenger, P. Beming, and M. Persson, "The high speed packet data evolution of WCDMA," *IEEE International Symposium on Personal, Indoor and Mobile Radio Communications*, pp. G27–G31, Sep. 2001.

[21] R. C. Qiu, W. Zhu, and Y.-Q. Zhang, "Third-generation and beyond (3.5G) wireless networks and its applications," *IEEE International Symposium on Circuits and Systems*, pp. I41–I44, May 2002.

[22] M. Döttling, J. Michel, and B. Raaf, "Hybrid ARQ and adaptive modulation and coding schemes for high speed downlink packet access," *IEEE International*

Symposium on Personal, Indoor and Mobile Radio Communications, pp. 1073–1077, Sep. 2002.

[23] M. Nakamura, Y. Awad, and S. Vadgama, "Adaptive control of link adaptation for high speed downlink packet access (HSDPA) in W-CDMA," *International Symposium on Wireless Personal Multimedia Communications*, pp. 382–386, Oct. 2002.

[24] R. Kwan, P. Chong, and M. Rinne, "Analysis of the adaptive modulation and coding algorithm with multicode transmission," *IEEE Vehicular Technology Conference*, pp. 2007–2011, Sep. 2002.

[25] T. E. Kolding, F. Frederiksen, and P. E. Mogensen, "Performance aspects of WCDMA systems with high speed downlink packet access (HSDPA)," *IEEE Vehicular Technology Conference*, pp. 477–481, Sep. 2002.

[26] S. Abedi and S. Vadgama, "Hybrid genetic packet scheduling and radio resource management for high speed downlink packet access," *International Symposium on Wireless Personal Multimedia Communications*, pp. 1192–1196, Oct. 2002.

[27] W. S. Jeon, D. G. Jeong, and B. Kim, "Design of packet transmission scheduler for high speed downlink packet access systems," *IEEE Vehicular Technology Conference*, pp. 1125–1129, May 2002.

[28] Y. Ofuji, A. Morimoto, S. Abeta, and M. Sawahashi, "Comparison of packet scheduling algorithms focusing on user throughput in high speed downlink packet access," *IEEE International Symposium on Personal, Indoor and Mobile Radio Communications*, pp. 1462–1466, Sep. 2002.

[29] Q. Zhang and H.-J. Su, "Methods for preventing protocol stalling in UMTS

radio link control," *IEEE International Conference on Communications*, pp. 2246–2250, May 2003.

[30] A. Morimoto, S. Abeta, and M. Sawahashi, "Performance of fast cell selection coupled with fast packet schedulling in high-speed downlink packet access," *IEICE Transcation on Communication*, vol. E85-B, no. 10, pp. 2021–2031, Oct. 2002.

[31] L. Davis, D. Garrett, G. Woodward, M. Bickerstaff, and F. Mullany, "System architecture and asics for a MIMO 3GPP-HSDPA receiver," *IEEE Vehicular Technology Conference*, pp. 818–822, April 2003.

[32] A. Hottinen, J. Vesma, O. Tirkkonen, and N. Nefedov, "High bit rates for 3G and beyond using MIMO channels," *IEEE International Symposium on Personal, Indoor and Mobile Radio Communications*, pp. 854–858, Sep. 2002.

[33] P. Lin and Y. B. Lin and I. Chlamtac, "Overflow control for UMTS high-speed downlink packet access," *IEEE Transaction on Wireless Communications*, vol. 3, no. 2, pp. 524–532, March 2004.

[34] M. Chatterjee, G. D. Mandyam, and S. K. Das, "Fast ARQ in high speed downlink packet access for WCDMA systems," *Proceedings of European Wireless*, pp. 451–457, Feb. 2002.

[35] D. K. Kim and S.-H. Hwang, "Capacity analysis of an uplink synchronized multicarrier DS-CDMA system," *IEEE Communications Letters*, vol. 6, no. 3, pp. 99–101, March 2002.

[36] J. Namgoong, T. Wong, and J. Lehnert, "Subspace multiuser detection for multicarrier DS-CDMA," *IEEE Trans. on Communications*, vol. 48, no. 11, pp. 1897–1908, Nov. 2000.

[37] S. Hara and R. Prasad, "Overview of multicarrier CDMA," *IEEE Communications Magazine*, vol. 35, no. 12, pp. 126 – 133, Dec. 1997.

[38] L. Loyola and T. Miki, "A new transmission and multiple access scheme based on multicarrier CDMA for future highly mobile networks," *IEEE International Symposium on Personal, Indoor and Mobile Radio Communications*, vol. 2, pp. 1944 – 1948, Sept. 2003.

[39] D. K. Kim and S.-H. Hwang, "Capacity analysis of an uplink synchronized multicarrier DS-CDMA system," *IEEE Communications Letters*, vol. 6, no. 3, pp. 99–101, March. 2002.

[40] L.-L. Yang and L. Hanzo, "Serial acquisition performance of single-carrier and multicarrier DS-CDMA over Nakagami-m fading channels," *IEEE Transaction on Wireless Communications*, vol. 1, no. 4, pp. 692–702, Apr. 2002.

[41] L.-L. Yang and L. Hanzo, "Performance of generalized multicarrier DS-CDMA over Nagagami-m fading channels," *IEEE Trans. on Communications*, vol. 50, no. 6, pp. 956–966, June 2002.

[42] L.-L. Yang and H. L., "Multicarrier DS-CDMA: a multiple access scheme for ubiquitous broadband wireless communications," *IEEE Communications Magazine*, vol. 41, no. 10, pp. 116–124, Oct. 2003.

[43] L.-L. Yang, W. Hua, and L. Hanzo, "A multicarrier DS-CDMA system using both time-domain and frequency-domain spreading," *IEEE Vehicular Technology Conference*, vol. 4, pp. 2426–2430, Oct. 2003.

[44] C. W. You and D. S. Hong, "Multicarrier CDMA systems using time-domain and frequency-domain spreading codes," *IEEE Trans. on Communications*, vol. 51, no. 1, pp. 17–21, January. 2003.

[45] C.-M. Yang, P.-H. Lin, G.-C. Yang, and W. C. Kwong, "2D orthogonal spreading codes for multicarrier DS-CDMA systems," *IEEE International Conference on Communications*, vol. 5, pp. 3277–3281, May. 2003.

[46] P.-W. Fu and K.-C. Chen, "Multi-rate MC-DS-CDMA with multiuser detections for wireless multimedia communications," *IEEE Vehicular Technology Conference*, vol. 3, pp. 1536–1540, May 2002.

[47] J. Zhang, W. Cao, M. Peng, and W. Wang, "Investigation of hybrid ARQ performance for TDD CDMA HSDPA," *IEEE Vehicular Technology Conference*, pp. 2721–2724, April 2003.

[48] A. Das, F. Khan, A. Sampath, and H.-J. Su, "Adaptive, asynchrounous incremental redundancy (A^2IR) fixed transmission time intervals (TTI) for HSDPA," *IEEE International Symposium on Personal, Indoor and Mobile Radio Communications*, pp. 1083–1087, Sep. 2002.

[49] R. Love, B. Classon, A. Ghosh, and M. Cudak, "Incremental redundancy for evolutions of 3G CDMA systems," *IEEE Vehicular Technology Conference*, pp. 454–458, May 2002.

[50] A. Das, F. Khan, A. Sampath, and H.-J. Su, "Performance of hybrid ARQ for high speed downlink packet access in UMTS," *IEEE Vehicular Technology Conference*, pp. 2133–2137, Oct. 2001.

[51] P. Frenger, S. Parkvall, and E. Dahlman, "Performance comparison of HARQ with chase combining and incremental redundancy for HSDPA," *IEEE Vehicular Technology Conference*, pp. 1829–1833, Oct. 2001.

[52] 3GPP TR 25.848 v4.0.0(2001-03), "Physical layer aspects of UTRA high speed downlink packet access," Mar. 2001.

[53] 3GPP TSG-RAN WG2 R2-020945, "ACK/NACK power offsets in case of realistic channel estimation," May 2002.

[54] TSG RAN R2-021343, "LS on HARQ ACK/NACK error requirements for HS-DPA," May 2002.

[55] 3GPP TSG-RAN WG2 R2-021590, "Enhancements to stall avoidance mechanism," June 2002.

[56] 3GPP WG2-30 R2-021725, "Stall avoidance schemes in HARQ entity," June 2002.

[57] 3GPP WG2-31 R2-021974, "Stall avoidance schemes in HARQ entity," August 2002.

[58] L. Hanzo, L.-L. Yang, E.-L. Kuan, and K. Yen, *Single and multi-carrier DS-CDMA multi-user detection, space-time spreading, synchronization, networking and standards*, 1st ed. John Wiley & Sons, Ltd., 2003.

[59] L.-L. Yang and L. Hanzo, "Generalized multicarrier DS-CDMA using various chip waveforms," *IEEE Wireless Communications and Networking Conference*, vol. 51, no. 5, pp. 748–752, May. 2003.

[60] L.-L. Yang and L. Hanzo, "Performance of broadband multicarrier DS-CDMA using spacevtime spreading-assisted transmit diversity," *IEEE Transaction on Wireless Communications*, vol. 4, no. 3, pp. 885–894, May 2005.

[61] J.-H. Rhee, M.-Y. Woo, and D.-K. Kim, "Multichannel joint detection of multicarrier 16-QAM DS/CDMA system for high-speed data transmission," *IEEE Trans. on Vehicular Technology*, vol. 52, no. 1, pp. 37–47, Jan. 2003.

[62] L.-C. Wang, C.-W. Chang, and H. Huang, "An interference avoidance code assignment strategy for multi-rate mc-ds-cdma with time- and frequency-domain spreading," *to appear in IEEE internatinal conference on communications, June 2006.*

[63] 3GPP TS 25.308 V5.2.0, "High speed downlink packet access (HSDPA) overall description," March 2002.

[64] 3GPP TS 25.321 V5.0.0, "Medium access control (MAC) protocol specification," March 2002.

[65] G. Manuel and M. Rinne, "Performance of the medium access control protocol for the high speed downlink packet access," *Proceedings of the IASTED International Conference Communication Systems and Networks*, pp. 42–47, Sep. 2003.

[66] G. Manuel and M. Rinne, "Analysis of the transmission window for the delay performance of the high speed downlink packet access protocol," *International Conference on Software, Telecommunications and Computer Networks* , pp. 566–571, Oct. 2003.

[67] 3GPP TSG-RAN WG2 R2-A010016, "Dual-channel stop-and-wait HARQ," January 2001.

[68] C. W. You and D. S. Hong, "Multicarrier CDMA systems using time-domain and frequency-domain spreading codes," vol. 51, no. 1, pp. 17–21, January. 2003.

[69] L.-L. Yang and L. Hanzo, "Performance of generalized multicarrier DS-CDMA over Nagagami-m fading channels," vol. 50, no. 6, pp. 956–966, June 2002.

[70] K. S. Lim and J. H. Lee, "Performance of multirate transmission schemes for a multicarrier DS/CDMA system," *IEEE Vehicular Technology Conference*, vol. 2, pp. 767–771, Oct. 2001.

[71] S. Ulukus and R. D. Yates, "Stochastic power control for cellular radio systems," vol. 46, no. 6, pp. 784–798, June 1998.

[72] N. Kong and M. L.B., "Error probability of multicell CDMA over frequency selective fading channels with power control error," vol. 47, no. 4, pp. 608–617, Apr. 1999.

[73] Abrardo and D. Sennati, "On the analytical evaluation of closed-loop power-control error statistics in DS-CDMA cellular systems," *IEEE Trans. on Vehicular Technology*, vol. 49, no. 6, pp. 2071–2080, Nov. 2000.

[74] L.-C. Wang and C.-W. Chang, "Probability of false power control command in CDMA systems subject to measurement errors," *IEEE Communications Letters*, vol. 9, no. 4, pp. 298–300, April 2005.

[75] Y.-C. Tseng and C.-M. Chao, "Code placement and replacement strategies for wideband CDMA OVSF code tree management," *IEEE Trans. on Mobile Computing*, vol. 1, no. 4, pp. 293–302, Oct.-Dec. 2002.

[76] Y.-C. Tseng, C.-M. Chao, and L.-C. Wang, "Reducing internal and external fragmentations of OVSF codes in WCDMA systems with multiple codes," *IEEE Wireless Communications and Networking Conference*, vol. 1, pp. 693–698, Mar. 2003.

[77] L.-L. Y. Hua Wei and L. Hanzo, "Time- and frequency-domain spreading assisted MC-DS-CDMA using interference rejection spreading codes for quasi-

synchronous communications," *IEEE Vehicular Technology Conference*, vol. 1, pp. 389–393, Sept. 2004.

[78] ——, "Interference-free broadband single-and multicarrier DS-CDMA," *IEEE Communications Magazine*, vol. 43, no. 2, pp. 68–73, Feb. 2005.

[79] U. M. M. Amadei and M. Merani, "On the assignment of walsh and quasi-orthogonal codes in a multicarrier DS-CDMA system with multiple classes of users," vol. 1, pp. 841–845, Nov. 2002.

[80] U. Manzoli and M. Merani, "Multicarrier DS-CDMA performance with different assignment strategies of quasi-orthogonal codes," *IEEE International Symposium on Personal, Indoor and Mobile Radio Communications*, vol. 4, pp. 1477–1481, Sept. 2002.

[81] S. Sureshkumar and H. H. N. E. Shwedyk, "Mai-minimized signature waveforms for MC-DS-CDMA systems," *IEEE Vehicular Technology Conference*, vol. 1, pp. 305–309, June 2005.

[82] S. P. Chang and K. B. Lee, "Transmit power allocation for BER performance improvement in multicarrier systems," *IEEE Trans. on Communications*, vol. 52, no. 52, pp. 1658–1663, Oct. 2004.

[83] H. Long and Y. H. Chew, "An adaptive subcarrier allocation scheme for MC-DS-CDMA systems in the presence of multiple access interference," *IEEE International Conference on Communications*, vol. 5, pp. 2894–2898, June 2004.

[84] H. Holma and A. Toskala, *WCDMA for UMTS Radio access for third generation mobile communications*, 2nd ed.   WILEY, 2002.

[85] 3GPP TR 25.855 V5.0.0, "High speed downlink packet access overall UTRAN description," Sep. 2001.

[86] H. Lin and S. K. Das, "Performance study of link layer and MAC layer protocols to support TCP in 3G CDMA systems," *IEEE Trans. on mobile computing*, vol. 4, no. 5, pp. 489–502, Sept./Oct. 2005.

[87] M. Fisz, *Probability Theory and Mathematical Statistics*, 1st ed. New York, 1963.

[88] T. Ottosson and A. Svensson, "On schemes for multirate support in DS-CDMA systems," vol. 6, no. 3, pp. 265–287, Mar. 1998.

[89] H.-J. Su and E. Geraniotis, "Adaptive closed-loop power control with quantized feedback and loop filtering," *IEEE Transaction on Wireless Communications*, vol. 1, no. 1, pp. 76–86, Jan. 2002.

[90] M. Abramowitz and I. A. Stegun, *Handbook of Mathematical Functions with Formulas, Graphs, and Mathematical Tables*. U.S. Department of Commerce National Bureau of Standards Applied Mathematics Series 55, 1964.

[91] Li-chun Wang and Chih-Wen Chang, "Performance analysis of multicarrier DS-CDMA with imperfect power control and variable spreading factors," *IEEE global telecommunications conference*, vol. 6, pp. 3897–3901, Nov. 2005.

[92] L.-C. Wang, C.-W. Chang, and C.-J. Chang, "On the performance of an indicator-based stall avoidance mechanism for high speed downlink packet access systems," *IEEE Trans. on Vehicular Technology*, vol. 55, no. 2, pp. 691–703, March 2006.

[93] L.-C. Wang and C.-W. Chang, "Gap-processing time analysis of stall avoidance schemes for high speed downlink packet access with parallel HARQ mechanisms," *to appear in IEEE Transactions on mobile computing (accepted in Jan. 2006)*.

[94] ——, "On the performance of multi-carrier DS-CDMA with imperfect power control and variable spreading factors," *to appear in IEEE Journal on Selected Areas in Communications, Special issue on Advances in Multicarrier CDMA, second quarter of 2006 (accepted in Nov. 2005).*

[95] L.-C. Wang, C.-W. Chang, and H. Huang, "An interference avoidance code assignment strategy for MC-DS-CDMA with TF-domain spreading," *submitted to IEEE Transactions on Wireless Commmunications, Nov. 2005 (Major revised in Feb. 2006).*

[96] L.-C. Wang and C.-W. Chang, "A joint subcarrier power allocation and interference avoidance code assignment strategy for MC-DS-CDMA with TF-domain spreading," *to be submitted.*

[97] S. Hara and R. Prasad, "Design and performance of multicarrier CDMA system in frequency-selective Rayliegh fading channels," *IEEE Trans. on Vehicular Technology*, vol. 48, no. 5, pp. 1584–1595, Sep. 1999.

[98] L. Rugini and P. Banelli, "BER of MC-DS-CDMA systems with CFO and nonlinear distortions," vol. 4, pp. iv773 – iv776, May 2004.

[99] H. Kim and Y. Han, "A proportional fair scheduling for multicarrier transmission systems," *IEEE Communications Letters*, vol. 9, no. 3, pp. 210–212, March 2005.

[100] M. Hamza, H. T. Huynh, and P. Fortier, "Fixed and multiple step power control for MC-DS-CDMA in indoor and outdoor environments," *IEEE International Conference on Communications*, vol. 5, pp. 2965 – 2969, June 2004.

[101] Y. Zhu and E. Gunawan, "Performance of MC-CDMA system using controlled

MRC with power control in Rayleigh fading channel," *IEE Electronics Letters*, vol. 36, no. 8, pp. 752–753, April 2000.

[102] C. S. Park and K. B. Lee, "Transmit power allocation for BER performance improvement in multicarrier systems," *IEEE Trans. on Communications*, vol. 52, no. 10, pp. 1658–1663, Oct. 2004.

Vita

Chih-Wen Chang (IEEE student member'02) was born in HsinChu, Taiwan R.O.C, in 1976. He received the B.S. and M.S. degree in electrical engineering from National Sun Yat-Sen University, Kaohsiung, Taiwan, in 1998 and 2000, respectively. He obtained the Minor M. S. in applied mathematics and Ph.D degree in communication engineering from National Chiao-Tung University HsinChu, Taiwan, in 2005 and 2006, respectively. He was awarded the IEEE student travel grant for ICC 2006 and the membership of the Phi Tau Phi scholastic honor society in 2006. His current research interests include wireless communications, wireless networks, and cross-layer design.

Publication List

Journal Paper (published or accepted)

1. Li-Chun Wang and Chih-Wen Chang, "Gap-processing time analysis of stall avoidance schemes for high speed downlink packet access with parallel HARQ Mechanisms," to appear in IEEE Transactions on mobile computing (accepted in Jan. 2006).

2. Li-Chun Wang and Chih-Wen Chang, "On the Performance of Multi-carrier DS-CDMA with imperfect power control and variable spreading factors," IEEE Journal on Selected Areas in Communications, Special issue on Advances in Multicarrier CDMA, vol.24, no.6 pp.1154-1166, June 2006.

3. Li-Chun Wang, Chih-Wen Chang, and Chung-Ju Chang, "On the performance of an indicator-based stall avoidance mechanism for high speed downlink packet access systems," IEEE Trans. on Vehicular Technology, vol.55, No.2, pp.691-703, Mar. 2006.

4. Li-Chun Wang and Chih-Wen Chang, "Probability of false power control command in CDMA systems subject to measurement errors," IEEE Communications Letters, vol. 9, no. 4, pp. 298-300, Apr. 2005.

Journal Paper (Revision)

1. Li-Chun Wang, Chih-Wen Chang, Howard Huang, "An interference avoidance code assignment strategy for MC-DS-CDMA with TF-domain Spreading," submitted to IEEE Transactions on Wireless Commmunications, Nov. 2005 (Major revised in Feb. 2006).

Journal Paper (In preparation)

1. Chih-Wen Chang and Li-Chun Wang, "A joint Subcarrier power allocation and interference avoidance code assignment strategy for MC-DS-CDMA with TF-domain spreading," to be submitted.

2. Li-Chun Wang, Assane Laina, and Chih-Wen Chang, "A novel stall avoidance scheduling for high speed downlink packet access, " to be submitted.

Patent

1. Li-Chun Wang and Chih-Wen Chang, "An interference avoidance code assignment strategy for MC-DS-CDMA with TF-domain Spreading," filed for Taiwan and China patents in Jan. 2006.

International Conference Paper

1. Li-Chun Wang, Chih-Wen Chang, and Howard Huang, "An interference avoidance code assignment strategy for MC-DS-CDMA with TF-domain Spreading," accepted by 2006 IEEE International Conference on Communications.

2. Li-Chun Wang and Chih-Wen Chang, "Performance Analysis of Multicarrier DS-CDMA with Imperfect Power Control and Variable Spreading Factors", IEEE Global Telecommunications Conference, vol. 6, pp. 3897-3901, Nov. 2005.

3. Li-Chun Wang and Chih-Wen Chang, "Gap-processing time analysis of stall avoidance mechanisms for high speed downlink packet access with parallel HARQ Mechanisms," IEEE International Conference on Wireless Networks, Communications and Mobile Computing, vol. 1, pp. 81-86, June 2005.

4. Li-Chun Wang, Chih-Wen Chang, and Chung-Ju Chang, "On the performance of an indicator-based stall avoidance mechanism for high speed downlink packet access systems," IEEE Vehicular Technology Conference, vol. 2, pp. 1159-1163, Sept. 2005.

5. Li-Chun Wang, Chih-Wen Chang, Han-Kuang Chang, Chin-Yang Hsieh, and Sam Jiang, "Performance Comparison of Stall Avoidance Mechanisms for High Speed Downlink Packet Access in the WCDMA System," IEEE Personal, Indoor, and Mobile Radio Conference (PIMRC), vol. 3, pp. 2431-2436, Sept. 2003.

6. Li-Chun Wang and Chih-Wen Chang, "Impact of measurement errors on the closed loop power control for CDMA systems," IEEE Wireless Communications and Network Conference (WCNC), vol. 3, pp. 735-740, Mar. 2003.

7. Li-Chun Wang and Chih-Wen Chang, "Error statistics of closed-loop power control in Multirate DS-CDMA cellular systems," IEEE Wireless Communications and Network Conference (WCNC), vol. 2, pp. 712-716, Mar. 2002.

International Conference Paper (submitted)

1. Chih-Wen Chang and Li-Chun Wang, "A joint Subcarrier power allocation and interference avoidance code assignment strategy for MC-DS-CDMA with TF-domain spreading," submitted to IEEE Globecom 2006.

2. Li-Chun Wang, Assane Liana and Chih-Wen Chang, "A novel stall avoidance scheduling for high speed downlink packet access," submitted to IEEE APWCS 2006.